Julius-Maximilians-Universität Würzburg

Theodor-Boveri-Institut für Biowissenschaften

Fakultät für Biologie

Humanized mouse model: a system to study the interactions of human immune system with vaccinia virus-infected human tumors in mice

Dissertation

zur Erlangung des naturwissenschaftlichen Doktorgrades

der Julius-Maximilians-Universität Würzburg

vorgelegt von Desislava Tsoneva

aus Sofia, Bulgarien

Würzburg, September 2015

Eingereicht am: _____

Mitglieder der Promotionskommission:

Vorsitzender: _____

Erstgutachter: _____

Zweitgutachter: _____

Tag des Promotionskolloquiums: _____

Doktorurkunde ausgehändigt am: _____

Table of Contents

Summary

According to the World Health Organization cancer remains responsible for millions of deaths worldwide. The inability of conventional cancer treatment modalities to always lead to a complete cure or even to prolong the life of all cancer patients, requires finding new less invasive and more effective cancer treatment options, which can be used alone or in combination with the conventional therapies. A promising new approach for the treatment of human cancer is the use of oncolytic viruses, which exhibit a natural or genetically engineered tumor tropism. One of the top candidates in this area is the oncolytic vaccinia virus (VACV), which has already shown promising results in animal studies and in several Phase I and II clinical trials. However, due to discrepancies in both innate and adaptive immunity between mice and men the evaluation of the vaccinia virus' interactions with the host immune system in mice are not fully conclusive of what is actually happening in human cancer patients after systemic administration of vaccinia virus. Also, ethical and legal concerns as well as risk of potential toxicity limit research involving human patients. Therefore, a good *in vivo* model for testing interactions between vaccinia virus and human immune cells, avoiding the numerous limitations and risks associated with human studies, could be a humanized mouse model. This is an excellent small animal model that could improve our understanding of the physiology of the human immune system and the immune responses to diseases and pathogen agents.

The attenuated vaccinia viruses used in this thesis, LIVP-1.1.1, GLV-2b372, GLV-1h68, GLV-1h375, GLV-1h376 and GLV-1h377, were kindly provided by Genelux Corporation and Dr. Chen and initially evaluated in cell cultures before being used in humanized mice. The large cloning capacity of VACV allowed the insertions of different transgenes into the viral genomes. GLV-2b372 was constructed by inserting TurboFP635 expression cassette into the *J2R* locus of the parental LIVP-1.1.1 virus. GLV-1h375, -1h376 and -1h377 recombinant VACVs, which were constructed to encode the human CTLA4-blocking single-chain antibody (CTLA4 scAb), were engineered by Genelux Corporation in particular to be tested in the here presented novel humanized tumor mouse model. Performed replication and cytotoxicity assays demonstrated that all six viruses were able to infect, replicate in and kill human tumor cells in virus-dose- and time-dependent fashion. For the used viruses, transgene

expression in infected cell cultures was assessed by various methods. GLV-2b372-mediated TurboFP635 and GLV-1h68-, -1h375-, -1h376- and -1h377-mediated GFP expression were visualized by direct fluorescent microscopy and correlated well with replication and cytotoxicity data. LIVP-1.1.1 had naturally disrupted *J2R* locus but no transgenes inserted into its genome and therefore provided no option for visualization of the infection in cells. CTLA4 scAb and β-glucuronidase (GusA) expression as well as plaque forming units in GLV-1h376-infected cell cultures were analyzed by ELISA, β-glucuronidase assay and standard plaque assay, respectively, and compared. Indeed, an excellent correlation with correlation coefficients R^2>0.9806 were observed, indicating that each of the three parameters could be used to estimate the amount of the other two when tested in cell culture and presumably also in mouse blood or tumor samples. GLV-1h376-encoded CTLA4 scAb was successfully purified from supernatants of infected CV-1 cells and demonstrated *in vitro* affinity to its human CTLA4 target and lack of cross-reactivity to mouse CTLA4. In activated Jurkat cells, CTLA4 scAb was functional and able to further intensify the activation process. After being studied *in vitro* and in cell culture, LIVP-1.1.1, GLV-2b372, GLV-1h68 and GLV-1h376 were used in non-tumorous and/or tumor-bearing humanized mice.

The establishment of a new humanized mouse model with subcutaneous human tumor, which could potentially allow investigation of the oncolytic properties of vaccinia virus in the context of the human immune system without the limitation of experimentation in humans, was major task of this doctoral thesis. Initially, it was demonstrated that injection of human cord blood-derived $CD34^+$ stem cells into the liver of preconditioned newborn NSG mice let to a successful systemic reconstitution with human immune cells. Cells from lymphoid and myeloid lineage, $CD19^+$ B cells, CD4 and CD8 single positive $CD3^+$ T cell, $NKp46^+CD56^-$ and $NKp46^+CD56^+$ NK cells as well as $CD33^+$ myeloid cells, developed. At early time points after engraftment, majority of the human hematopoietic cells detected in the mouse blood were $CD19^+$ B cells and only a small portion were $CD3^+$ T cells. With time a significant change in $CD19^+/CD3^+$ ratio was reported with a decrease of B cells and an increase of T cells. Spleens of the humanized mice were reconstituted mainly with B cells. Implantation of human A549 lung cancer cells under the skin of those humanized NSG mice 10 - 13 weeks after engraftment resulted in a successful tumor cell implantation and subsequent progressive tumor growth, described for the first time in this thesis.

Successful colonization of subcutaneous A549 tumors with VACVs was visualized and demonstrated by detection of GLV-2b372- and GLV-1h68- and -1h376-mediated TurboFP635 and GFP expression, respectively, as well as by standard plaque assay and immunohistochemistry of LIVP-1.1.1- and GLV-2b372-treated tumors. In contrast to blood and spleens, the human $CD45^+$ cell population in tumors was represented mainly by $NKp46^+CD56^{bright}$ NK cells and a large portion of activated $CD4^+$ and cytotoxic $CD8^+$ T cells. However, no significant differences were observed between control and LIVP-1.1.1-infected tumors, suggesting that the recruitment of NK and activated T cells were more tumor tissue specific than virus-dependent. Unfortunately, virus-mediated CTLA4 scAb expression in the GLV-1h376-infected tumors was also not able to significantly increase activation of T cells compared to control and GLV-1h68-treated mice. Importantly, ELISA, β-glucuronidase and standard plaque assays showed an excellent correlation with correlation coefficients R^2>0.9454 between CTLA4 scAb, GusA concentrations and plaque forming units in tumor samples from those GLV-1h376 treated mice. The excellent correlations indicated that each of the three parameters could be used to estimate the amount of the other two when tested in tumor samples, making the GuaA assay, which is the most cost-, labor-, sample usage- and time-efficient of the three assays, the assay of choice to be performed when testing viral titers, GusA and CTLA4 scAb concentrations in tumor-bearing humanized mice-derived samples after treatment with GLV-1h376.

T cells isolated from the spleens of such control or GLV-1h68- or -1h376-treated A549 tumor-bearing mice were functional and could successfully be activated with commercially available beads, designed to mimic dendritic cells and to specifically activate human T cells. However, although no significant difference was observed between the three mouse groups, a slightly higher percentage of the GLV-1h376-treated mice-derived T cells were expressing CD25 and producing IFN-ɣ after *ex vivo* activation, probably due to the CTLA4 blockade by the virus-encoded CTLA4 scAb in the GLV-1h376-treated mice. Also, slightly higher levels of IL-2 were detected in the culture supernatant of those splenocytes compared to control samples. In contrast to the activation with beads, T cells from all three mouse groups were not able to recognize and to be activated by A549 tumor cells *ex vivo*, most likely due to the reported functional impairments of the phenotypically immature dendritic cells in stem cell engrafted animals. To be able to understand and more precisely interpret these

results in the model system being used in the particular study however further characterization of the developed immune cell types and proof of their functionality will be necessary.

Many humanized mouse models and approaches to improve the functionality of the human innate and adaptive immunity in those mice have already been developed. Our model has the specific advantage that tumors develop under the skin of the humanized mice, which allows accurate monitoring of the tumor growth and evaluation of the oncolytic virotherapy. Therefore it is important to choose the right approaches for its further improvement to be able to better understand the complex interaction between the vaccinia virus and the tumor in the context of the human immune system.

Zusammenfassung

Nach Angaben der Weltgesundheitsorganisation Krebs bleibt verantwortlich für Millionen Todesfälle weltweit. Die Unfähigkeit von traditionellen Krebsbehandlungsmodalitäten immer zu einer vollständigen Heilung zu führen oder sogar das Leben aller Krebspatienten zu verlängern, erfordert die Suche nach neuen weniger invasiven und effektiveren Krebsbehandlungsmöglichkeiten, die allein oder in Kombination mit den traditionellen Therapien verwendet werden können. Ein vielversprechender neuer Ansatz zur Behandlung von Krebs beim Menschen ist die Verwendung von onkolytischen Viren, die einen natürlichen oder gentechnischen Tumor-spezifischen Tropismus aufweisen. Einer der Top-Kandidaten in diesem Bereich ist das onkolytische Vaccinia Virus (VACV), das bereits vielversprechende Ergebnisse in Tierversuchen und in mehreren klinischen Phase I und II Studien gezeigt hat. Aber die von den *in vivo* in tierischen Modellen erhaltenen Resultate könnten ungenaue Informationen wegen der anatomischen und physiologischen Unterschiede zwischen den Spezies liefern. Andererseits sind Studien in Menschen aufgrund ethischer Erwägungen und potenzieller Toxizität nur limitiert möglich. Die zahlreichen Einschränkungen und Risiken, die mit den Humanstudien verbunden sind, könnten mit der Verwendung eines humanisierten Mausmodells vermieden werden. Diese erst kürzlich entwickelten immundefizienten Mausmodelle mit rekonstituiertem menschlichen Immunsystem sind ausgezeichnete Werkzeuge zur Erforschung des menschlichen Immunsystems und der Immunantworten gegen Krankheiten und Krankheitserreger.

In der vorliegenden Arbeit wurden die VACV Stämmen LIVP-1.1.1, GLV-2b372, GLV-1h68, GLV-1h375, GLV-1h376 and GLV-1h377 untersucht. Alle Viren wurden freundlicherweise von der Genelux Corporation und Dr. Chen zur Verfügung gestellt. Vor ihrer Anwendung in Mäusen, wurden die Viren zunächst in Zellkultur untersucht. Das große Genom der VACVs macht es möglich, verschiedene Transgene in einzufügen. GLV-2b372 wurde durch Einfügen der TurboFP635 Expressionskassette in den *J2R* Genlocus des parentalen LIVP-1.1.1-Stammes konstruiert. GLV-1h375, -1h376 and -1h377, welche das Gen für den menschlichen CTLA4-blockierenden Einzelketten-Antikörper (CTLA4 scAb) kodiert, wurden von der Genelux Corporation hergestellt, um in dem hier vorgestellten neuartigen humanisierten Tumormausmodell

getestet zu werden. Befunde aus Replikations- and Zytotoxizitätsstudien zeigten, dass alle sechs Viren Tumorzellen infizieren, sich in ihnen replizieren und sie in Zellkultur schließlich ebenso dosis- und zeitabhängig effizient abtöten konnten. In infizierten Zellkulturen wurde die Transgenexpression durch verschiedene Verfahren untersucht. GLV-2b372- und GLV-1h68-, -1h375-, -1h376- and -1h377-vermittelte TurboFP635- und GFP-Expression wurden durch direkte Fluoreszenzmikroskopie sichtbar gemacht und korrelierten gut mit der Virusreplikation und Zytotoxizität. LIVP-1.1.1 hatte einen natürlich unterbrochenen *J2R* Genlocus aber keine Transgene in seinem Genom und übermittelte daher keine Möglichkeit zur Visualisierung der Infektion in Zellen. CTLA4 scAb und β-Glucuronidase (GusA) Expression sowie Virus Titer in GLV-1h376-infizierten menschlichen A549-Zellen wurde anhand von ELISA-, β-Glucuronidase- and Standard Plaque-Assays bestimmt. Hierbei zeigte sich eine ausgezeichnete Korrelation mit Korrelationskoeffizienten R^2>0.9806, was darauf hindeutet, dass jeder der drei Parameter verwendet werden kann, um die Menge der beiden anderen zu bestimmen, wenn sie in Zellkultur und auch in Mausblut oder Tumorproben getestet werden. Der durch das GLV-1h376 kodierte CTLA4 scAb wurde erfolgreich aus Überständen von infizierten CV-1-Zellen gereinigt. CTLA4 scAb hat eine hohe *in-vitro*-Affinität zu seinem menschlichen CTLA4-Zielmolekül sowie abwesende Kreuzreaktivität gegenüber murine CTLA4 gezeigt. In aktivierten Jurkat-Zellen war CTLA4 scAb funktional und in der Lage, den Aktivierungsprozess weiter zu intensivieren. Nachdem sie *in vitro* und in Zellkultur untersucht wurden, wurden LIVP-1.1.1, GLV-2b372, GLV-1h68 und GLV-1h376 in nicht-tumorösen und/oder tumortragenden humanisierten Mäusen getestet.

Die Hauptaufgabe dieser Arbeit war die Entwicklung eines neuen humanisierten Mausmodells, welches die Untersuchung der onkolytischen Eigenschaften von VACV im Rahmen des menschlichen Immunsystems ermöglichen kann. Zunächst wurde gezeigt, dass die Injektion von menschlichen Nabelschnurblut-abgeleiteten $CD34^+$ Stammzellen in die Leber von vorkonditionierten neugeborenen NSG Mäusen zu einer erfolgreichen systemische Rekonstitution mit menschlichen Immunzellen geführt hat. Es wurden Zellen aus lymphoiden und myeloiden Linie entwickelt. $CD19^+$-B-Zellen, $CD4^+$- und $CD8^+$-$CD3^+$-T-Zellen, $NKp46^+CD56^-$ und $NKp46^+CD56^+$-NK-Zellen sowie $CD33^+$-myeloischen Zellen wurden detektiert. Die Mehrheit der nachgewisenen humanen hämatopoetischen Zellen im Mäuseblut in den ersten Wochen nach der

Humanisierung waren $CD19^+$-B-Zellen, und nur ein kleiner Teil waren $CD3^+$-T-Zellen. Mit der Zeit wurde eine signifikante Veränderung in $CD19^+/CD3^+$-Verhältnis beobachtet, die parallel zur Abnahme der B-Zellen und einem Anstieg der T-Zellen kam. Die Milzen der humanisierten Mäuse wurden vor allem mit B-Zellen rekonstituiert. Die Implantation von menschlichen A549-Zellen unter die Haut dieser Mäuse von 10 bis 13 Wochen nach der Humanizierung führte zu einer erfolgreichen Implantation der Tumorzellen und einem anschließenden progressiven Tumorwachstum. Bildgebende Verfahren zur Detektion von Virus-vermittelter TurboFP635- und GFP-Expression, Standard Plaque Assays sowie immunohistochemische Analysen bestätigten die erfolgreiche Invasion der Viren in die subkutanen Tumoren. Im Gegensatz zu Blut und Milz wurde die humane $CD45^+$-Zellpopulation in Tumoren hauptsächlich durch $NKp46^+CD56^{bright}$-NK-Zellen und einen hohen Anteil von aktivierten $CD4^+$- und zytotoxische $CD8^+$-T-Zellen dargestellt. Es wurden jedoch keine signifikanten Unterschiede zwischen den Kontroll- und LIVP-1.1.1-infizierten Tumoren beobachtet, was darauf hindeutete, dass die Rekrutierung von NK- und aktivierten T-Zellen, mehr Tumorgewebe-spezifisch als Virus-abhängig waren. Die GLV-1h376-vermittelten CTLA4 scAb-Expression in den infizierten Tumoren war ebenfalls nicht in der Lage, die Aktivierung von Tumor-infiltrierenden T-Zellen im Vergleich zur Kontrolle und GLV-1h68-behandelten Mäusen, signifikant zu erhöhen. ELISA-, β-Glucuronidase- and Standard Plaque-Assays zeigten eine eindeutige Korrelation mit den Korrelationskoeffizienten R^2>0,9454 zwischen CTLA4 scAb- und GusA-Konzentrationen und Virus Titer in Tumorproben von GLV-1h376-behandelten Mäusen. Diese Korrelationen zeigte, dass jeder der drei Parameter verwendet werden kann, um die Menge der beiden anderen zu bestimmen. Weil der β-Glucuronidase-Assay der kostengünstigste, arbeitsparendste und zeiteffizientste der drei Assays ist, ist dieser der Assay der Wahl bei der Untersuchung der genannten drei Parameter in Maus-Proben nach Behandlung mit GLV-1h376.

T-Zellen, die aus der Milz dieser Kontroll- oder GLV-1h68- oder -1h376-behandelten A549 Tumor-tragenden Mäuse isoliert wurden, waren funktionell und konnten erfolgreich mit Beads, entworfen, um dendritische Zellen zu imitieren, aktiviert werden. Obwohl kein signifikanter Unterschied zwischen den drei Maus-Gruppen beobachtet wurde, wurden mehr $CD25^+$ und IFN-γ^+ T-Zellen in der GLV-1h68-Gruppe gefunden, wahrscheinlich aufgrund der CTLA4-Blockade durch die Virus-vermittelte CTLA4

scAb-Expression in den GLV-1h376-behandelten Mäusen. Außerdem wurde eine höhere Konzentration von IL-2 in dem Kulturüberstand von diesen Splenozyten im Vergleich zu Kontrollproben nachgewiesen. Im Gegensatz zu der Aktivierung mit Beads konnten T-Zellen von allen drei Maus-Gruppen nicht durch A549 Tumorzellen *ex vivo* aktiviert werden. Der Grund dafür könnte Funktionsbeeinträchtigungen von phänotypisch unreifen dendritischen Zellen oder anderen Immunzellen in den humanizierten Mäusen sein. Um diese Ergebnisse genauer zu interpretieren, sind jedoch weitere Charakterisierung der entwickelten Immunzelltypen und den Nachweis ihrer Funktionalität notwendig.

Viele humanisierte Mausmodelle und Ansätze, um die Funktionalität des menschlichen angeborenen und adaptiven Immunität bei den Mäusen zu verbessern, wurden bereits entwickelt. Unser Mausmodell hat den besonderen Vorteil, dass sich Tumoren unter der Haut der humanisierten Mäuse entwickeln, was eine genaue Überwachung des Tumorwachstums und Auswertung der onkolytischen Virotherapie ermöglicht. Daher ist es wichtig, die richtigen Ansätze zu seiner weiteren Verbesserung auszuwählen, um das komplexe Zusammenspiel zwischen dem Vaccinia Virus und dem Tumor in Zusammenhang mit dem menschlichen Immunsystem besser zu verstehen.

1. Introduction

1.1 Cancer

Cancer is a generic term for a group of diseases characterized by uncontrolled growth and spread of abnormal body's own cells in the living organism leading to the formation of malignant tumors and when not treated to the organism's death [1]. According to the World Health Organization (WHO) cancer remains the second leading cause of death with 14.1 million new cancer cases and 8.2 million cancer deaths in 2012 worldwide, and the number of new cases is expected to rise by about 70% over the next 2 decades. Highest incidence rates in economically developed or developing countries were observed for breast, prostate, lung and colorectal or lung, breast, colorectal and liver cancer, respectively. Most common cause of cancer death in both areas remains the lung cancer. Increasing knowledge about tumorigenesis should help to avoid major risk factors for cancer. At the same time, the improvement of screening techniques would facilitate early disease detection, before symptoms appear, so cancer can be treated before it enters an advanced stage with better outcomes [2].

Tumor development is a complex multistep process of progressive conversion of normal human cells into malignant cancer cells [3]. The accumulation of alterations in the cellular machinery, regulating proliferation, differentiation and death, disrupts critically important homeostatic mechanisms of the cell. In 2000, Hanahan and Weinberg formulated a small number of underlying cellular defects that are shared in the cells of almost all the malignant cell types. Mutant cells possess a variety of selective advantages, which change their behavior within the normal tissue and allow their uncontrolled growth. A major adaption of perhaps all cancer cell types is to become resistant against apoptosis, which is the natural barrier to cancer development. Malignant cells have greatly reduced dependence on exogenous growth stimulation, because of producing their own stimulating signals, and simultaneously can block anti-proliferative signals coming from the surrounding normal tissue environment. They are capable of limitless doubling and skipping of senescence most probably due to the upregulated levels of telomerase enzyme expression in these cells. Therefore, tumor cells can proliferate and induce building of a complex solid

tumor microenvironment [4]. The intratumoral heterogeneity is composed of proliferating tumor cells in different differentiation states including cancer stem cells, endothelial cells forming the tumor-associated vasculature, infiltrating immune cells as well as an extracellular matrix. The interactions between malignant and normal cells are highly complex and can change over time during tumorigenesis. Growing tumors induce and sustain angiogenesis, via activation of an “angiogenic switch” [3, 5]. The tumor-associated neovasculature provides oxygen and nutrients supply for the growing tumor tissue. This continuous tumor cell growth and proliferation is also supported by a reprogrammed cancer cell energy metabolism [4]. At some stage of the tumor development a small number of cancer cells undergoes cell-biologic changes, including changes in shape, downregulated expression of cell-to-cell and cell-to-extracellular matrix adhesion molecules or upregulation of molecules associated with the cell migration etc. This allows them to spread from the primary tumor mass to distant organs using the blood or lymphatic system [3, 4]. The metastatic cells colonize new locations within the body and build secondary tumors. Metastases formation is an incompletely understood complex multistep process, which is the reason for 90% of the cancer deaths. Therefore, goal of most traditional and novel cancer therapies is not only to remove the primary tumor mass but also to eliminate the metastases.

1.2 Oncolytic virotherapy: novel approach for cancer treatment

Conventional cancer treatment modalities such as surgery, chemotherapy and radiation therapy require expensive equipment and often fail to induce a complete cure [2, 6]. Surgery can radically remove primary tumors but cannot eliminate metastases recurrence. Chemotherapy and radiotherapy have a narrow therapeutic index i.e. low doses can result in tumor cell resistance to these agents but increasing the doses is limited by toxicity to normal tissues [7]. One promising new approach for the treatment of human cancer is the use of oncolytic viruses, which exhibit a natural or genetically engineered tumor tropism. These tumor-selective replicating viruses have a high therapeutic index with the ability to induce cancer tissue damage by direct lysis of

infected cells leaving the surrounding normal cells unaffected [8]. Their replication is restricted to the targeted tumor tissue, where the input virus amplifies exponentially. This replication in the neoplastic tissue makes the pharmacokinetic properties of the novel viral agents distinct from the traditional anticancer therapeutics [9]. The new viral particles produced in the tumor can move directly to neighboring tumor cells, take control over the transcriptional and the translational machinery, and then replicate in and destroy them before infecting the next tumor cell. The reason why many viruses preferentially replicate in transformed cells is their ability to take advantage of the same cellular defects that promote tumor growth, such as uncontrolled proliferation, disruption of apoptotic pathways and ability to evade host anti-viral immune responses [10].

The increase of tumor selectivity of the oncolytic viruses is of exceptional importance for successful and safe treatment of cancer patients. Recent progress in the fields of genetics, virology and tumor molecular biology made the engineering of recombinant viruses possible. The new virus strains are genetically altered to attenuate their virulence in normal tissues but display high intratumoral levels of viral replication. This was achieved by deletion or insertional inactivation of genes critical for replication in normal tissues but not necessary in tumor cells. [7, 8, 10] Insertion of transgenes, for example such as biomarkers or immunostimulatory factors, into the viral genome add additional mechanisms, which could improve the oncolytic therapy by allowing monitoring of the spatial distribution of the live therapeutic or successful tumor lysis, or by provoking host antitumor immune responses, respectively.

Such oncolytic virus strains engineered to specifically target, replicate in and destroy tumor cells are promising novel antitumor therapeutic agents. Many of them have already been tested in preclinical and clinical trials. Ones of the top candidates in this area are the oncolytic vaccinia viruses.

1.3 Vaccinia virus

Vaccinia virus (VACV) belongs to the family *Poxviridae*, the subfamily *Chordopoxviridae*, and the genus *Orthopoxvirus* [11].

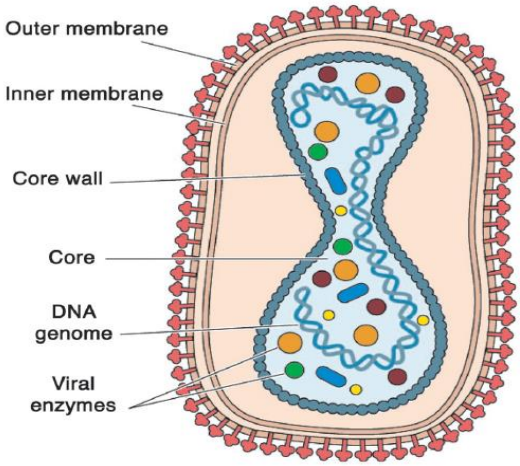

Figure 1. Genome organization of Vaccinia virus [11].

Intracellular mature vaccinia virion (IMV) and the extracellular enveloped virion (EEV) are both infectious forms of vaccinia virus delimited by one or respectively two lipid bilayer membranes that surround an inner core, containing double-stranded viral DNA genome and viral enzymes.

It is a large enveloped virus of 350 nm in diameter [10] (Figure 1). Viral core contains linear double-stranded DNA whose ends are covalently connected by single-stranded hairpin loops and associated viral proteins [11]. The intracellular mature virion (IMV) and the extracellular enveloped virion (EEV) are two infectious forms of the virus, which have one or two lipid bilayer membranes, respectively.

Vaccinia virus has had a critical role in one of the mankind's greatest medical triumphs, the eradication of the smallpox [11, 12]. It is the virus used in the variola virus vaccine. The use of vaccinia virus for the smallpox vaccination provided important information on its behavior in humans after intradermal vaccinia inoculation. Although VACV is not a human pathogen and could not naturally cause any known human disease, vaccination is usually followed by minimal reactions such as transient flu-like symptoms with fever, and is sometimes associated with rare complications such as generalized vaccinia infections and postvaccinal encephalitis [13] To overcome severe adverse reactions, associated with the smallpox vaccine, a number of approved and experimental antiviral agents for treatment of poxvirus infections, including vaccinia immune globulin, cidofovir etc, are available [14]. Because it is the virus with the longest and the most extensive history of use in humans, vaccinia virus has become the model of choice for the investigation of poxvirus biology and pathogenesis.

1.3.1 Morphogenesis of vaccinia virus

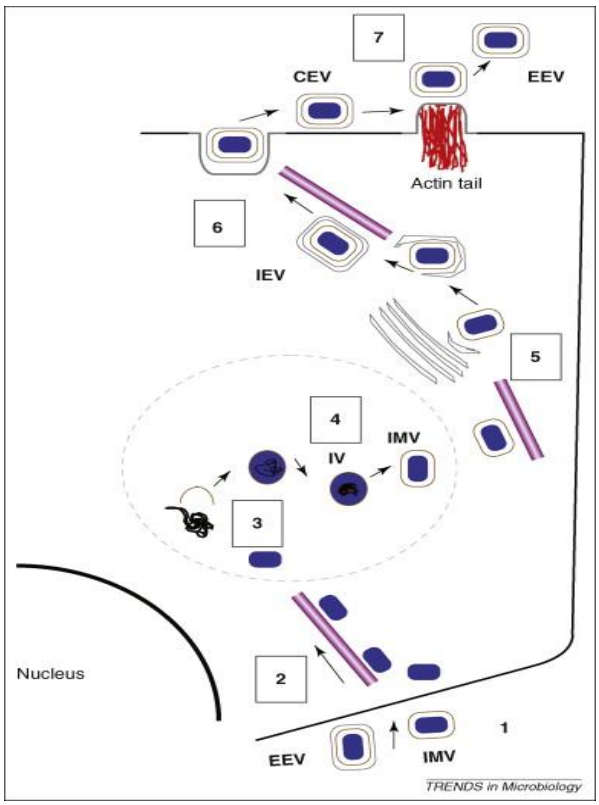

Figure 2. Overview of the vaccinia virus life cycle [15].

See 1.3.1 Morphogenesis of vaccinia virus for a detailed description of each illustrated step.

The uptake mechanism of vaccinia virus into susceptible host cells is highly complex and employs a large number of viral and cellular proteins [16]. In general, its infectious forms, IMV or EEV, attach to and enter the cell by direct fusion with the plasma membrane or using the endocytic internalization mechanisms (Figure 2 – 1). Both virions could exploit macropinocytosis, which is the most suitable form of endocytosis for large particles into non-phagocytic cells [17]. After vesicular transport in the maturing endosomes, the single membrane of the mature virion fuses with the endosomal membrane releasing the core into the cytosol [16]. The outer membrane of the enveloped virion is disrupted upon contact with the plasma membrane or with the cellular membrane of the endocytic vesicle and the underlying single-membrane mature virion-like particle fuses with those membranes like the mature virions. Primary uncoating takes place and the viral core enters the cell [10, 11] It is then transported along microtubules deeper into the cytoplasm to the place of the early viral gene

expression (Figure 2 – 2) [15]. After a second uncoating event the viral genome and its associated proteins are released into the cytoplasm (Figure 2 – 3) [11]. Part of these proteins are the viral DNA-dependent RNA polymerase and other proteins necessary for the transcription of the first early mRNAs. These early transcripts are then translated by the host cell translation machinery. One of the early expressed viral proteins is the vaccinia growth factor (VGF), which is secreted from the infected cell and binds to the epidermal growth factor receptor (EGFR) of the same cell and its neighboring cells, inducing proliferation [14]. Proteins modulating the host cell immunity are also part of the early protein products encoded by the vaccinia virus genome [10].

The early gene expression is followed by intermediate and late phase of the infection, during which different transcription factors, structural and other viral proteins are produced [11]. The actual genome replication occurs in distinct sites within the cells, named viral factories (Figure 2 – 4) [10]. The first infectious viral particles are the IMVs, which are coated in one membrane with controversial origin [11, 15]. They can be released from the infected cells only by cell lysis [10]. Some of these particles are coated with a second membrane from the trans-Golgi network or early endosomes (Figure 2 – 5), becoming intracellular enveloped viruses (IEVs). IEVs move to the cell surface along microtubules (Figure 2 – 6) and remain attached to the cell as cell-associated enveloped virus (CEV) particles, inducing formation of an actin tail (Figure 2 – 7), which drive virions toward neighboring uninfected cells for direct cell-to-cell spread or dissociate from the membrane as another infectious form of the virus, EEV.

1.3.2 Vaccinia as an oncolytic virus

Although VACV is the virus with the longest track record of use in humans, the use of vaccinia virus for the smallpox vaccination provided important information on its behavior after intra dermal inoculations but not after systemic administration via intravenous injection. Systemic administration of VACV would be beneficial when the virus is used as an oncolytic agent because this would allow VACV to reach more easily not only the main tumor mass but also eventually disseminated remote tumor metastases. The injection of the virus into the bloodstream of cancer patients and its systemic delivery through the leaky tumor vasculature into solid tumors and their

metastases in mouse models and clinical trials has already shown promising results [18-20] (www.clinicaltrials.gov; keywords: GL-ONC1 and vaccinia). A major challenge for the oncolytic VACV treatment using the blood route would be the already existing mature and effective adaptive immunity that can react against the therapeutic virus in patients, who have participated in the smallpox vaccination program [9]. To avoid host immune responses during spreading in immunocompetent patient VACV rely on its EEV, which outer membrane antigenically differ from the IMV membrane by displaying only low recognition by antibodies [10]. Also, the host immune system is not prepared to counter the large amount of virus delivered directly into the blood stream as it is in the case of the oncolytic virotherapy. Thus, the ideal oncolytic virus dose needed for sufficient infection of the tumor in immunocompetent patient but avoiding unwanted toxicity should be determined by appropriate dose escalation studies.

The oncolytic VACV is known to infect a vast variety of mammalian cell lines. Infectious virions may be internalized into the host cells through macropinocytosis or directly fuse with the plasma membrane [16, 17]. VACV replicates fast and efficient in the infected cells and spreads the infection rapidly from cell to cell [21]. Because its replication takes place exclusively within the cytoplasm of the infected host cell [10, 11], the risk of viral DNA integration into the host genome is inconsiderable. The large genome and respectively large cloning capacity of VACV [7, 22] together with its preferential infection of tumor cells [10] make it a useful research tool for the tumor biology field. The specificity of the virus for replication in tumors was further increased with the deletion of genes, such as the thymidine kinase, that are critical for the viral replication in healthy cells but redundant in cancer cells [10, 22]. The integration of reporter gene systems like the green fluorescent protein (GFP) into the genome of these attenuated tumor targeting vaccinia viruses allow optical-imaging and monitoring of the viral infection *in vivo* over time [22, 23]. Beta-glucuronidase is another example for such reporters, which allows viral infection monitoring in cell culture, *in vivo* in mouse models and *ex vivo*, when measured in blood plasma [24] (Tsoneva, Stritzker 2015, unpublished data).

With all these features and its highly immunogenic nature vaccinia virus meets all requirements for one virus to be a very promising oncolytic agent candidate [9] with the potential to effectively treat patients with cancer [10, 14, 25, 26].

1.4 Reporter gene systems for monitoring of oncolytic therapy

The monitoring of different biological processes within cell cultures or live organisms has outstanding importance for understanding the way they function and to troubleshoot malfunctions. Numerous imaging reporter systems are available and are being used in multiple branches of the biological science. But most of the imaging technologies for noninvasive imaging of processes in living subjects are very time consuming or have other big disadvantages like low sensibility, expensive equipment requirements etc.

Since cancer is one of the deadliest diseases among the human population and morbidity is increasing, gaining knowledge in the antitumor therapy has an exceptional importance. The discovery of the oncolytic viruses' ability to preferentially and specifically infect and lyse cancer cells led to the establishment of the novel oncolytic virus therapy and its progress in clinical testing. Development of appropriate and reliable tools for monitoring of successful tumor colonization during oncolytic therapy will be useful for one good controlled treatment, and genetically modified virus strains engineered to express different kind of reporter genes have already been described [22, 23, 27-29].

1.4.1 *E.coli* β-glucuronidase as vaccinia virus-encoded biomarker

The *E.coli* β-glucuronidase (GusA) is an enzyme encoded by the *gusA* gene isolated originally from the bacterium *Escherichia coli* [30]. It is a hydrolase that can cleave a vast variety of commercially available substrates depending on the type of assay that has to be performed. GusA can be detected by excitation with UV light (excitation peak at 365 nm).

Human and other mammalian β-glucuronidases are located in the lysosomes and work under acidic conditions. For that reason these enzymes have a strongly reduced capacity at neutral blood and tissue pH and are not suitable for reporter gene systems.

In contrast, the *E.coli* β-glucuronidase is more active in neutral or slightly alkaline pH and works optimal in the range of pH 6.8 - 7.7 [31]. This feature of the bacterial enzyme is making it a better reporter gene for biomarker studies by distinguishing between the *E. coli* glucuronidase encoded by the virus and the endogenous mammalian glucuronidase present in blood serum [32].

The β-glucuronidase assay is a very promising reporter system. For the first time it was used as a gene fusion marker in plant physiology studies [30, 33] but was less extensively investigated in mammals. In 2011 Hess, Strizker et al. published very promising data for the application of the 4-MUG (4-Methylumbelliferyl-β-D-glucuronide) fluorimetric β-glucuronidase assay for noninvasive *ex vivo* detection of successful tumor colonization during oncolytic virotherapy in nude mice [24]. 4-MUG is one of the substrates of the β-glucuronidase enzyme used for fluorimetrical analysis. It is non-fluorescent but when cleaved by β-glucuronidase produces the fluorigenic product 4-MU, which is highly fluorigenic at pH 9.5 - 10.5 [34]. Moreover, another substrate, FDGlcU (Fluorescein Di-β-D-Glucuronide), was used for *in vivo* imaging of the β-glucuronidase expressing tumors [24]. The *gusA* expression cassette for the bacterial hydrolase was delivered to the cells of interest using attenuated recombinant vaccinia virus strains. Because the engineered vaccinia virus has the ability to colonize solid tumors and tumor metastasis very specifically, but not other healthy organs, and its replication occurs in the cytoplasm of the host cells, *E.coli* β-glucuronidase is produced only in the infected tumor cells. The enzyme is not secreted and remains within the cell. Its amount increase during viral replication. When the quantity of the newly assembled viral particles becomes too high, the host tumor cell is lysed and the β-glucuronidase is released into the surrounding blood and tissue environment which is offering an optimal pH and therefore advantage for the bacterial hydrolase over the endogenous one. The enzyme was shown to have a high stability in blood and blood serum samples. On these grounds measured enzymatic activity by hydrolytic cleavage of the 4-MUG substrate in blood serum one can obtain information on tumor cell destruction during the therapy. The method is very specific and can detect the β-glucuronidase activity in a single lysed cell. Thus, GusA activity in serum is an indicator not only of vaccinia virus infection and replication, but also tumor cell lysis. Therefore, it was proposed that in patients the activity of the biomarker in the blood would be a more direct indicator of virus induced oncolysis than lactate dehydrogenase (LDH)-

measurements (Tsoneva, Stritzker 2015, unpublished data). Indeed, a good correlation between the GusA amounts and LDH was observed at all stages of virus infection when measured in the supernatants of GusA-encoding rVACV infected tumor cell lines. Also, an improved sensitivity of the GusA assay was reached when assayed with CMUG (6-Chloro-4-methylumbelliferyl β-D-glucuronide) as substrate compared to those obtained with 4-MUG and FDGlcU. Therefore, this was substrate used in this study.

Particular advantages of this quantitative enzyme assay are the easy handling, the small sample volume needed, its accuracy, relatively cheap substrates and the potential of this method to be used in other biological therapy approaches. The great number of its useful features is making β-glucuronidase assays an attractive candidate for reliable biomarker for monitoring of oncolytic virotherapeutical efficiency in cell culture, animal studies and human patients. Because high sensitivity of the assay even with small sample volumes would be very useful features especially in humanized mouse studies, this assay was in particular interest for this work. Studies with humanized mice require routinely blood withdraws for analyzing the reconstitution levels with human immune cells. Therefore, a small blood volume needed for monitoring a successful virus replication in the tumor of these mice after oncolytic viral therapy would be very helpful to reduce the frequency of blood withdraws. GusA assay could also be very useful to test the viral load in the samples from excised humanized mice-derived tumors by increasing the accuracy and reducing the human labor when compared to the standard plaque assay.

1.5 Virus-induced immunologic cell death

Oncolytic viruses were originally used to selectively replicate in and destroy tumors by direct virus-mediated oncolysis [35]. However, to achieve a complete destruction of the tumor and to ensure elimination of any distant tumor metastases a virus-induced engagement of the host immune system would be necessary. During the multistep process of tumorigenesis tumors adopt mechanisms allowing them to damp antitumor immune responses [36], which are part of the host antitumor immunosurveillance. Also some tumors attract excessive levels of immune tolerance-inducing components of

the host immune system, such as suppressor myeloid and inhibitory T regulatory (Treg) cells [35]. On the other hand, vaccinia virus itself possesses a large panel of immunosuppressive gene products involved in evading of the innate immunity and the development of T helper 1 (Th1) immune responses [10]. This delay in the host antiviral immune response provide a valuable time for the virus to multiply in the infected cells. However, the highly efficient VACV replication ultimately leads to tumor cell lysis and release of large amounts of both virus- and tumor-associated antigens (VAA and TAA, respectively), as well as viral (pathogen-associated molecular pattern (PAMPs)) and cellular (danger-associated molecular pattern (DAMPs)) danger signals [14]. Dendritic cells (DCs) recognize the virus derived PAMPs with the help of their pattern recognition receptors, migrate to the secondary lymph nodes and activate T cells to differentiate to effector cells, by presenting them the virus antigens [35]. These immune effector cells are then able to infiltrate the tumor site and to attack the virus-infected malignant cells. Another way of activating the host immune system is the inducing of immunogenic cell death (ICD) through the released DAMPs. Vaccinia virus replicates in the cytosol of the host cells and uses the cellular translational machinery to produce its viral proteins. The intensive production of viral proteins overwhelms this machinery and cause reactive oxygen species induced endoplasmic reticulum (ER) stress. This cause the translocation of the ER chaperone calreticulin on the plasma membrane as well as release of the adenosine triphosphate (ATP) and high-mobility group box 1 (HMGB1) immunomodulatory molecules. The release of these danger signal stimulates DC to take up TAAs and to present them again to the T cells in the lymph nodes. Activated effector T cells move to the tumor site and contribute to the killing of malignant cells. The presentation of TAAs in the context of the strong local immune response to the viral infection could lead to the generation of highly potent adaptive antitumor cytotoxic T cell response to diverse antigen targets [14, 36] thereby dramatically enhancing the therapeutic effect of the oncolytic virus [10] This potent inflammatory response initiated by all of these factors should take place at all tumor sites, i.e. at all sites of metastases too, infected by the intravenously delivered virus [36]. It should also be able to overcome the localized immune suppression that is typically found within the tumor and provide long-term cancer immunosurveillance for prevention of tumor relapse and metastases.

Antitumor immunity could be further increased with the engineering of recombinant vaccinia virus strains encoding for immunostimulatory factors, such as CTLA4-blocking antibodies, to optimally shape the host immune responses at the tumor site.

1.5.1 Blocking CTLA4 immune checkpoint to enhance antitumor immunity

The immune system is using immune checkpoints to maintain peripheral tolerance to self-antigens and to prevent normal tissue from damage by regulating and dampening excessive immune responses during pathogenic infections [37, 38]. An example for such important immune checkpoint is the cytotoxic T-lymphocyte-associated antigen 4 (CTLA4). CTLA4 is an inhibitory receptor expressed exclusively on T cells [38], which plays an important role in the shaping of the T cell immune responses. For their activation, cytotoxic $CD8^+$ T cells require T cell receptor (TCR)-mediated recognition of antigens bound to major histocompatibility complex (MHC) molecules on professional antigen-presenting cells (APCs) [37]. To enhance this initial signal into a potent activation signal, T cells need a second costimulatory signal through the CD28 receptor, which is also expressed on the T cell surface and interacts with CD80 (B7-1) and CD86 (B7-2) molecules, expressed on the APCs. Activated effector T cells then proliferate and travel to the site of antigen origin, execute their effector functions and produce inflammatory molecules [38]. To avoid an excessive cytotoxicity in such highly inflammatory environment host immune system possesses negative feedback mechanisms, such as the CTLA4 pathway. CTLA4 is expressed on the T cell surface upon activation and regulates the early stage of the activation process by counteracting the CD28-mediated signal, due to its higher affinity for both CD80 and CD86 ligands, thereby dampening the activation. Aside from surveilling the effector $CD8^+$ T cell responses, CTLA4 play a critical in the regulation of the $CD4^+$ T cell subset. It downregulates immune responses by decreasing helper T (Th) cell- and increasing regulatory T (Treg) cell-activities. In addition to the natural Treg cells there is also a second subtype of them called induced T cells, which accumulate at the tumor site, where together with myeloid derived suppressor and other inhibitory cells creates a niche of innate and adaptive tumor induced immune suppression [37, 38].

Inhibiting this important immune checkpoint through CTLA4-blocking antibodies (Abs) could therefore help the host to overcome the tumor induces immune suppression and generate a potent antitumor immune response by enhancing the tumor-specific cytotoxic T cell responses, activating Th cells and depleting Treg cells from the tumor site. This concept was proved by the use of the Ipilimumab, the first US Food and Drug Administration-approved fully humanized CTLA4-blocking monoclonal antibody [38, 39]. This new therapeutic increased patient long-term survival by 18%. But the systemic administration of CTLA4-blocking antibodies in preclinical and clinical studies was also accompanied with some degree of immune toxicity [38, 40]. This systemic immune toxicity could be overcome by combining the CTLA4-blocking antibody with the oncolytic vaccinia virus into one recombinant CTLA4-blocking antibody-encoding vaccinia virus. The ability of VACV to selectively infect tumorous but not healthy tissue will limit the expression of the blocking Ab to the tumor site and also limit the unwanted systemic activation of the immune system. The anti-CTLA4 Ab could be expresses under the control of weaker or stronger promotor, thereby regulating the amount of Ab to be produced. Such targeted activity of the CTLA4-blocking Ab to the tumor could be able to disrupt the tumor induced immunosuppression and together with the oncolytic virus could build a specific antitumor immune response. Additionally, when choosing a CTLA4-blocking Ab, the replacement of the monoclonal Ab used in the clinic with a smaller single-chain one would facilitate its distribution within the tumorous tissue. To test this concept, Genelux engineered an anti-human CTLA4 single-chain antibody-encoding rVACV. Its potential to increase levels of tumor-infiltrating lymphocytes in A549 tumors was evaluated in the here presented humanized mouse model.

1.6 Humanized mouse models

Studies on tumorigenesis, bacterial or viral infections, gene or stem cell therapies, transplantation, vaccine development or the normal human physiology are very limited or impossible *in vitro*. Those in humans are also limited because of ethical considerations and the risk of potential toxicity. Therefore, many experimental therapies are being tested *in vivo* in animal models. The widest used and the most cost-efficient laboratory animal model is the mouse. Mice are mammals and have

many similarities with humans. However, there have important differences, and in many cases the results obtained in experiments utilizing this model may not precisely represent the situation in humans. The advances in mammalian genetics during the last 30 years led to the development of new immunodeficient mouse models. These models have been extensively used to study the engraftment and reconstitution of human hematopoietic stem cells, autoimmune disorders, development of the human immunodeficiency virus infection, vaccine design etc. [41-44]. Because such immunodeficient mice with reconstituted human immune system could be a perfect tool to study the interactions between vaccinia virus and the human immune system the development of such humanized mice was one of the major tasks of this work.

Two methods for reconstitution of immunodeficient mice with human immune cells have been developed [45]. The first one involves an implantation of a small intact fragment of human fetal thymus under the murine kidney capsule [41] or its coimplantation with a small piece of human fetal liver [46] and subsequent transplantation with autologous hematopoietic stem cells obtained from the same fetal liver that has been previously implanted into the animal [47]. The development of the second model, which was utilized in this thesis, requires a transplantation of human hematopoietic cells only.

1.6.1 Transplantation of human hematopoietic (stem) cells into different immunodeficient mouse strains

A widely used method of reconstitution of immunodeficient mice without surgical manipulations is the implantation of these mice with human peripheral blood mononuclear (PBMCs) or hematopoietic stem cells.

Engraftment of human immune cells into immunodeficient mouse was first possible and initially performed in severe combined immunodeficient (SCID) mice. The *scid* mutation in the gene for the catalytic subunit of a DNA-dependent protein kinase responsible for the rearrangement of the immunoglobulin gene segments was first described in 1983 in C.B-17 mouse strain [48, 49]. The homozygous C.B-17 *scid* mice have defects in B and T cell development i.e. severely deficient in adaptive immune

system because of this mutation but they do have innate immune systems. In the same year, Mosier et al reported delivery of mature human PBMCs by intraperitoneal injection into SCID mice [50]. However, the human lymphocytes in this model showed relatively inefficient engraftment and high incidence of human graft versus disease (GVHD) in the mouse host. Relatively high engraftment rates with human cells were observed later in the bone marrow of sublethally irradiated and then transplanted with human hematopoietic $CD34^+$ stem cells SCID mice [51].

The SCID mice have functional elements of the innate immune system in addition to high levels of natural killer (NK) cells, with the ability to eliminate human cells from the mouse blood, a possible reason for insufficient reconstitution of the peripheral blood of these mice [49, 52-54]. This problem has been overcome in a new mouse strain, resulting from the transfer of the *scid* mutation onto the nonobese diabetic (NOD) strain by Shultz and colleagues at The Jackson Laboratory (Bar Harbor, ME, USA) [49, 55, 56]. However, NOD/SCID mice have a short lifespan because of the expression of the endogenous ectopic murine leukemia provirus locus “EMV30”, on chromosome 11 coming from the NOD-strain. The resulting thymoma causes the death of most of the animals within 4 to 8 months [55]. This mouse strain has significantly reduced innate immune system activity due to additional defects in NK, macrophages, antigen-presenting cells and complement functions. The decreased levels of NK cells allowed better engraftment with human hematopoietic cells and the generation of B lymphocytes in this *in vivo* model [45, 57].

Following the report of Greiner and coworkers in 1995 that NOD/SCID mice exhibited enhanced reconstitution levels with human spleen-derived hematolymphoid cells as compared to SCID mice [57], Hogan et al. published promising data for the engraftment of NOD/SCID mice with umbilical cord blood-derived $CD34^+$ cells [58]. However, the levels of reconstitution with human immune cells in the different mouse tissues varied, and the principal cells in the initial humanized mouse models were the B cells, with only limited presence of T cells [45].

More recently, studies performed with newborn RAG2-/-ɣc-/- mice implanted with human hematopoietic stem or progenitor cells demonstrated efficient human immune cells reconstitution [59]. The recombinase activating gene-2 (RAG2) and common cytokine receptor gamma chain (ɣc) double mutant mice lack mature B and T

lymphocytes and also NK cells [60, 61]. The intraperitoneal injection of human fetal liver-derived $CD34^+$ cells into sublethally irradiated newborn RAG2-/-γc-/- mice led to rapid multi lineage reconstitution with human $CD45^+$ cells in 83% of the mice, but only in 42% of the mice the reconstitution was over 50%. Remarkable reconstitution with B lymphocytes, monocytes, NK cells, plasmacytoid dendritic cells and T lymphocytes in various peripheral organs or in the circulation was presented. B lymphocytes were the most abundant immune cell type. Because a large T cell repertoire was present in this model, but not in previous studies with adult mice, it was suggested that the more atrophic thymus in addition to the more active innate immune system of the adult when compared to the newborn immunodeficient mice could not provide a good environment for T cell development.

Another important improvement of this model was the injection of the human umbilical cord blood-derived $CD34^+$ cells directly into the liver of the neonate mice [62]. Fetal liver in mammalian fetus during the first weeks of development serves as major hematopoietic organ. When human $CD34^+$ cells were injected into the liver of newborn RAG2-/-γc-/- mice, this resulted in excellent engraftment of the hematopoietic stem and progenitor cells. The long-term and multi-lineage reconstitution led to increase in the splenic and thymic cellularity of the mice and development of mesenteric lymph nodes. Human immune cells in these organs were able to form lymphoid structures. B cells were capable of Ig isotype class switching. The full B cell maturation together with the development of systemic T cell homeostasis and dendritic cells in this model supported the generation of adaptive immune response against tetanus toxoid (TT) and Epstein-Barr virus (EBV).

The level of human cell engraftment in the newborn mouse model was further increased by using the NOD/SCID/IL2rγ^{null} mouse strain, which also lacks the IL-2 family common cytokine receptor γ chain gene (IL2rγ) [63, 64]. The problem with the residual NK activity in these mice was overcome, no murine T, B or NK cells could develop [65]. Important advantage of this new mouse strain was its longer lifespan – up to 95 weeks of age, due to the fact that these mice do not develop thymoma as reported in the NOD/SCID mice. Intravenous injection of human cord blood-derived $CD34^+$ cells via a facial vein of a newborn NOD/SCID/IL2rγ^{null} mice resulted in a successful, highly efficient (between 50-80% in each mouse) and long-term robust multilineage development of functional human immune cells for both systemic and

mucosal immunity [66]. Surprisingly, cells of the myeloerythroid system, e.g. erythroid cells and megakaryocytes, were also present. The successful maintenance of human immune system for more than 24 weeks after transplantation and the development of human erythropoiesis and thrombopoiesis make the NOD/SCID/IL2rγ^{null} newborn mouse model a primary choice of a small animal model for studying the human immune system *in vivo*. The only drawback of this system was the development of the human T cells in the murine thymus.

The constantly improving humanized mouse models lead to a better understanding of human hematopoietic stem cell biology, homeostasis and the complexity of the human innate and adaptive immune system, transplantation immunology etc. Another important feature of the human immune system, namely anticancer immunity, could not be studied because of potential rejection of the implanted tumor cells in the humanized mice due to mismatched MHC between the human immune cells and the cancer cells. This problem was solved with the development of the humanized tumor mouse model in 2011 [67]. This model involves a co-transplantation of human umbilical cord blood-derived CD34^{+} cells and human cancer cells into the liver of newborn NOD/SCID/IL2rγ^{null} mice. As previously reported, the injection of the hematopoietic stem cells resulted in stable, long-term, multilineage reconstitution of a functional human immune system and at the same time development of solid tumors and tumor metastases without sign of rejection.

The humanized tumor mice model is the small animal system closest to the real situation in cancer patients. It allows investigation of the cancer development in the context of the human immune system and testing of potential therapeutic interventions like antibody-based anticancer therapies, oncolytic virotherapy, etc. This model could be a wonderful experimental system for evaluation of the complex relationships between the vaccinia virus, the human immune system, and different tumors and their metastases during oncolytic virotherapy. For example, evaluation of the human cytokine levels before and after administration of the virus could provide important information for the immune responses provoked by the virus in the context of the human immune system. It could also be a good *in vivo* system to test the ability of vaccinia virus expressing the Cytotoxic T lymphocyte Antigen 4 (CTLA4) antibodies to enhance the anticancer activity of the human T cells by CTLA4 mediated blockade in the tumor area. This model could also allow evaluation of the possible infection of the

human immune cells by the virus upon vaccination with vaccinia virus or during oncolytic therapy. This system is much more precise than any *in vitro* assay and can predict with higher accuracy the possible outcome of different therapeutic interventions in humans.

2 Materials

2.1 Chemicals

1X Red Blood Cell Lysis Buffer	eBioscience
3x FLAG® Peptide	Sigma
β-glucuronidase	Sigma
Acetic acid	Sigma
Anti-Flag® M2 Affinity Gel	Sigma
BD™ stabilizing fixative	Becton Dickinson
Bovine serum albumin (BSA) Fraction V	Fisher Scientific
Carboxymethylcellulose (CMC)	MP Biomedicals, LLC
Citrate buffer	Sigma
CMUG	Glycosynth™
Collagenase D	Roche Diagnostics
Crystal violet	Sigma
Dehydration Alcohol 100	EMD Millipore
Difco™ Skim Milk	Becton Dickinson
Dimethyl sulfoxide (DMSO)	Sigma
Dispase®	Roche
DMEM-medium without phenol red	Mediatech, Inc.
DNAse I type IV	Sigma
Dulbecco's Modification of Eagle's Media (DMEM)	Mediatech, Inc.
Dulbecco's Phosphate-buffered /Saline (1xDPBS)	Mediatech, Inc.
Ethyl Alcohol Pure, 200 Proof	EMD Millipore
Ethylenediaminetetraacetic acid (EDTA)	Fisher Scientific
Fetal bovine serum (FBS)	Mediatech, Inc.
Ficoll-Paque™Plus	GE Healthcare
Formaldehyde (37 %)	VWR International
Glutamine (L)	Mediatech, Inc.
Hank's Balanced Salt Solution (HBSS 1x)	Thermo Scientific
Hepes	Mediatech, Inc.

Human AB serum	GEMINI Bio-Products
Hyaluronidase type V	Sigma
Hydrochloric acid (HCL)	VWR
Hydrogen peroxide solution	Sigma
HyPure™Cell Culture Grade Water	Thermo Scientific
ImmPACT DAB Peroxidase (HRP) Substrate	VECTOR
Ionomycin	Sigma
Ipilimumab (YERVOY™)	Bristol-Myers Squibb
Isopropyl alcohol	EMD Millipore
Laemmli Sample Buffer 2x	Bio Rad
MACS Buffer	Miltenyi Biotec
MEM - medium without phenol red	Mediatech, Inc.
MEM Nonessential Amino Acids	Mediatech, Inc.
Methanol	Sigma
McCoy's 5A medium	Mediatech, Inc.
NuPAGE® Novex® LDS Sample Buffer (4x)	Invitrogen
NuPAGE® Novex® MOPS SDS Running Buffer (20x)	Invitrogen
NuPAGE® Novex® Transfer Buffer (20X)	Invitrogen
Paraformaldehyde	Electron Microscopic Science
Paraplast® Tissue embedding medium	McCormick Scientific
Penicillin/Streptomycin	Sigma
Phosphate buffered saline, powder	Sigma
Precision Plus Protein™ Dual Color Standards	Bio Rad
Phorbol 12-myristate 13-acetate (PMA)	Sigma
Protein Standard I, Bovine γ-globulin	Bio Rad
Recombinant human B7-1/CD80 Fc Chimera	R&D Systems
Recombinant human B7-2/CD86 Fc Chimera	R&D Systems
Red Blood Cell Lysis Solution (10x)	Miltenyi Biotec
Richard-Allan Scientific™ Mounting Medium	Thermo Scientific
RPMI 1640	Mediatech, Inc.
RPMI 1640 without phenol red	Mediatech, Inc.
Sodium azide	Fisher Scientific

Sodium pyruvate	Mediatech, Inc.
StemSpan Cytokine Cocktail CC100	StemCell Technologies
StemSpan Serum-free Medium SFEM	StemCell Technologies
Thiazolyl Blue Tetrazolium Bromide (MTT)	Sigma
TMB (3,3′,5,5′-tetramethylbenzidine)	Sigma
Trypan blue solution	Mediatech, Inc.
Trypsin EDTA	Mediatech, Inc.
Tween 20	Bio Rad
VECTOR Hematoxylin QS	VECTOR
Xylene Substitute	Sigma
Z-Fix (Buffered aqueous zinc formalin)	Anatech LTD

2.2 Buffers and solutions

Acidified Isopropanol	41.7 ml 12 N HCL 458 ml 100% Isopropanol
Coomassie staining solution	0.25% Coomassie blue R 45% CH_3OH 10% CH_3COOH
Coomassie destaining solution	25% CH_3OH 7.5% CH_3COOH
Crystal violet solution	1.3 g crystal violet 50 ml C_2H_5OH 300 ml 37% formaldehyde 650 ml ddH_2O
FACS buffer	500 ml PBS 2.5 g BSA (final 0.5%) 0.04% sodium azide
Freezing medium	90% Human AB serum 10% DMSO

PBS+	500 ml PBS 5 ml Penicillin/Streptomycin
PBS+++	500 ml PBS 5 ml Penicillin/Streptomycin 2.5 g BSA (final 0.5%) 2 mM EDTA Filter through 0.22 µm
PBS-Tween 20	0.005% Tween 20 in PBS
MTT solution	2.5 mg/ml MTT in RPMI w/o Phenol red
Resin wash buffer	0.5 M Tris-HCl 1.5 M NaCl pH 7.4

2.3 Antibodies

2.3.1 Antibodies for flow cytometry

Antibody	**Clone**	**Manufacturer**
Human BD Fc Block™	-	BD
Mouse anti-human CD 3 APC-H7	SK7	BD
Mouse anti-human CD 4 PE	SK3	BD
Mouse anti-human CD 4 PE-Cy7	SK3	BD
Mouse anti-human CD 8 FITC	HIT8a	BD
Mouse anti-human CD 8 PE	HIT8a	BD
Mouse anti-human CD 19 FITC	HIB19	BD
Mouse anti-human CD 25 BV421	M-A251	BD
Mouse anti-human CD 33 PerCP-Cy5.5	P67.6	BD
Mouse anti-human CD 45 APC	HI30	BD
Mouse anti-human CD 56 PE	MY31	BD

Mouse anti-human CD 69 FITC	FN50	BD
Mouse anti-human CD 152 PE	BN13	BD
Mouse anti-human IFN-ɣ PerCP-Cy5.5	B27	BD
Mouse anti-human NKp46 PE-Cy7	$9E_2$/NKp46	BD
Mouse BD Fc Block™	2.4G2	BD

2.3.2 Antibodies for Western blot and ELISA

Antibody	**Manufacturer**
Goat Anti-Rabbit IgG (H+L)-HRP Conjugate	Bio Rad
Rb pAb to DDDDK tag	Abcam

2.3.3 Antibodies for tissue sections

Antibody	**Manufacturer**
Rabbit polyclonal IgG to Vaccinia Virus	Abcam

2.4 Kits

Kit	**Manufacturer**
BD Cytofix/Cytoperm™Plus Fixation/Permeabilization Kit with BD GolgiStop™	BD Bioscienses
DC™ Protein Assay Reagents Package Kit	Bio Rad
Direct CD34 Progenitor Cell Isolation Kit, human	Miltenyi Biotec
FLAG® Immunoprecipitation Kit	Sigma
Human IFNɣ ELISA Kit	Thermo Scientific
Human IL-2 ELISA Kit	Thermo Scientific
LIVE/DEAD® Fixable Dead Cell Stain Kit	Invitrogen
Opti-4NC™ Substrate Kit	Bio Rad
T-cell Activation // Expansion Kit, human	Miltenyi Biotec
VECTASTAIN Elite ABC Kit (Rabbit IgG)	VECTOR

2.5 Cell lines and growth media

Cell line	Description	Media
1936-MEL	Human skin cancer. Source: chest wall mass.	RPMI
888-MEL	Human skin cancer. Source: subcutaneous.	RPMI
A549	Adherent growing human lung carcinoma cells	RPMI
CV-1	Adherent growing cells derived from Cercopithecus aethiops monkey kidney	DMEM

2.5.1 Special cell culture media

1936- and 888-MEL medium	1 mM Sodium pyruvate 1% MEM nonessential amino acids 10% FBS
A549 and CV-1 medium	10% FBS
CMC overlay medium	15 g CMC 50 mL FBS 10 mL Penicillin/Streptomycin 1 L DMEM
CTL medium	500 ml RPMI 1640 medium without phenol red 1% Penicillin/Streptomycin 2 mM Glutamine 1 mM Sodium pyruvate 10 mM Hepes 1% MEM nonessential amino acids 2%, 5% or 10% human AB serum

2.6 Human tissues

Human peripheral blood	Advanced Bioscience Resources
Human cord blood	Cryopoint

2.7 Equipment and other materials

375 Hotplate/Stirrer	VWR International
384 well plate	Thermo Scientific
Alcohol Prep Pad (medium)	Professional Disposables International, Inc
Amicon Ultra-15, PLGC Ultracel-PL Membrane, 10 kDa	EMD Millipore
Biosafety cabinet	The Baker Company
Blotting pad	VWR
Blotting Paper, 703	VWR
Cell culture plates and flsks	Corning
Cell scraper	Corning
Cell strainer (40 µl, 70 µl)	Becton Dickinson
Controlled rate freezing container	Thermo Scientific
Cotton Tipped Applicator (15 cm)	Henry Schein Inc
Cryo vials, 1.5 ml size with screw caps	Thermo Scientific
Durable Slidebox	VWR International
EDTA-coated capillary tubes	Drummond Scientific
FACS tubes with closures (5 ml)	VWR International
Falcon (15 ml, 50 ml)	Becton Dickinson
Forceps	Fine Science Tools, Roboz Surgical Instruments Co., Inc
Histosette® II Tissue processing/ embedding cassettes	Simport
HP Scanjet G3110	HP
IEC MicroCl 21 centrifuge	Thermo electron corporation
Incubator	Thermo electron corporation
Leica M165 FC	Leica Microsystems

Leica RM2125	Leica Biosystems
MACSIMAG	Miltenyi Biotec
MACSIMIX	Miltenyi Biotec
MACS Multi Stand	Miltenyi Biotec
MACS® Separation Columns	Miltenyi Biotec
MagNA Lyser	Roche Diagnostics
MagNA Lyser green beads	Roche Diagnostics
Nitrile gloves	E&K Scientific
Nitrocellulose Transfer Membrane, 0.45micrometer Nitro Bind	Fisher Scientific
Novex® XCell Sure Lock® Mini-Cell	Invitrogen
Novex® XCell II™ Blot Module	Invitrogen
NuPAGE® Novex® 12% Bis-Tris Protein Gels, 1.0 mm, 10 wells	Invitrogen
OCTO MACS	Miltenyi Biotec
Olympus IX71 microscope	Olympus
Olympus MicroFire® digital CCD camera	Olympus
Petri dishes	VWR International
Pipettes	Pipetman
Pipet Tips	VWR
PowerPac™ Universal Power Supply	Bio Rad
Pre separation filter (70 µl)	Miltenyi Biotec
Providone-Iodine Prep Pad	Professional Disposables International, Inc
PTFE coated microtome blades	DURAEDGE
RadSource RS 2000 irradiator	Rad Source Technologies
Reagent reservoir	Sigma-Aldrich®
Rocking platform	VWR
Round Preparation Tissue Bath	Boekel Scientific
Scale	Sartorius, Mettler toledo
Scalpel	Sklar Instruments
Scissors	Fine Science Tools
Slide warmer	Barnstead/ Lab-Line
Slimsette™ Biopsy cassettes	Simport

Small animal Imager	Carestream
Sonifier 450	Branson
Syringes	Becton Dickinson
Tissue embedding center	Reichert-Jung
Unifrost Microscope Slides, silane coated surfaces	Azer Scientific
Vacuum filtration system (0.2 µl)	VWR International, Sigma-Aldrich®
Vortex	Fisher Scientific, Baxter
Water bath ISOTEMP 210	Fisher Scientific

2.8 Software

FlowJo Version 10	FLOWJO
Leica Application Suite V3.7	Leica Microsystems
Microsoft Excel	Microsoft Corporation
Molecular Imaging Software "MI" 7.1 for Windows	Bruker

2.9 Viral vectors

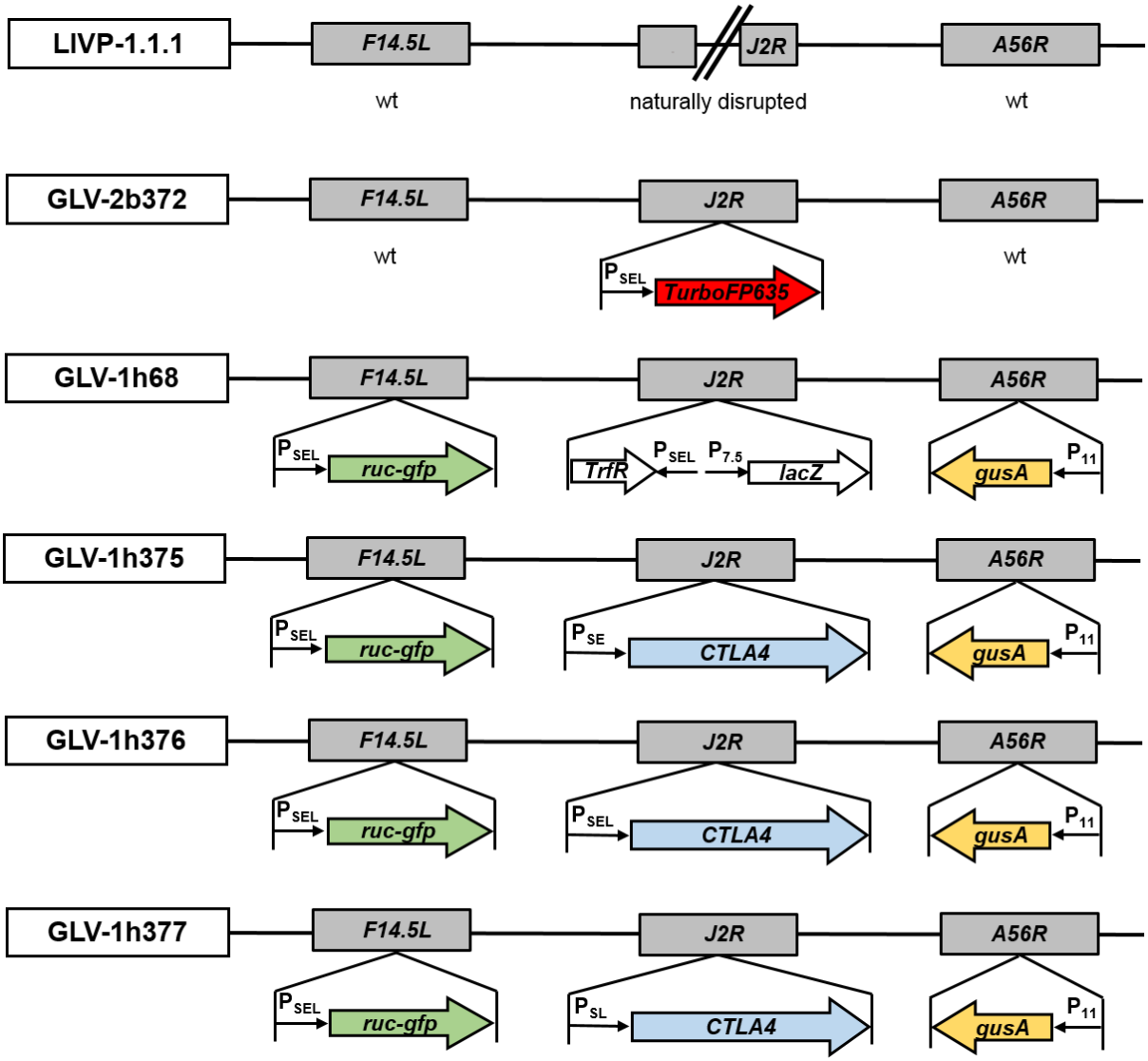

Figure 3. Schematic overview of vaccinia virus (VACV) constructs and marker genes.

All recombinant vaccinia viruses shown in Figure 3 and used in this work have been kindly provided by and engineered at Genelux Corporation in San Diego, CA, USA. LIVP-1.1.1 is an isolate from the wt LIVP with naturally disrupted *J2R* locus. GLV-2b372 was delivered from LIVP-1.1.1 by inserting the far-red fluorescent protein TurboFP635, also called Katushka, (*TurboFP635*) expression cassette at the *J2R* locus under the control of the VACV synthetic early/late promoter (P_{SEL}). The wt LIVP was also used to generate the recombinant GLV-1h68 according to Zhang *et al*. [22].

This triple mutant was constructed by insertion of *Renilla* luciferase-Aequorea green fluorescent protein fusion (*ruc-gfp*), β-galactosidase (*TrfR lacZ*) and β-glucuronidase (*gusA*) expression cassettes into the *F14.5L*, *J2R* and *A56R* loci and under the control of VACV synthetic early/late (P_{SEL}), VACV 7.5K early/late ($P_{7.5}$) and VACV late promoter (P_{11}), respectively. The human transferrin receptor encoding cDNA (*TrfR*) was inserted in the reverse orientation to its promotor (P_{SEL}), and is therefore not expressed. GLV-1h375, -1h376 and -1h377 were delivered from GLV-1h68 by replacing the *TrfR lacZ* expression cassette at the *J2R* locus with the anti-human CTLA4 FLAG-tagged single-chain antibody (*CTLA4*) expression cassette under three different VACV synthetic early (P_{SE}), early/late (P_{SEL}) and late (P_{SL}) promoters, respectively.

2.10 Experimental animals

Figure 4. NSG mouse (www.jax.org).

All *in vivo* experimental studies for the generation of the humanized mice were performed with NOD.Cg-*Prkdc*^{scid} *Il2rg*^{tm1Wjl}/SzJ (Common name: NOD scid gamma or NSG, Stock number: 005557) mice provided by The *Jackson Laboratory* (Figure 4).

The combination of the NOD/ShiLtJ background, the severe combined immune deficiency (scid) mutation and the true null interleukin-2 receptor gamma chain mutation in these mice cause multiple defects in adaptive and innate immunity [56, 65](www.jax.org). These mutants lack mature T- and B- Lymphocytes or functional NK

cells. They are characterized by absent hemolytic complement activity and defects in the differentiation and function of APCs. The NSG mice are deficient in cytokine signaling. Serum Ig in these mice in not detectable.

This comprehensive impairment of immunological functions allows efficient engraftment of human hematopoietic cells.

3 Methods

3.1 Techniques for work with mouse and human blood

3.1.1 Isolation of human peripheral blood mononuclear cells (PBMCs) from whole blood

Heparinized whole blood samples were obtained from healthy blood donors. PBMCs were isolated by standard density gradient centrifugation on Ficoll-Hypaque. The blood was diluted with PBS. Forty ml of the diluted cell suspension were carefully layered over 10 ml of Ficoll-Hypaque in a 50 ml falcon tube. After centrifugation at 400xg for 30 min at 20°C without brake, the mononuclear cell layer containing the lymphocytes, monocytes and the thrombocytes, was transferred to a new tube, washed twice with PBS and centrifuged at 1200 rpm for 7 min at RT with brake. After the second wash step cell pellet was gently suspended in an appropriate amount of CTL medium.

3.1.2 Isolation of PBMCs from humanized mouse-derived whole blood

Peripheral blood was collected from the Saphenous vein or the retroorbital sinus using EDTA-coated capillary tubes and EDTA-treated tubes. At the final day of the experiment blood was collected by cardiac puncture. Erythrocytes were lysed with 1 x RBC Lysis Buffer from eBioscience by mixing one volume of the blood with 10 volumes of the buffer. PBMCs were washed twice with FACS buffer.

3.1.3 Isolation of mononuclear cells from human cord blood

Standard density gradient centrifugation on Ficoll-Hypaque (see 3.1.1) was used to isolate the mononuclear cells from human cord blood. After second wash step, cell pellet was prepared for magnetic separation of $CD34^+$ cells by gently suspending in an appropriate amount of MACS Separation Buffer. Cell count was determined.

3.1.3.1 Magnetic separation of $CD34^+$ cells from human cord blood-derived mononuclear cells

The $CD34^+$ cells were isolated from the cord blood-derived mononuclear cells using the CD34 MicroBead Kit according to the manufacturer's instructions. The $CD34^+$ cells were magnetically labeled with CD34 MicroBeads and retained within a MACS Column, which was placed in the strong magnetic field of the MACS Separator. At the end of the magnetic separation, $CD34^+$ cells could be eluted from the column as a highly pure $CD34^+$ fraction. The purity was analyzed by flow cytometry. The hematopoietic stem and progenitor cells were washed twice in PBS++ and prepared to be stored.

3.1.3.2 Freezing of cord blood-derived $CD34^+$ cells

After magnetic separation, the $CD34^+$ cells were washed twice with PBS++ and centrifuged at 300xg for 10 min at 4°C. Then they were resuspended in cold freezing medium (10% DMSO and 90% human AB serum). Cold cryo fluid was added to the cells drop-wise over a period of 2 minutes. One ml aliquots were transferred to cryo-vials and placed in the pre-cooled to 4°C "Mr. Frosty" container, which provides -1°C/minute cooling rate. The controlled rate freezing container was placed in a -80°C freezer. Twelve hours later cells were transferred into liquid nitrogen and stored until transplantation there.

3.1.3.3 Thawing of cryopreserved cord blood-derived $CD34^+$ cells

Cells were taken from the liquid nitrogen and placed into a 37°C water bath. The vial was kept in the water until no ice remained in it. Then it was washed with 70% isopropanol and placed in a laminar flow hood. Before transferring the cells into a 15 ml-conical tube with 10 ml cool StemSpan Serum-free medium a 10 µl aliquot was taken to determine the cell count. Cell suspension was centrifuged at 200xg for 10 min at 4°C. Cell pellet was resuspended with care in 10 ml cool StemSpan Serum-free medium. Cells were placed in the refrigerator. After 20 min they were spun down again at 200xg for 10 min at 4°C. Cell pellet was resuspended with care in an appropriate amount of PBS buffer and transported on ice upon implantation.

3.2 Cell biological methods

3.2.1 Cell culture

The growth of mammalian cells under controlled conditions in the laboratory is called cell culture. Cells that are directly isolated from mammalian tissues are known as primary cell cultures. After several divisions these cells can die or become immortal and keep dividing. The cell culture offers perfect conditions for bacteria and yeast to grow. Because they are dividing much faster than the mammalian cells, they can easily overgrow and destroy the cell culture. That is why all the following cell culture techniques were carried out under sterile conditions in a laminar flow hood. All the used materials were sterilized and sprayed with 70% Isopropyl alcohol before entering the hood.

The different cell lines were grown in different cell culture media, which constituents are a variety of nutrients, vitamins, salts and buffer substances. Phenol red was frequently used as pH indicator in most of the media. Media were supplemented with 5-10% heat-inactivated fetal bovine serum (FBS) or human AB serum and kept at 4°C in the refrigerator and warmed up in a 37°C water bath before use to ensure gentle treatment of the cells.

All cell lines were grown under standard cell culture conditions at 37°C in a cell incubator, which maintained a constant thermal environment, a 5% CO_2 content of the atmosphere and 100% relative humidity inside. By working with cells they were kept out of the incubator for as little time as possible.

Cells can be grown either in suspension or adherent cultures.

3.2.1.1 Culturing of adherent growing cells

The A549 (human lung carcinoma) and the CV-1 (African green monkey kidney fibroblasts) were obtained from the American Type Culture Collection (ATCC). The 1935-MEL and 888-MEL melanoma cell lines were kindly provided by AG Szalay (Biocenter, University of Würzburg, Germany) and cultured in RPMI 1640 supplemented with 1 mM sodium pyruvate, 1 x MEM nonessential amino acids solution and 10% FBS under standard cell culture conditions (37°C, 5% CO_2 and over 95% humidity). CV-1 cells were cultured in DMEM supplemented with 10% FBS. A549 cells were cultured in RPMI 1640 instead of DMEM.

These four adherent growing cell lines were cultured in tissue-culture treated flasks and plates which allow cell adhesion and spreading. Their cell growth undergoes three distinct phases. After the culture is seeded the cells are adapting to the new media and environment and grow slow. This is the lag phase. It is followed by the logarithmic phase (log phase) where the cell number increases exponentially until the surface is occupied or some or all the nutrients in the media are depleted, indicated by color change from red to yellow, when pH-indicator media is available. When this happens the number of the cells remains constant because the proliferation is greatly reduced. This final phase is called plateau phase and it should be avoided in cell culture. Therefore before reaching 100 % confluence cells were harvested and passaged.

Every 3-4 days the used medium was aspirated and the cells were washed ones with PBS and prepare the cells to the next step, where enough trypsin-EDTA was added to cover the bottom of the culture flask to enable the detachment of the cells from the flask. The culture was placed in the 37°C incubator for 2-5 min. The cells were released from the surface by gentle tap to the dish. After that the reaction was stopped

with fresh culture medium containing 10% FBS, cells were resuspended, washed and counted. The needed cell count was transferred into a new cell culture flask and supplied with fresh medium.

3.2.1.2 Culturing of suspension cells

Most of the cells in the human bloodstream naturally live in suspension and do not attach any surface.

3.2.1.2.1 Culturing of Jurkat cells

Jurkat cells are acute human T cell leukemia and were obtained from the American Type Culture Collection (ATCC). They were cultured in RPMI 1640 supplemented with 10% FBS under standard cell culture conditions. Small volume of the cell culture was transferred into a new cell culture flask and supplied with fresh medium once a week.

3.2.1.2.1.1 Activation of Jurkat cells

Two methods for activation of Jurkat cells were used. First, Jurkat cells were activated using the T Cell Activation/Expansion Kit from Miltenyi Biotech according to the manufacturer's instructions. The MACSiBead™ Particles from this Kit are conjugated with anti-biotin antibodies on their surface. One day before the T cell activation they were loaded with biotinylated CD2, CD3 and CD28 antibodies under slow rotation for 2 hours in the MACSmix™ Tube Rotator at 4°C. These particles were used to activate resting T cells by mimicking antigen-presenting cells. Next, cells were activated with a mixture from 0.003 µg/ml phorbol 12-myristate 13-acetate (PMA), 0.3 µg/ml ionomycin, 0.5 µg/ml recombinant human B7-1 Fc Chimera and 0.5 µg/ml recombinant human B7-2 Fc Chimera. The used concentrations were obtained from previous publication [68], but were adapted for this experiment. Additionally, 1.2 µg/ml purified GLV-1h376-encoded CTLA4-blocking single-chain antibody or 25 µg/ml CTLA4-blocking monoclonal antibody, Ipilimumab (YERVOY™), were added to some of the wells in order to investigate if the activation of the Jurkat cells could be intensify by the

addition of the checkpoint inhibitor. Cells were cultured with the loaded beads for 48 hours. Successful activation was determined by low cytometry.

3.2.1.2.2 Culturing of human PBMCs and mouse-derived splenocytes

Freshly isolated human PBMCs and humanized mouse-derived splenocytes were cultured up to 48 hours in CTL media under standard cell culture conditions.

3.2.2 Cell counting

For most in vitro experiments in cell culture the number of cells per unit volume of a suspension needs to be determined. Cells were counted using a counting chamber called a hemocytometer (Figure 5). It is a slide with a grid of squares of different sizes etched into the glass.

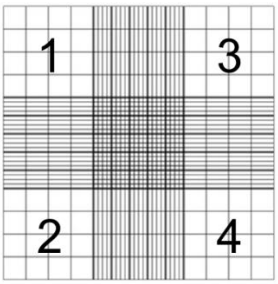

Figure 5. Hemocytometer

Prior to counting a cover glass was placed over the counting surface of the hemocytometer. 10 µl of the cell suspension were mixed with 10 µl trypan blue and 10 µl of this mix was loaded between the chamber and the cover glass to cover the counting surface. The chamber was placed under an inverse bright field microscope. Cells that were on the top and right lines of a grid square were not counted. The number of cells counted in 4 big squares, each of them consisting of 16 small squares, was divided by 4 and multiplied by the dilution factor of suspension (2) and then multiplied by 10^4 in order to determine the total number of cells per ml of cell suspension. The cell count was calculated using the following formula:

$$\frac{\text{Cell number in 4 big squares}}{4} \times \text{Dilution factor} \times 10^4 = \frac{\text{Cell count}}{\text{ml}}$$

3.3 Virological methods

3.3.1 Vaccinia virus infection of cells

All the vaccinia virus strains were stored at -80°C. Prior to infection they were thawed and then kept on ice. To prevent the formation of virus aggregates the stocks were sonicated for 3 x 30 sec at 4°C prior to infection.

The cell count per infection was determined through utilizing the hemocytometer. The required virus amount was calculated using the following formula:

$$\frac{\text{MOI} \times \text{Cell count}}{\text{Virus titer}} = \text{Virus amount}$$

The concentration of each virus used for the infections is defined as pfu (Plaque forming units) or the virus particles capable to form plaques per milliliter. MOI (Multiplicity of infection) is the ratio of infectious virus particles to cells. For example MOI of 0.1 means 0.1 virus particles per cell or 1 plaque forming units per 10 cells. The virus amount needed per infection was calculated this way. The infection medium was prepared by diluting the required volume of virus stock in medium supplemented with 1% antibiotic-antimycotic solution (10,000 units/ml penicillin G, 10,000 µg/ml streptomycin, 25 µg/ml amphotericin B) and 2% FBS.

3.3.1.1 Infection of adherent growing tumor cells

Cells were seeded onto 24-well plates one day before infection. Prior to infection they were washed once with PBS. Then 200 µl of infection medium containing the desired amount of plaque forming units per infection were added to each well. Plates were incubated for 1h at 37°C with gentle agitation every 20 min. The infection medium was then replaced with fresh growth medium without phenol red, supplemented with 1% antibiotic-antimycotic solution.

3.3.2 Viral replication assay

After infection the cells were grown for 24, 48, 72, 96 or 120 hours. At each of these time points supernatants and cells from three wells, were harvested separately.

Supernatant was removed and stored at -80°C. Fresh medium (1 ml) was added to the infected cells which were then frozen at -80°C. After thawing, all cell fragments were mechanically removed from the plates by pipetting.

3.3.3 Plaque assay

The viral titer in the samples from the replication assay was determined by standard plaque assay. The plaque assay is a method to determine the concentration of viruses in a suspension. All the samples underwent three freeze and thaw cycles and were sonicated three times for 30 sec. Tenfold dilutions of the samples in DMEM containing 2% FBS were prepared. As host cells for the infections were used CV-1 cells. They were grown in 24-well plates until they reached 100% confluence. The medium of the CV-1 cells was aspirated prior to infection and 200 µl from the virus containing samples were placed into each well. All dilutions were plated in duplicate to improve reliability of the method. Cells were infected for 1 hour at 37°C. Plates were shaken every 20 min. After this incubation time cells were covered with 1 ml CMC (carboxymethyl cellulose) which prevent further virus spreading. Cells were incubated for 48 hours at 37°C. During this incubation period the viruses replicate in the infected cells, these cells are lysed and virus particles spread into the neighboring cells generating plaques. After two days 500 µl of crystal violet were added to each well. Cells were stained overnight. Plates were washed from the staining solution. Plaques in wells containing between 12 and 100 plaques were counted. The virus titer was calculated in plaque pfu per milliliter using the following formula:

$$\text{Plaque forming units} \times \text{Dilution factor} \times 5 = \text{Viral titer [pfu/ml]}$$

3.3.4 MTT assay

MTT assay is a colorimetric assay used to assess the amount of viable tumor cells after infection with vaccinia virus in cell cultures. Tumor cells were seeded onto 24-well plates, cultured for 18-24 h and infected in triplicates with the viral constructs at an MOI of 0.005, 0.1, and 1 or mock-infected with infection medium alone. At 24, 48, 72 and 96 hpi shortly before performing the assay, the yellow tetrazolium salt MTT (3-(4,5-Dimethyl-2-thiazolyl)-2,5-diphenyl-2H-tetrazolium bromide) was solubilized in RPMI medium 1640 without phenol red at a final concentration of 2.5 mg/ml, resulting in light-sensitive yellowish solution. Culture medium supernatant of the infected and untreated control cells was removed and replaced with 250 µl of the MTT solution under aseptic conditions in a laminar flow hood. Plates were placed back in the incubator for 2 hours. Yellow MTT was reduced by metabolically active cells to intracellular insoluble purple formazan product [69]. MTT solution was then removed and plates were stored at -80°C. After collecting the plates from all time points they were thawed and 500 µl of 1 N HCL diluted in isopropanol were added to all control and test wells to dissolve the formazan crystals. 200 µl from each sample were transferred to a 96-well plate. Absorbance was measured at 570 nm in a Spectra Max M5 microplate reader (Molecular devices, Sunnyvale, CA). Decreasing quantities of formazan due to the death of the infected tumor cells over the time led to decrease in the absorbance. Uninfected cells were considered as 100% viable. Cytotoxicity was calculated in Microsoft Excel using the following formula:

$$\text{Percentage of viable cells} = \frac{\text{OD (infected cells)}}{\text{OD (control cells)}} \times 100$$

3.4 Protein analytical methods

3.4.1 Protein quantitation

Protein concentration was assayed using the colorimetric DC Protein Assay Kit according to the manufacturer's instructions. Serial dilutions of 1 mg/ml, 0.8 mg/ml, 0.6 mg/ml, 0.4 mg/ml, 0.2 mg/ml and 0 mg/ml of standard Bovine ɣ-globulin (standard

l) for establishing the standards curve were prepared for each measurement. 20 µl of Reagent S were added to 1 ml of Reagent A to create Reagent A'. 5 µl of standard and samples were dispensed into the wells of a 96-well clear flat bottom plate. 25 µl of Reagent A' and then 200 µl of Reagent B were added to the 5 µl of sample per well. Samples were incubated in the dark at room temperature for 15 min. Absorbance, also called optical density (OD), was measured at 750 nm at room temperature using a Spectra Max M5 plate reader. Protein concentrations of the samples were calculated using the standard curve.

3.4.2 Gel electrophoresis

Protein containing test samples were placed in Eppendorf tubes. For cell culture supernatants, after adding of 2.5 µl LDS Sample Buffer (4X) to each tube sample volume was adjusted to 10 µl with deionized water. Samples were heated at 70°C for 10 min and then immediately cooled down on ice. For cell lysates, Laemmli sample buffer was added to the samples according to the manufacturer's instructions. Samples were heated at 90°C for 10 min and then immediately cooled down on ice.

A new NuPAGE® Novex® Pre-Cast Gel cassette was placed into the Xcell SureLock™ Mini-Cell gel running tank. The inner and outer buffer chambers were filled with 1x MOPS SDS Running Buffer. After rinsing the gel wells each test sample and the protein standard were carefully loaded into a separated wells.

The voltage was set at 80 V constant and the gel was run until the migration front reached the bottom of the gel cassette. After turning off the power it was immediately proceeded to Coomassie staining or Western blot.

3.4.3 Coomassie stain

After electrophoresis gel was placed in a staining container with Coomassie staining solution on a shaker. After one hour the staining solution was discarded and replaced with Coomassie destaining solution. Gel was destained until the excess dye has been removed leaving blue colored protein bands but a clear gel.

Gel was scanned using a HP Scanjet G3110 scanner. Pictures were processed using the HP Scanjet G3110 Solution Center Software.

3.4.4 Western blot

A wet transfer using the Novex® XCell II™ Blot Module was performed (Figure 6). Four sponge pads, 2 blotting filters and a nitrocellulose membrane, cut to the dimensions of the gel, were soaked in 1X NuPAGE® Transfer Buffer containing 10% methanol. The gel and the membrane were sandwiched between the other pre-soaked components in the following order shown in Figure 6 over the anode core.

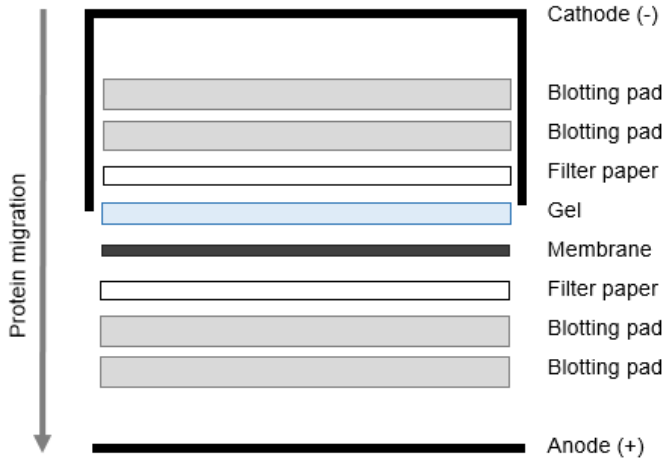

Figure 6. Western blot assembly.

All air bubbles trapped between the gel, filters and pads were carefully removed by rolling a plastic pipette over the assembly. After closing with the cathode core the Blot Module was placed in the Novex® XCell Sure Lock® Mini-Cell. The blot module was filled with the transfer buffer and the outer buffer chamber with deionized water.

Transfer was performed at a constant voltage of 30 V for 1 hour. After blotting, all unbound membrane sites were blocked with 5% non-fat milk in PBS 0.05% Tween 20 blocking buffer on a shaker at room temperature. After 1 hour, blocking buffer was removed and membrane was placed in diluted primary antibody with gentle agitation overnight at 4°C. Next morning membrane was washed with 20 ml of PBS 0.05%

Tween 20 to remove excessive antibody and incubated in diluted HRP-conjugated secondary antibody with gentle agitation for 1 hour at room temperature. After washing with 20 ml of PBS 0.05% Tween 20 it was proceeded with detection using the Opti-4NC™ Substrate Kit and following the manufacturer's instructions.

3.4.5 Purification of flag-tagged single-chain antibody

CV-1 cells were seeded in T-225 flasks and cultured at 37°C overnight. Growth medium was replaced by 15 ml DMEM containing GLV-1h376 at an MOI of 2 for 24 h. After removing the viral particles using a 0.1 µl syringe filter the CTLA4 scAb-containing supernatant was concentrated by centrifugation with Amicon Ultra-15 columns (Millipore). FLAG-tagged single-chain antibody was purified from the concentrate using the FLAG® Immunoprecipitation Kit. The correct molecular mass of the purified antibody was verified on Coomassie stained gel. Its concentration was measured using the DC™ Protein Assay Kit.

3.4.6 ELISA

The presence of CTLA4 scAb in cell culture and mouse tumor and serum samples was tested by ELISA assays. Ninety-six-well plates were pre-coated with recombinant human CTLA4 Fc Chimera (R&D Systems), blocked and incubated for 1 h at room temperature with the test samples and standard dilutions (500 ng/ml, 250 ng/ml, 125 ng/ml, 62.5 ng/ml, 31.25 ng/ml, 15.625 ng/ml, 7.8125 ng/ml and 0 ng/ml), followed by a primary rabbit anti-DDDDK antibody and a secondary horseradish peroxidase-labeled anti-rabbit IgG antibody. Wells were washed with PBS/0.05% Tween after each incubation step. Color was developed using 3,3′,5,5′-tetramethylbenzidine and reaction was stopped by adding 2 N HCl. Absorbance was measured at 450 nm in a Spectra Max M5 microplate reader.

3.5 Mouse experiments

Eleven to fifteen days pregnant NOD.Cg-Prkdcscid Il2rgtm1Wjl/SzJ (NSG) mice were purchased at The Jackson Laboratory and allowed to acclimatize for 3 to 6 days before giving birth under pathogen-free conditions in HEPA-filtered, individually ventilated disposable cages (Innovive) with irradiated food and pre-bottled acidified water (Innovive) in the animal facilities of Explora Biolabs at the San Diego Science Center. Newborn pups were irradiated with 0.8 Gy using a RadSource RS 2000 irradiator and transplanted into the liver within 3 h with 1.8 x 10^5 - 3 x 10^5 human $CD34^+$ cells, isolated from umbilical cord blood. The peripheral blood collected from $CD34^+$ cell engrafted animals was routinely evaluated for human hematopoietic engraftment starting at 6 week posttransplantation (p.t.). Nine to ten weeks p.t. mice were implanted subcutaneously (s.c.) with 5 x 10^6 A549 cells into the right hind leg. When tumors reached a size of 250 - 350 mm^3, VACV was administered systemically by retro-orbital (r.o.) inoculation of 6 x 10^6 plaque forming units (pfu) in 100 µl PBS at day 0. Mice were observed daily for any adverse effects, including signs of morbidity or virus related toxicity. More blood and different organs were collected at the end of each experiment, when animals were sacrificed.

All animal studies were approved by and performed in strict accordance with the guidelines of the Institutional Animal Care and Use Committee of Explora Biolabs (IACUC), San Diego Science Center (Approval number: EB12-018). All efforts were made to minimize stress and suffering.

3.5.1 Preparation of single-cell suspensions and mononuclear cell isolations

Humanized mouse-derived PBMCs were isolated as described in (3.1.2). Spleens, livers and tumors were excised, weighted, inspected and prepared for flow cytometry analyses. Spleen tissue was homogenized between the frosted ends of microscopic slides, passed 3 x through an 18 G needle and filtered through a 70 µl cell strainer. RBC were lysed with 1 x RBC Lysis Buffer from eBioscience by mixing one volume of the blood with 10 volumes of the buffer. Tumor and liver tissue was cut into small

pieces and placed in RPMI 1640 supplemented with 0.5 mg/ml Collagenase D, 0.2 mg/ml hyaluronidase type V, 0.0015 mg/ml DNAse I type IV and 1% FBS for 1 h at 37°C and pipetted up and down every 20 min. Tumor suspension was then filtered through a 70 µl cell strainer and washed with FACS buffer. The mononuclear cells from the filtered liver suspension were isolated by Ficoll-Hypaque gradient separation and washed in FACS buffer. Human reconstitution levels were evaluated by flow cytometry.

3.5.2 Tumor homogenates

Tumors were excised, weighted and gently disrupted into small pieces on ice and then homogenized using a MagNA Lyser at 6000 rpm for 30 sec, followed by three subsequent freeze (-80°C)/thaw (37°C) cycles. Viral titer, β-glucuronidase and CTLA4 scAb concentrations were determined by standard plaque assay, β-glucuronidase assay and ELISA, respectively.

3.5.3 Activation of splenocytes

Single-cell suspension of spleens from A549-tumor-bearing humanized mice were prepared and the suspension from each mouse spleen was distributed into three groups. The T cells from group 1 were activated using a human T Cell Activation/ Expansion Kit according to the manufacturer's instructions. Next, to assess the ability of the human immune cells to recognize and be activated by the A549 cells *ex vivo*, tumor cells were irradiated with 30 Gy using a Cesium-137 irradiator at the Moores UCSD Cancer Center (San Diego, CA, USA) and added to the spleen suspension of group 2 (tumor-to-immune cell ratio 1:4). Untreated cells from group 3 were used as a control. All three groups were cultured in CTL medium under standard cell culture conditions. Forty-eight hours later samples from all three groups were stained for human immune cell surface antigens, CD45, CD3, CD4, CD8 and CD25, and intracellular human IFN-ɣ. Interferon-ɣ was stained using a BD Cytofix/Cytoperm™Plus Fixation/Permeabilization Kit with BD GolgiStop™ protein transport inhibitor containing monensin, following the manufacturer's instructions, and

an anti-human IFN-ɣ-PerCP-Cy5.5 antibody. The untreated cells from control group 3 were used to set the location of gates in the following flow cytometry analysis.

3.5.4 Immunohistochemistry: Preparation of paraffin sections

Humanized and control mice were euthanized by CO_2 asphyxiation. Tissues for histopathologic examination were fixed, dehydrated and embedded in paraffin.

3.5.4.1 Fixation

Tissues were cut to a size of 10 x 10 x 3 mm or smaller, placed into embedding cassettes and fixed in 10% neutral buffered formalin overnight. Any remaining fixative is washed out by placing the blocks in 0.9% NaCl for 1 hour on shaker. It was processed to dehydration.

3.5.4.2 Dehydration

To dehydrate tissues were passed through a series of increasing alcohol concentrations. The embedding cassettes were transferred sequentially to 30% dehydration alcohol in 0.9% NaCl, 50% dehydration alcohol in 0.9% NaCl, 70% dehydration alcohol in water, 80% dehydration alcohol in water, 90% dehydration alcohol in water, and 100% ethanol for 1 hour each, at room temperature and on shaker. The tissues were then placed in a second 100% ethanol solution to ensure that all water is removed and stored in the fridge before embedding.

3.5.4.3 Embedding

Tissues were transferred sequentially to fresh 100% ethanol, ethanol/xylene (1:1) and xylene at room temperature and on shaker and then to xylene/wax (1:1) and wax (three times) at 58°C in the incubator for 1 hour each step. Subsequent to paraffin infiltration

tissues were placed into embedding molds. Molds were covered with the embedding cassette and filled with paraffin. After cooling paraffin blocks were removed from the molds and subjected to sectioning.

3.5.4.4 Sectioning

Paraffin blocks were sectioned at 5 µm. Sections were placed in water bath (45°C), mounted on microscope slides and allowed to dry overnight at room temperature.

3.5.4.5 Immunohistochemical staining of formalin-fixed paraffin-embedded tissues

Immunohistochemical staining was performed using the VETASTAIN Elite ABC Kit according to the manufacturer's instruction. Sections were rehydrated and citrate buffer was used for antigen retrieval. Tissue was blocked with normal goat serum, peroxidase treated, incubated with primary rabbit-polyclonal IgG to vaccinia virus, biotinylated goat anti-rabbit IgG secondary antibody provided with the kit and then with VECTASTAIN Elite ABC Reagent. Suitable staining was developed with ImmPACT DAB Peroxidase Substrate. After counterstaining with hematoxylin, section was dehydrated. A coverslip was carefully lowered onto the drop of mounting medium.

3.6 Imaging techniques

3.6.1 Noninvasive imaging

Noninvasive fluorescence *in vivo* imaging of the tumor growth in the mice were performed on the Carestream small animal imager. Tumor-bearing mice infected with GLV-2b372 were imaged for TurboFP635 (Katushka) expression at 3, 8 and 15 days post infection (dpi). A 2% isoflurane source was plugged into the machine and kept the animals anesthetized during the whole imaging procedure. The obtained images

and results in relative fluorescent units (RFU) were processed using the Molecular Imaging Software "MI" 7.1 for Windows and Microsoft Excel.

3.6.2 Microscopy

3.6.2.1 Fluorescence microscopy

The fluorescence microscopy is an essential tool in biology and the biomedical science, allowing monitoring of different physiological and pathological processes in tissues and cultured cells. The cells or the cell structures of interest can be visualized very precisely using different fluorophores. When exposed to certain wavelengths, they can be excited to emit light at a longer wavelength than the light source. Some cells, biological structures or molecules can naturally emit light when they have absorbed specific wavelengths. Example for such proteins are the *green fluorescent protein* (GFP) [70], originally isolated from the jellyfish *Aequorea victoria*, and the far-red fluorescent protein TurboFP635 [71], which is a far-red mutant of the red fluorescent protein from the sea anemone *Entacmaea quadricolor*. *Renilla* luciferase-GFP protein fusion [22] and TurboFP635 expression cassettes were inserted into the genomes of the recombinant vaccinia virus strains GLV-1h68 and GLV-2b372, respectively, and used as reporters to monitor the ability of the virus to infect tumor cells.

GFP and TurboFP635 expression in A549 cell cultures infected with oncolytic VACV GLV-1h68 and GLV-2b372 at an MOI of 0.1 was imaged at 24, 48, 72, 96 and 120 hpi using an inverted Olympus IX71 microscope with an Olympus MicroFire® digital CCD camera and a PictureFrame™ software.

The expression of the GFP protein in GLV-1h68-infected A549 tumors was imaged *ex vivo* using a Leica M165 FC Fluorescence Stereomicroscope and a Leica Application Suite V3.7.

3.6.2.2 Light microscopy

Light microscopic images were obtained with an inverted Olympus IX71 microscope using visual light and an Olympus MicroFire® digital CCD camera and a PictureFrame™ software.

3.6.3 Flow cytometry

Flow cytometry or fluorescence activated cell sorting (FACS) is a routine procedure used in many scientific laboratories or in the clinic to analyze cells based on their physical and molecular properties, including cell size and granularity. Cells are often labeled with fluorescent antibodies against different cell surface or intracellular markers or analyzed based on their expression of fluorescent proteins like GFP. The cells from the samples are hydrodynamically focused and forced into the center of stream of liquid before intercepting a light source. Monochromatic lasers are usually used as a light source. When activating the light source, the cells scatter the light according to their physical and chemical characteristics, and the fluorophore-absorbed light excites to a higher energy level and then emits energy as photons. Scattered and emitted light are then analyzed by detectors, providing information about the size and the molecular characteristics of each individual cell.

Activated human T cells and mouse reconstitution with human immune cells in different organs were assessed by multicolor flow cytometry. Samples were stained using the monoclonal antibodies (mAb). To determine the viability of cells, samples were incubated with LIVE/DEAD® Fixable Aqua Dead Cell Stain Kit according to the manufacturer's instructions. Samples were acquired with a FACSCanto flow cytometer (BD Pharmingen, CA) at the VA hospital Flow Cytometry Core facility (San Diego, CA, USA) using established protocols. Data analysis was performed using a FlowJo Version 10 software. Dead cells were excluded from the analysis by gating out low forward scatter and brightly aqua fluorescent reactive dye-retaining cells.

3.6.4 Glucuronidase assay

Beta-glucuronidase assay is a fluorescence based detection method. To detect β-glucuronidase expression in cell culture and mouse samples, 5 µl of test sample or standard solution with a known β-glucuronidase concentration were added to black 384-well optical bottom plates. After addition of 75 µl of PBS supplemented with 2% FBS and 0.2 µl of 36.5 mM 6-Chloro-4-methylumbelliferyl β-D-glucuronide (CMUG) stock solution in dimethyl sulfoxide, plates were incubated for 1h at 37°C. Fluorescence was measured at excitation and emission wavelengths of 365 and 455 nm in a Spectra Max M5 microplate reader. Results were presented in relative fluorescent units (RFU). Serial dilutions of standard β-glucuronidase for establishing the standards curve were prepared for each measurement. Because all sample signals have to be within the linear range of the standard curve some of the samples were diluted.

3.7 Statistical analysis

Statistical analysis were performed in Microsoft Excel. Mean values ± standard errors were presented. Statistical differences between two groups were calculated with Student's t-test. P-values <0.05 were considered statistically significant. Statistical significance is indicated by asterisks as follows: * ($p<0.05$), ** ($p<0.01$), *** ($p<0.001$), **** ($p<0.0001$).

4 Results

4.1 Establishment of humanized subcutaneous tumor-bearing NSG mouse model and treatment with LIVP-1.1.1 and GLV-2b372 vaccinia virus strains

To evaluate the vaccinia virus potential to overcome the localized tumor-mediated immune suppression and to increase antitumor immunity by attracting tumor-infiltrating effector lymphocytes, LIVP-1.1.1 VACV was systemically delivered into A549 tumor-bearing humanized NSG mice. LIVP-1.1.1 is an attenuated isolate from the wt LIVP with naturally disrupted *J2R* locus and allowed investigation of the VACV effect on the immune system without addition of any potentially immunogenic transgenes' products or any fluorescent imaging gene products that could interfere with the subsequent flow cytometry analysis. Successful *in vivo* infection of the tumors after systemic administration of the virus as well as lack of "off-target" infectivity were assessed by treating a small group of mice with GLV-2b372. GLV-2b372 was delivered from LIVP-1.1.1 by inserting the TurboFP635 expression cassette into the *J2R* locus, so it is practically the same virus but provide monitoring option. Before their application in A549 tumor-bearing animals, the ability of both viruses to infect and replicate in as well as their potential to kill A549 cancer cells were investigated in cell culture.

4.1.1 Comparison of GLV-2b372 and LIVP-1.1.1 replication efficiencies

The replication capability of the recombinant GLV-2b372 virus and the parental LIVP-1.1.1 strain were evaluated and compared in A549 cell cultures (Figure 7). A549 cells were infected with either one of the viruses at an MOI of 0.005 or 0.1. Supernatants and cells of infected cultures were collected separately and in triplicates at 24, 48, 72, 96 and 120 hpi. Viral titers were determined in triplicates by standard plaque assay in CV-1 cell monolayers.

Figure 7 shows that both vaccinia virus strains could efficiently replicate in A549 cells in culture. Viral titers were plotted against the course of time. For both tested MOIs the titer values from the cell lysates were considerably higher compared to the supernatants. Viral titers from MOI 0.005 infected cultures (Figure 7, left panel) showed a slight but constant increase during the whole course of the replication assay and no plateau was reached. Highest titers found 120 hpi in supernatant and cell lysate samples were 1.12 x 10^3 and 2.27 x 10^5 pfu/ml, for GLV-2b372, and 1.08 x 10^3 and 2.08 x 10^5 pfu/ml, for LIVP-1.1.1, respectively. Constant viral titer increase was observed also for the supernatants of the cell cultures infected at an MOI of 0.1 (Figure 7, right panel). Highest titers found 120 hpi were 1.97 x 10^4 and 1.47 x 10^4 pfu/ml for GLV-1h372 and LIVP-1.1.1, respectively. Viral loads in GLV-2b372 infected cell lysates peaked 24 hours after infection and reached a plateau but those in the LIVP-1.1.1 infected lysates were slightly increasing through the whole time of the infection. However viral titers for both viruses were close at each time point. Viral loads measured 120 hpi were 6.50 x 10^5 and 6.33 x 10^5 pfu/ml for GLV-2b372 and LIVP-1.1.1, respectively.

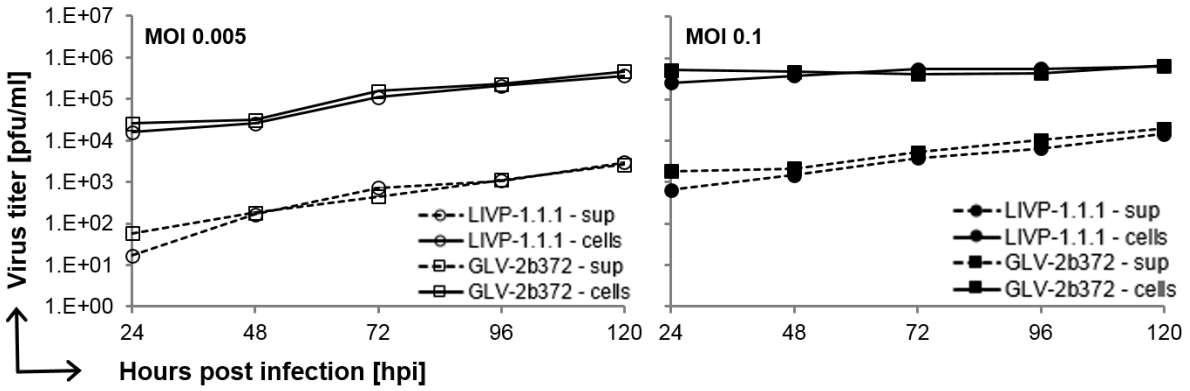

Figure 7. Virus replication assay. Replication efficiency of LIVP-1.1.1 (circles) and GLV-1h2b372 (squares) in A549 cancer cell cultures infected at an MOI of 0.005 (left panel) or 0.1 (right panel). Supernatants and cells of infected cultures were collected separately and in triplicates at 24, 48, 72, 96 and 120 hours post infection (hpi). Viral titers were determined in triplicates as plaque forming units (pfu) per milliliter of medium by standard plaque assay. Mean values (n=3) and standard errors are plotted.

GLV-1h2b372 replicated in the cancer cell line in a dose- and time-dependent fashion and in a similar manner to the parental LIVP-1.1.1, reaching comparable viral titers at each time point. The insertion of the TurboFP635 expression cassette into the GLV-2b372 genome did not alter the replication capability of the virus.

4.1.2 LIVP-1.1.1- and GLV-2b372-mediated A549 cytotoxicity

To evaluate whether the TurboFP635 expression affects the cytotoxic potential of GLV-2b372 on A549 cells in comparison to the parental LIVP-1.1.1, cells were infected with either one of the viruses at an MOI of 0.005 or 0.1 and MTT assay was performed (Figure 8). Tumor cell viability was monitored in triplicates at 0, 24, 48, 72, 96 and 120 hpi. Viable cells were calculated as percentage from the mock-infected control cells for each time point, which were considered to be 100% viable.

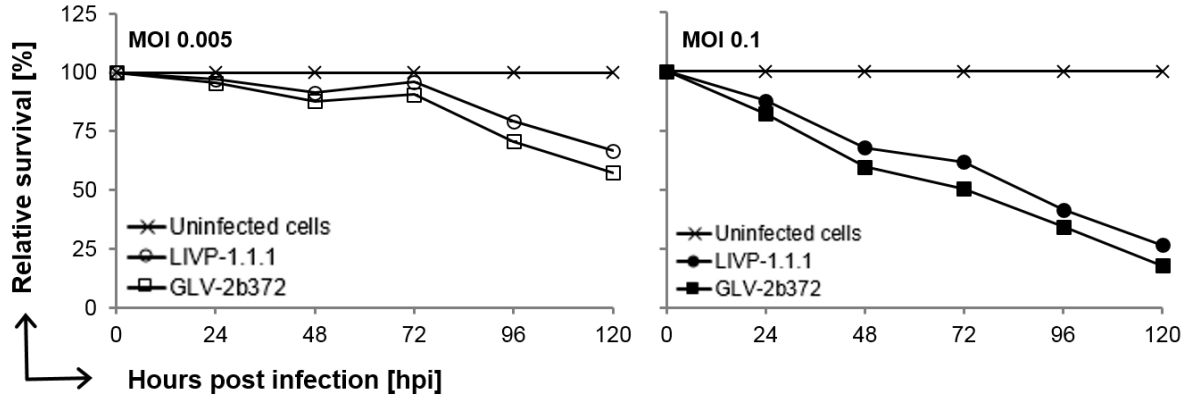

Figure 8. Cytotoxicity assay. Viability of A549 cells infected with LIVP-1.1.1 (circles) and GLV-1h2b372 (squares) at an MOI of 0.005 (left panel) or 0.1 (right panel) was monitored in triplicates over 120 hours using an MTT assay. Viable cells were calculated as percentage from the mock-infected control cells for each time point, which were considered to be 100% viable. Mean values (n=3) and standard errors are plotted.

Both viruses showed efficient cytotoxicity on A549 cancer cells. GLV-1h2b372 virus killed the cancer cell line in a time- and MOI-dependent fashion and in a similar manner

to the parental LIVP-1.1.1. Its cytotoxic effect followed the same path as the parental virus but was able to lyse slightly (≤ 10%) more tumor cells than LIVP-1.1.1 by both tested MOIs. At 120 hpi 57.35 ± 0.23% and 66.63 ± 0.13% of the cells infected at an MOI of 0.005 with GLV-2b372 and LIVP-1.1.1, respectively, were still viable (Figure 8, left panel). Much stronger cytotoxic effect was observed with an MOI of 0.1 (Figure 8, right panel). Only 17.83 ± 0.03% and 26.54 ± 0.06% of the cells infected with GLV-2b372 and LIVP-1.1.1, respectively, survived 120 hours after the infection.

With the performed MTT assay was demonstrated that the TurboFP635 expression did not alter the oncolytic efficacy of GLV-2b372, suggesting that this virus has the potential to treat A549 tumors in mouse models and could be used instead of LIVP-1.1.1, when *in vivo* monitoring of the infection is desired.

4.1.3 GLV-2b372-mediated TurboFP635 protein expression in A549 cells

To evaluate the expression of the reporter protein TurboFP635 in cell culture, A549 human lung carcinoma cells were infected with GLV-2b372 at an MOI of 0.005 or 0.1 (Figure 9). TurboFP635 expression was assessed daily at 24, 48, 72, 96 and 120 hpi by fluorescence microscopy.

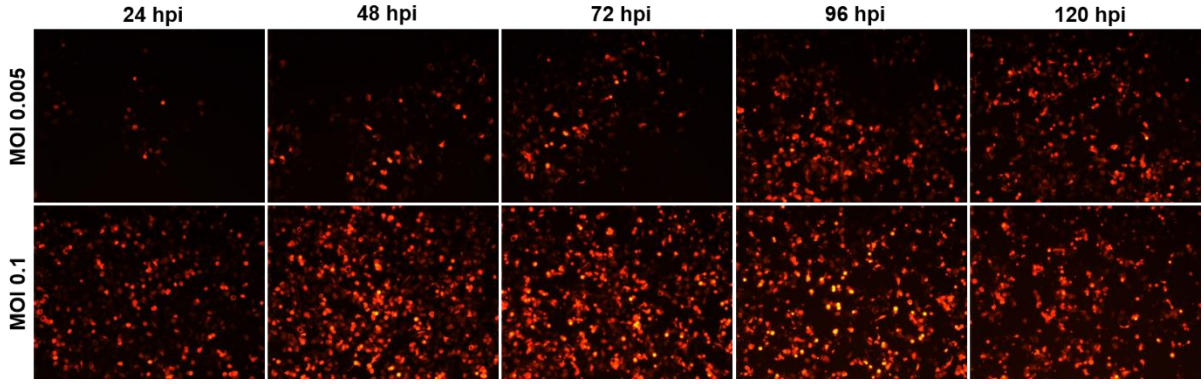

Figure 9. GLV-2b372-mediated red fluorescent TurboFP635 (Katushka) protein expression. A549 lung carcinoma cell cultures were infected with GLV-2b372 vaccinia virus at an MOI of 0.005 and 0.1 and monitored over 120 hours. TurboFP635 expression in infected cell cultures was visualized by direct fluorescent microscopy and increased in virus-dose- and time-dependent fashion. The use of a higher MOI resulted in faster initial signal increase but subsequent decrease due to virus-mediated cancer cell killing. All pictures were taken at the same magnification.

Infection with an MOI of 0.005 showed increasing marker gene expression during the whole course of the assay with highest fluorescent signal obtained at 120 hpi (Figure 9, upper row). In contrast, TurboFP635 expression in cells infected at an MOI of 0.1 increased over the first 72 hours after the infection followed by a decline due to viral cytotoxicity and subsequent tumor cell death (Figure 9, lower row).

TurboFP635 expression is time- and dose-dependent and correlate well with the virus replication and cytotoxicity data obtained in 4.1.1 and 4.1.2.

4.1.4 Macroscopic analyses of humanized A549 tumor-bearing NSG mice-derived tumors and spleens

Subcutaneous implantation of 5 x 10^6 human lung carcinoma A549 cells into the right hind leg of NSG mice 10 to 13 weeks post humanization resulted in a successful A549 tumor growth in all implanted animals during the course of this doctoral work. Majority of the tumors in non-humanized control NSG mice as well as in humanized NSG mice that have not been treated with vaccinia virus (Figure 10A (a, b and c)) showed large fluid filled necrotic areas, many blood vessels and large hemorrhagic regions. In contrast, VACV infected tumors (Figure 10A (d and e)) showed more compact structure, with less blood vessels and virtually no hemorrhagic areas. Representative pictures of tumors from one of the mouse studies are shown in Figure 10A.

Another interesting observation was the spleen size dependence on humanization and virus administration. Generally, humanized NSG mice (Figure 10B (g)) had larger spleens compared to non-humanized control mice (Figure 10B (f)). Compared to humanized mouse-derived spleens, enlarged spleens were observed in many of the VACV-injected humanized animals (Figure 10B (h)), suggesting a probable vaccinia virus-induced splenomegaly. Figure 10B is showing representative pictures of spleens from one of the mouse studies.

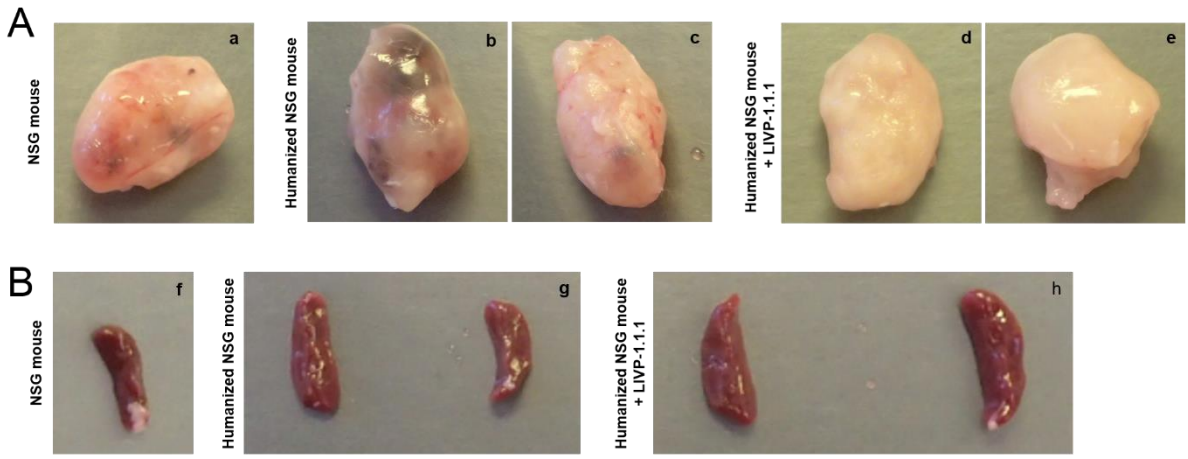

Figure 10. Macroscopic analyses of tumors and spleens. (A) Tumors were excited from A549 tumor-bearing non-humanized control NSG mouse (a) or humanized NSG mice 13 weeks post humanization and 5 weeks after tumor implantation (b, c, d and e) and 8 days after virus administration (d and e) to virus-treated mouse group. (B) Spleens were excited from non-humanized control (f) or humanized A549 tumor-bearing NSG mice 13 weeks post humanization (g and h) and 8 days after virus administration (h) to virus-treated mouse group.

4.1.5 Visualization of virus-mediated TurboFP635 expression in tumors

Successful colonization of subcutaneous A549 tumors with TurboFP635-encoding GLV-2b372 virus was visualized using the Carestream small animal imager (Figure 11). A549 tumor-bearing humanized NSG mice injected r.o. with 6 x 10^6 pfu of GLV-2b372 were imaged for TurboFP635 expression at 3 (n=4), 8 (n=3) and 15 (n=3) days post infection (dpi). Figure 11A shows images obtained from the tumor area of two representative mice. All virus-infected tumors were expressing GFP. No fluorescent signal was observed in the PBS treated control tumors (data not shown). The TurboFP635 signal was measured in RFU. Relative tumor signal change is shown in Figure 11B. Initial 22-fold increase of fluorescent signal during the first 8 days of the infection and consequent decrease in TurboFP635 expression by day 15 were observed.

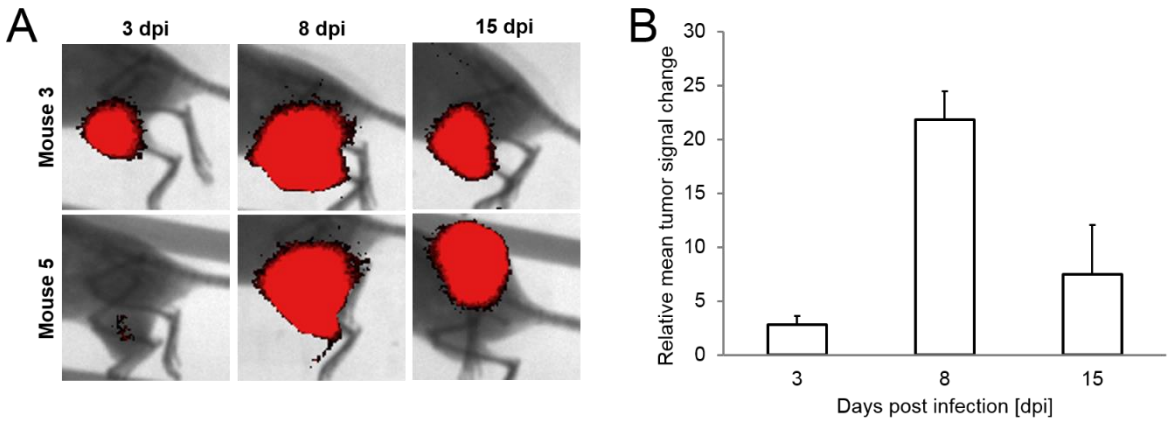

Figure 11. GLV-2b372-mediated red fluorescent TurboFP635 protein expression in tumors. A549 tumor-bearing humanized NSG mice were injected r.o. with 6 x 10^6 viral particles of GLV-2b372. Animals were imaged for TurboFP635 expression at 3 (n=4), 8 (n=3) and 15 (n=3) days post infection (dpi). (A) The images show the tumor area of two representative mice. (B) The TurboFP635 signal from the GLV-2b372 colonized A549 tumors was measured in RFU. Relative tumor signal change was monitored over 15 dpi. Mean values and standard errors are plotted.

4.1.6 Immunohistochemical analysis of vaccinia virus-infected tumors

Immunohistochemical staining for the detection of vaccinia virus in tumor tissues was performed to demonstrate the successful colonization of subcutaneous A549 tumors with LIVP-1.1.1 (Figure 12A) or GLV-2b372 (Figure 12B) and to investigate the progression of the infection and the corresponding histopathological changes in tumors. Tumors from A549 tumor-bearing humanized NSG mice injected r.o. with 6 x 10^6 pfu of LIVP-1.1.1 or GLV-2b372 were excited at 3, 8 and 15 dpi. Prepared sections were stained with vaccinia virus antibody and pictures from representative mice are shown in Figure 12.

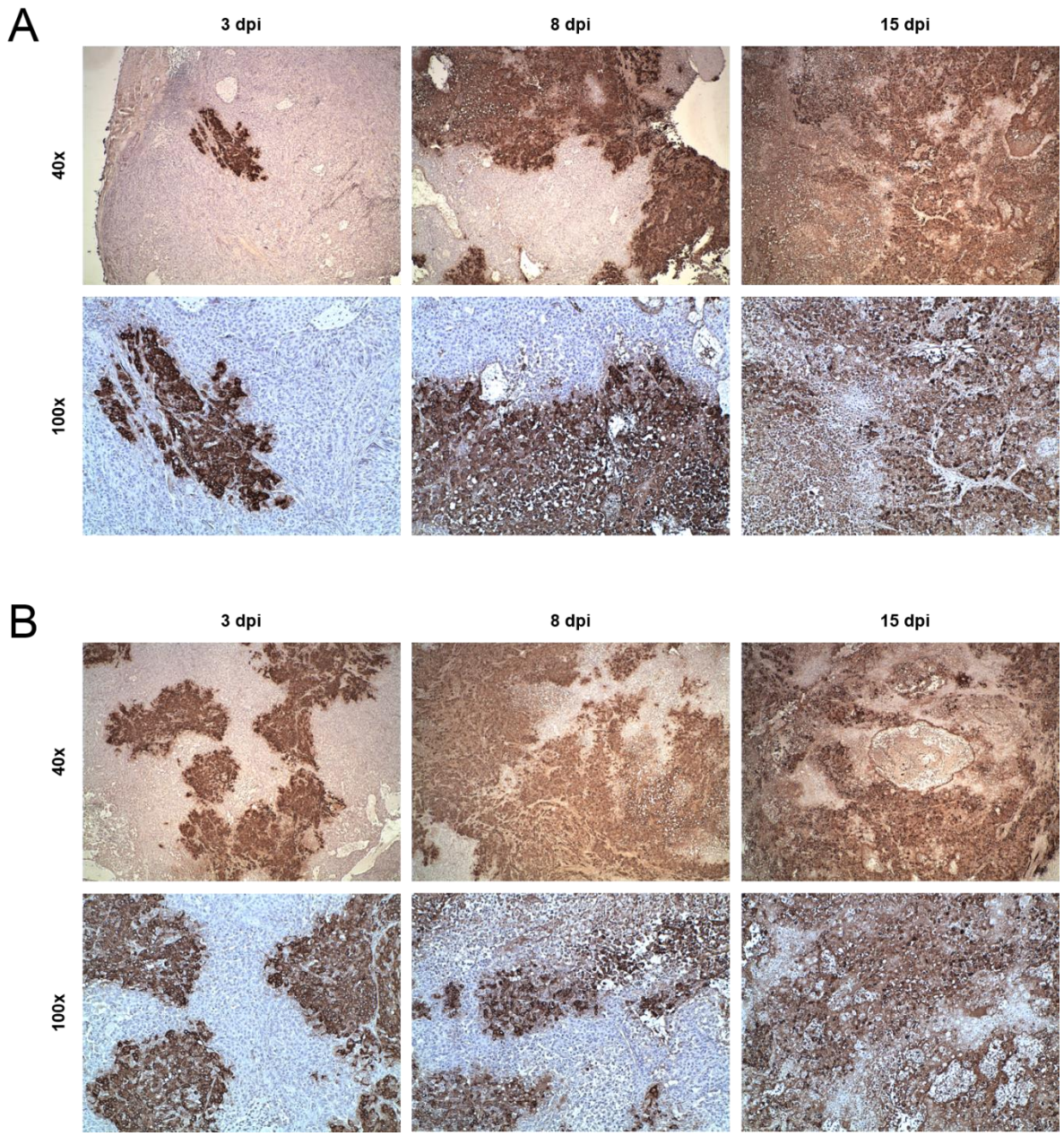

Figure 12. Immunohistochemical analysis of vaccinia virus-infected tumors. A549 tumor-bearing humanized NSG mice were left untreated or injected with LIVP-1.1.1 or GLV-2b372 at 14 weeks post humanization. At 3, 8 and 15 dpi tumors from all three mouse groups were excised for immunohistochemistry. Slides with tumor sections were stained for VACV and counterstained with hematoxylin. Sections from representative LIVP-1.1.1- (A) or GLV-2b372- (B) infected mice obtained at 40x and 100x magnification are shown. Time-dependent increase of VACV-infected areas leading to tumor tissue destruction was observed for both virus strains.

For both viruses, small areas of virus infection were observed at 3 dpi. These areas significantly increased in size by day 8 due to the fast virus spread. At the infection site tumor cells rounded up and detached, and tumor tissue had lost its integrity. At 15 dpi virtually the whole sections were positive for vaccinia virus. Much more extensive necrotic regions and lesions were observed. Similar infection progression was observed for both viruses. No virus-infected cells were detected in the tumors of control animals (data not shown).

4.1.7 Systemic reconstitution with human immune cells in humanized NSG mice

Intrahepatic transplantation of preconditioned newborn NSG mice with human cord blood-derived $CD34^+$ stem cells resulted in a successful systemic reconstitution with human immune cells. Cells from lymphoid and myeloid lineage developed. Human hematopoietic cells were stained with mouse anti-human monoclonal antibodies and analyzed by flow cytometry. Detectable levels of human immune cells were observed in blood of humanized animals by routine testing for engraftment. B cell, T cell, myeloid cell and NK cell subpopulations were first gated for human CD45 and then for the respective lineage-specific marker: CD19, CD3, CD33 and NKp46, respectively (Figure 13).

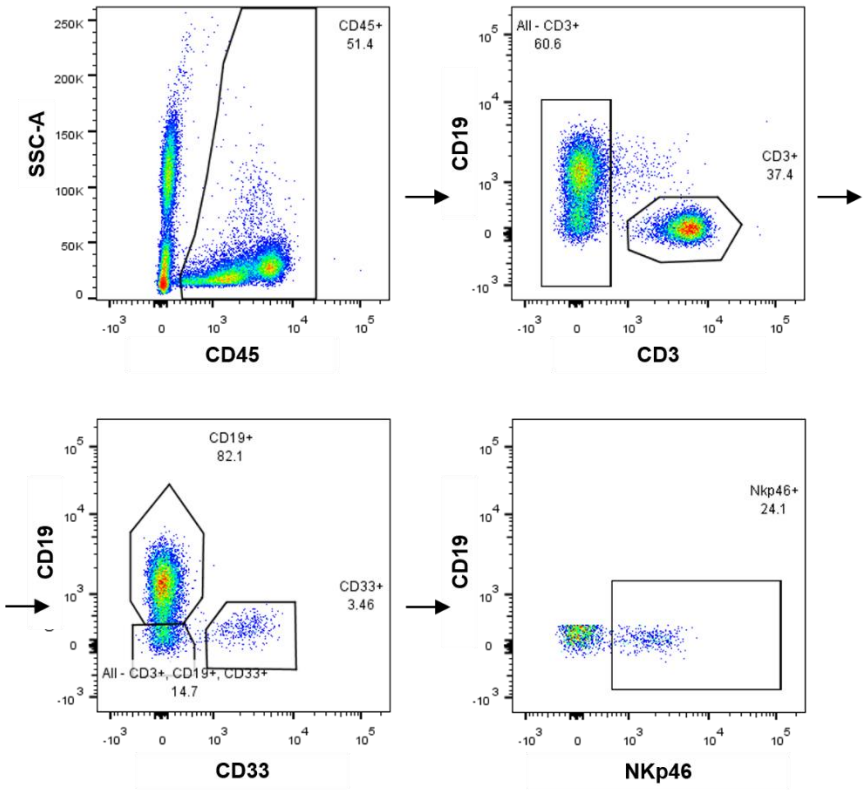

Figure 13. Reconstitution with human immune cells in mouse blood. Humanized mouse-derived blood was analyzed by flow cytometry for presence of human reconstitution 7 weeks after human CD34$^+$ stem cell engraftment. Cells were stained with mouse anti-human monoclonal antibodies. Gating strategy: CD45$^+$→(CD19$^+$,CD3$^+$, CD33$^+$ or NKp46$^+$). Data shown is from one representative humanized mouse.

Further analysis of the NKp46$^+$CD3$^-$ NK cell subset revealed that CD56$^+$ as well as CD56$^-$ NK cells were available in blood, spleens and tumors of all tested mice (Figure 14). However, highest percentages of CD56$^+$ cells among NKp46$^+$ NK cells were observed in tumors of A549 tumor-bearing mice, followed by spleens, and lowest ones were found in blood for the majority of the mice tested.

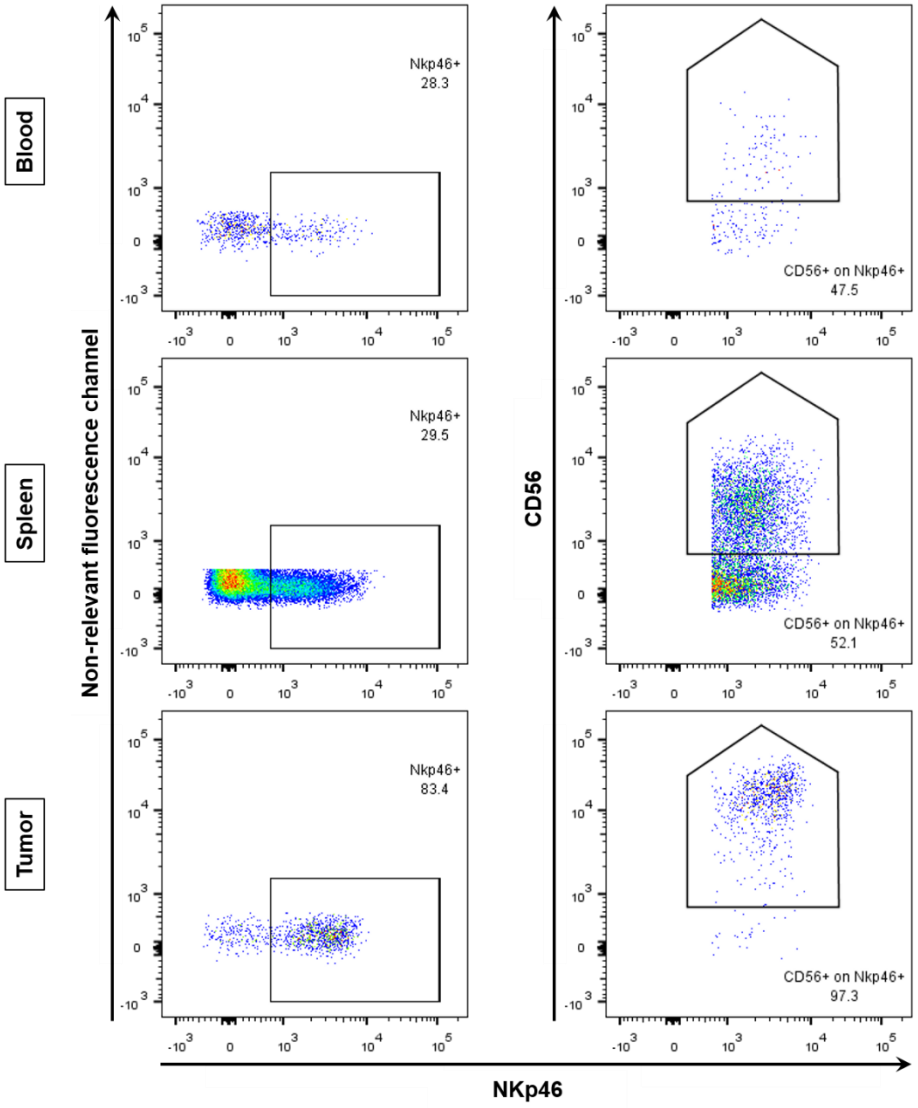

Figure 14. NK cells in humanized mice. Flow cytometric analysis of NK cell subset in blood, spleen and tumors of humanized A549 tumor-bearing mice. Analysis was performed 18 weeks after humanization and 5 weeks after tumor implantation. Cells were stained with mouse anti-human monoclonal antibodies. Gating strategy: $CD45^+ \rightarrow NKp46^+ \rightarrow CD56^+$. Data shown is from one representative humanized mouse.

Flow cytometric analyses of the $CD3^+$ T cell population demonstrated that both CD4 and CD8 single positive cells developed in this mouse model and could be found in the peripheral blood and spleens of the humanized NSG mice as well as in tumors of A549 cells-implanted mice (Figure 15).

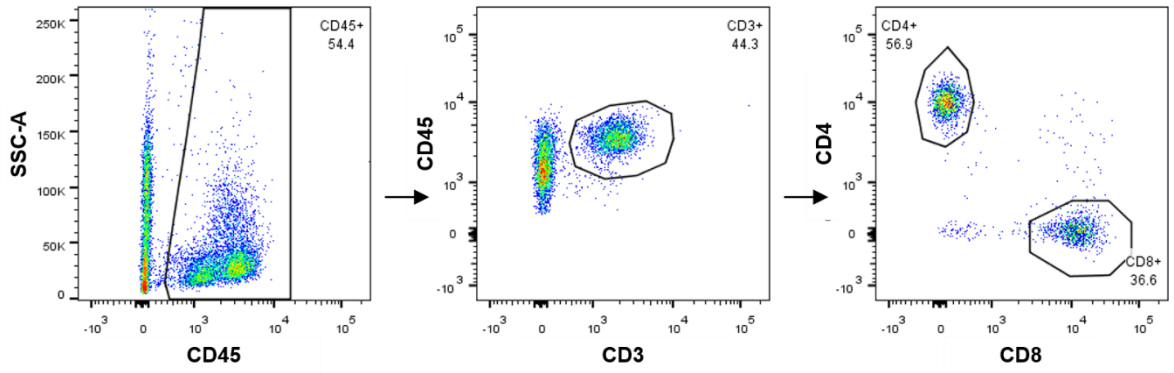

Figure 15. T cell population in mouse blood. Humanized mouse-derived blood was analyzed by flow cytometry for presence of human reconstitution 18 weeks after human CD34$^+$ stem cell engraftment. Cells were stained with mouse anti-human monoclonal antibodies. Gating strategy: CD45$^+$→CD3$^+$→(CD4$^+$ or CD8$^+$). Data shown is from one representative humanized mouse.

Further analyses of the CD4$^+$ and CD8$^+$ T cell subsets for expression of the late activation marker CD25 revealed that highest percentages of CD25 expressing cells among the CD4$^+$ and CD8$^+$ T cells could be found in the tumors of A549 tumor-bearing mice (Figure 16). Very few to almost none activated CD8$^+$ T cells were found in blood and spleen of most animals. In contrast, much higher percentages of the CD4$^+$ T cells in those two organs were expressing CD25.

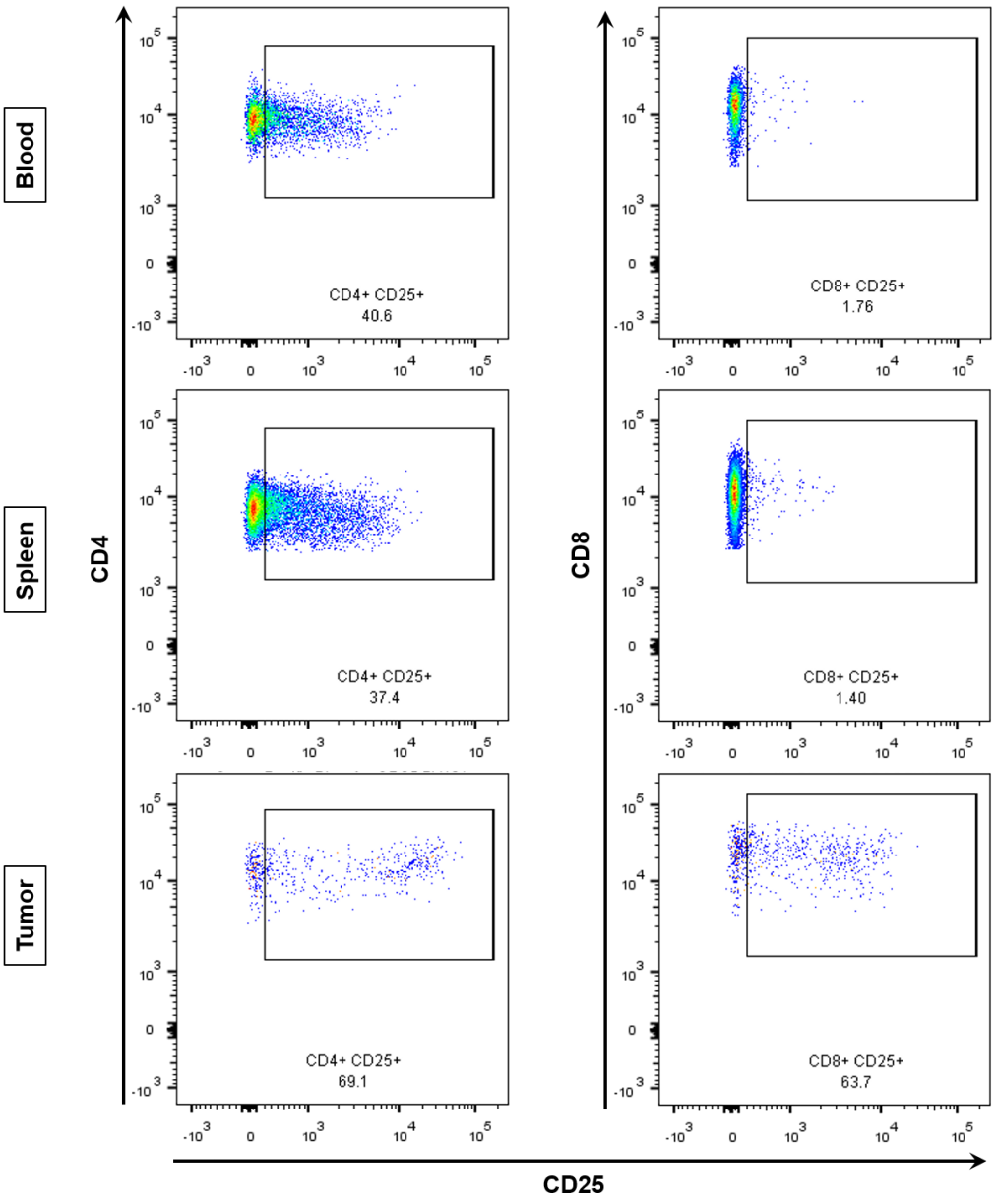

Figure 16. CD25 expression on T cells. Flow cytometric analysis of CD25 expression on $CD4^+$ and $CD8^+$ T cell subsets in blood, spleen and tumors of humanized A549 tumor-bearing mice. Analysis was performed 18 weeks after humanization and 5 weeks after tumor implantation. Cells were stained with mouse anti-human monoclonal antibodies. Gating strategy: $CD45^+ \rightarrow CD3^+ \rightarrow (CD4^+$ or $CD8^+) \rightarrow CD25$. Data shown is from one representative humanized mouse.

4.1.8 Peripheral human B and T cell reconstitution

Human $CD19^+$ B and $CD3^+$ T cell reconstitution was evaluated in humanized mouse blood. Newborn NSG mice were engrafted with human cord blood-derived $CD34^+$

stem cells and implanted subcutaneously with A549 cells at day 92 after humanization. Peripheral blood was withdrawn at certain time point and analyzed for human reconstitution by flow cytometry. Percentages of B and T cells among the human $CD45^+$ cells were calculated. Statistically significant change in $CD19^+/CD3^+$ ratio was reported for the observed time period with a decrease of B cells and an increase of T cells (Figure 17).

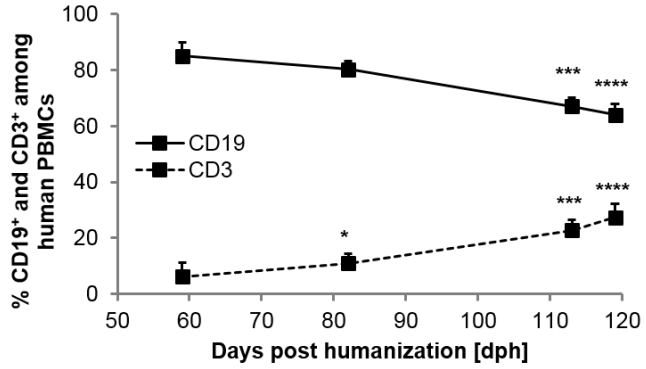

Figure 17. Peripheral human B and T cell reconstitution. Blood from humanized A459 tumor-bearing NSG mice (n=17) was collected at 59, 82, 113 and 119 days post humanization (dph) and analyzed by flow cytometry for presence of human immune cells. Gating strategy: $CD45^+ \rightarrow CD19^+$ or $CD3^+$. Percentages of $CD19^+$ and $CD3^+$ cells among human $CD45^+$ cells were calculated. Mean values and standard errors are plotted.

4.1.9 Flow cytometric analyses of humanized NSG mice derived blood and spleen samples

To evaluate the percentages of B, T and NK cells in blood and spleen of humanized NSG mice and more importantly to investigate the main two T cell subsets and their activation status in the presence or absence of vaccinia virus *in vivo*, first newborn NSG mice were humanized by intrahepatic injection of human cord blood-derived $CD34^+$ stem cells. Eight weeks post humanization half of the mice were retroorbitally injected with 6×10^6 pfu of LIVP-1.1.1. Because the evaluation of the T cell population in VACV infected animals was of great interest mice with an average of 7% more T cells were selected for the LIVP-1.1.1 group. Flow cytometric analysis of blood, spleen

and tumor samples was performed 7 days after virus administration (Figure 18 and 19).

4.1.9.1 Analyses of human B, T and NK cell subsets

Percentages of $CD19^+$ B cells, $CD3^+$ T cells and $CD3^-NKp46^+$ NK cells among the human $CD45^+$ cells as well as percentage of $CD56^+$ NK cells among $CD3^-NKp46^+$ NK cells are presented in Figure 18.

In spleens, B cells represented the main $CD45^+$ cell subpopulation for both mouse groups (Figure 18A). Highest percentage of B cells was observed for the non-virus group, where 77.17 ± 2.77% of the human hematopoietic cells were $CD19^+$, followed by 64.28 ± 5.75% for LIVP-1.1.1. In blood, B cells represented 62.16 ± 5.65% and 48.90 ± 6.79% of the human hematopoietic cells for control and LIVP-1.1.1 group, respectively.

Figure 18B illustrates the $CD3^+$ T cell portion among the total human $CD45^+$ cells. For both groups higher percentages of T cells were observed in the blood compared to the spleens. In blood, highest value of 27.27 ± 8.35% was measured for the LIVP-1.1.1 group. In spleens of the LIVP-1.1.1 injected mice T cells represented higher percentage of the human hematopoietic cells compared to the control. This was partly expected as mice with slightly higher T cell reconstitution were selectively grouped for virus treatment. However, the here obtained percentages showed a larger difference between the groups compared to the initial 7%, suggesting that the virus injection might have contributed to the further increase of the T cell population in the LIVP-1.1.1 group.

Only less than 2% of the human hematopoietic cells in blood and spleen were $CD3^-NKp46^+$ NK positive (Figure 18C). Further subset analysis of $NKp46^+$ NK cells revealed that $CD56^+$ as well as $CD56^-$ cells were present in the organs from both groups. In spleens, 51.70 ± 2.37% and 56.45 ± 2.63% of the $NKp46^+$ cells in control and LIVP-1.1.1 group, respectively, were expressing CD56 (Figure 18D). In contrast, only less than 2% of the NK cells in the blood were expressing CD56. Generally, no significant differences were observed between the mouse groups. Majority of the

NKp46^{+}CD56^{+} NK cells, around 90%, in blood and spleens of both mouse groups were CD56^{dim}, unlike the CD56^{bright} cells, which represented less than 12% of the total CD56^{+} NK cells in those two organs.

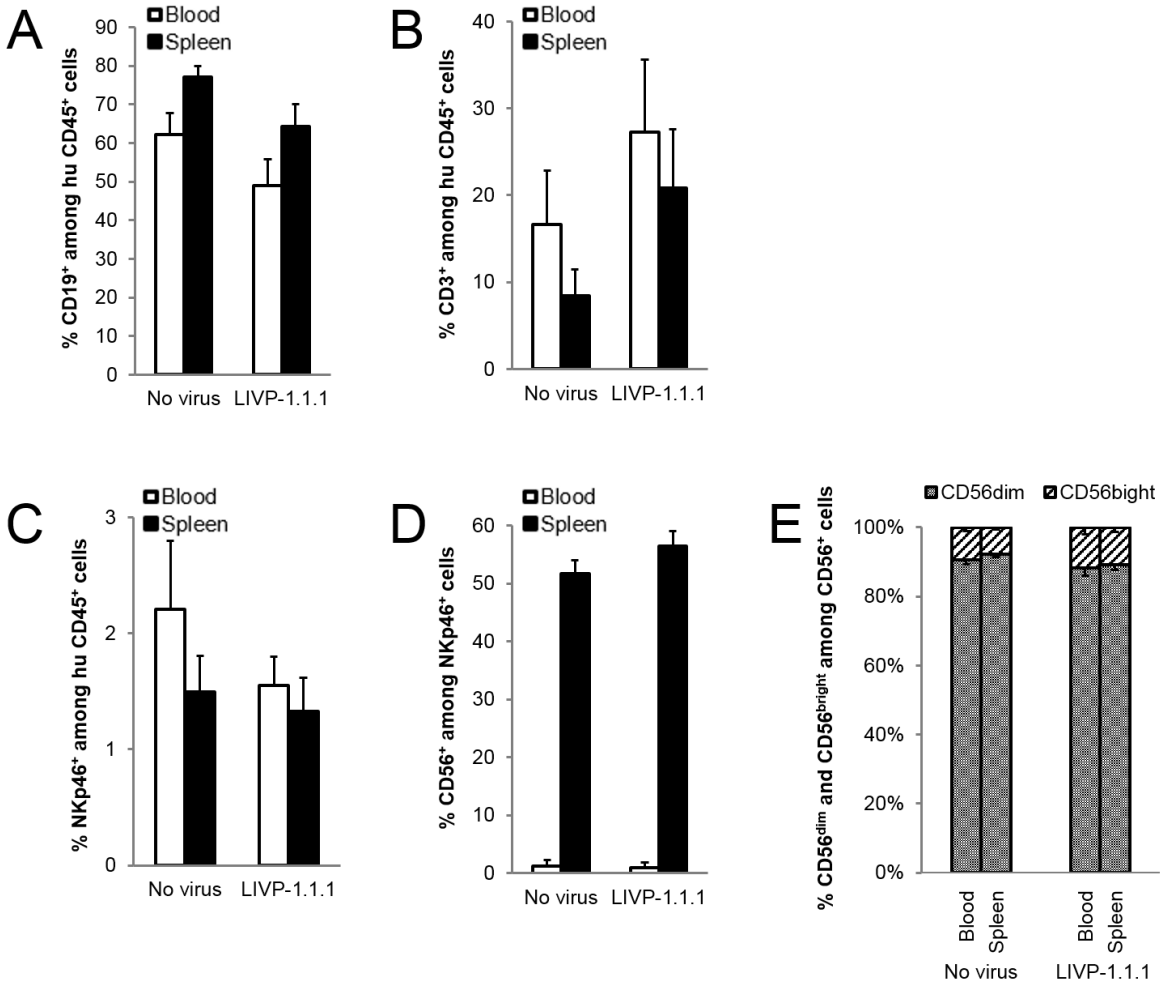

Figure 18. Human hematopoietic cells in humanized NSG mice. Blood and spleen samples from untreated (n=8) or LIVP-1.1.1 injected (n=9) humanized NSG mice were analyzed by flow cytometry for presence of human reconstitution. Analysis were performed 8 weeks post humanization and 7 days after virus administration to virus-treated mouse group. Human hematopoietic cells were stained with mouse anti-human monoclonal antibodies. B cell (A), T cell (B) and NK cell (C) subpopulations were first gated for human CD45 and then for the respective lineage-specific marker: CD19, CD3 and NKp46, respectively. Values are shown as percentage among the human CD45^{+} cells. (D) CD3^{-}NKp46^{+} subset was additionally examined for CD56 expression. (E) Percentage of CD56^{dim} and CD56^{bright} among CD3^{-} NKp46^{+}C56^{+} NK cells. Mean values and standard errors are plotted.

4.1.9.2 Analyses of human CD4 and CD8 single positive T cell subsets

Human T cell population was further investigated. Percentages of $CD4^+CD8^-$ and $CD8^+CD4^-$ cells among the human T cells as well as $CD4^+CD25^+$ and $CD8^+CD25^+$ among $CD4^+$ and $CD8^+$ T cells, respectively, are shown in Figure 19.

Figure 19A shows the percentages of differentiated CD4 (left panel) or CD8 (right panel) single-positive cells among the T cells in blood and spleen samples from LIVP-1.1.1 treated and control mouse groups. In blood, $CD4^+$ cells represented higher percentages of the $CD3^+$ cell fraction compared to the spleen samples (Left panel). Highest value of 45.97 ± 5.98% was observed for the LIVP-1.1.1 group. In spleens, again highest percentage of $CD4^+$ T cells was observed for the LIVP-1.1.1 group. Slightly smaller percentages of $CD4^+$ T cells were detected in blood and spleens from control mice. In contrast, higher percentage $CD8^+$ T cells were found in spleens of both groups compared to the blood samples (right panel). Highest value of 52.83 ± 5.02% was measured in spleens of LIVP-1.1.1 injected mice. However, no statistically significant differences were observed between both mouse groups.

Further analysis revealed that 29 - 34% or 36 - 39% of the $CD4^+$ T cells presented in the blood or the spleens, respectively, were expressing CD25 (Figure 19B, left panel). Although slightly higher percentages of $CD4^+CD25^+$ T cells were observed in spleens compared to blood, all values were very close.

Evaluation of the $CD8^+$ T cells revealed that only less than 4% of those cells in blood and spleen were activated in both mouse groups (Figure 19B, right panel). Again, no statistically significant differences were observed between the mouse groups.

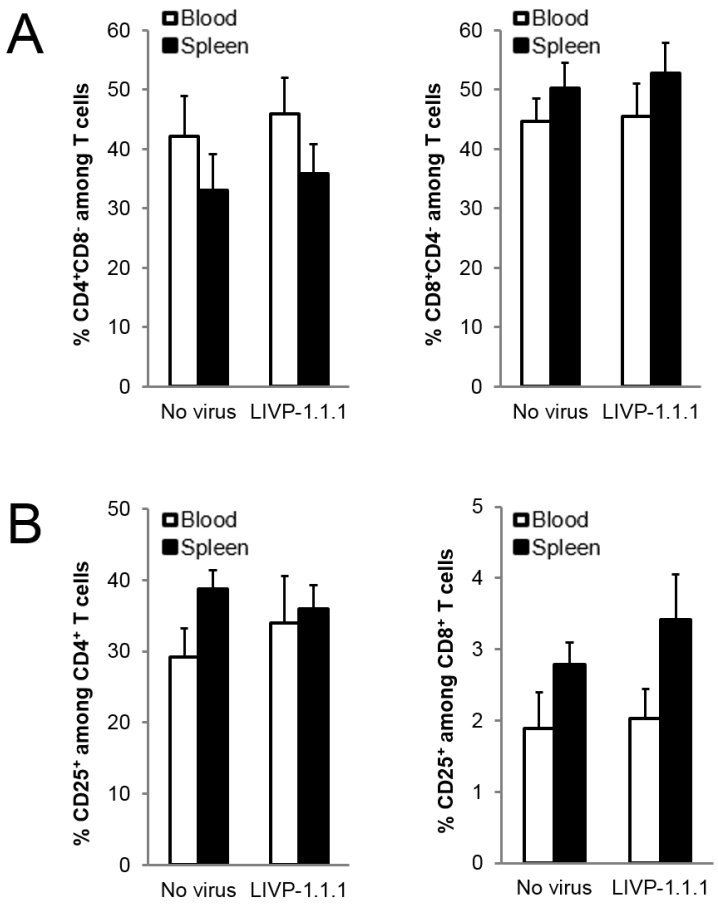

Figure 19. Flow cytometry analysis of T cell population in humanized NSG mice. Humanized NSG mice were left untreated (n=6) or injected with LIVP-1.1.1 (n=7) at 7 weeks post humanization. Seven days after virus administration the human T cell population in the blood and spleens of those mice were analyzed by flow cytometry. Cells were stained with mouse anti-human mAb and gated first for human CD45 and then for the respective lineage-specific marker. (A) CD4 (left panel) or CD8 (right panel) expression was determined following gating on all $CD3^+$ T cells. Gating strategy: $CD45^+ \rightarrow CD3^+ \rightarrow (CD4^+CD8^-$ or $CD8^+CD4^-)$. (B) CD4 (left panel) and CD8 (right panel) single positive cells were additionally examined for CD25 expression. Gating strategy: $CD45^+ \rightarrow CD3^+ \rightarrow (CD4^+CD8^-$ or $CD8^+CD4^-) \rightarrow CD25^+$. Mean values and standard errors are plotted.

4.1.10 Flow cytometric analyses of humanized A549 tumor-bearing NSG mice-derived blood, spleen and tumor samples

Aim of this mouse study was to evaluate the proportion of B, T and NK cells subpopulations among the human $CD45^+$ cell population in blood, spleens and tumors of humanized A549 tumor-bearing NSG mice and even more importantly to investigate

the main two T cell subsets and their activation status in the presence or absence of vaccinia virus *in vivo*. To start with, newborn NSG mice were humanized and 13 weeks later implanted subcutaneously with A549 cells. In four weeks the tumor volume reached an average of 400 mm^3 and mice were either injected retroorbitally with 6 x 10^6 pfu of LIVP-1.1.1 or left untreated as a control group. Because the evaluation of the T cell subpopulation in VACV infected animals was of great interest mice with an average of 20% more T cells were selected for the LIVP-1.1.1 group. Eight days after virus administration blood, spleen and tumor samples were analyzed by multiparametric flow cytometry (Figure 20 and 21).

4.1.10.1 Analyses of human B, T and NK cell subsets

Percentages of $CD19^+$ B cells, $CD3^+$ T cells and $CD3^-NKp46^+$ NK cells among the human $CD45^+$ cells as well as percentage of $CD56^+$ NK cells among $CD3^-NKp46^+$ NK cells are presented in Figure 20.

Spleens of the humanized mice were reconstituted mainly with B cells (Figure 20A). Highest percentages of B cells were observed for the non-virus group, where 61.01 ± 5.83% of the $CD45^+$ cells were $CD19^+$. In blood, B cells represented 17 - 31% of the human hematopoietic cells. In contrast, only 2 - 3 % of the tumor-infiltrating $CD45^+$ cells were $CD19^+$ cells.

Figure 20B illustrates the $CD3^+$ T cell portion among the total human hematopoietic cells. The smallest percentages of T cells, 22.49 ± 4.86% and 25.20 ± 5.50%, were observed in the spleens of control and LIVP-1.1.1 injected mice, respectively. In blood, highest value of 66.30 ± 4.98% was detected for the LIVP-1.1.1 group. T cells represented almost equal percentage of the tumor-infiltrating $CD45^+$ cells in both groups. However, slightly higher value of 42.86 ± 10.50% was detected in the virus group.

$CD3^-NKp46^+$ NK cells were the most abundant cell type among the human $CD45^+$ cells found in control tumors with value of 41.14 ± 21.11% (Figure 20C). In virus-treated tumors, NK cells represented the second largest leukocyte subpopulation infiltrating

the tumors after the T cells with value of 27.57 ± 19.01%. In contrast, less than 4% of the human hematopoietic cells in blood and spleen were NKp46 positive.

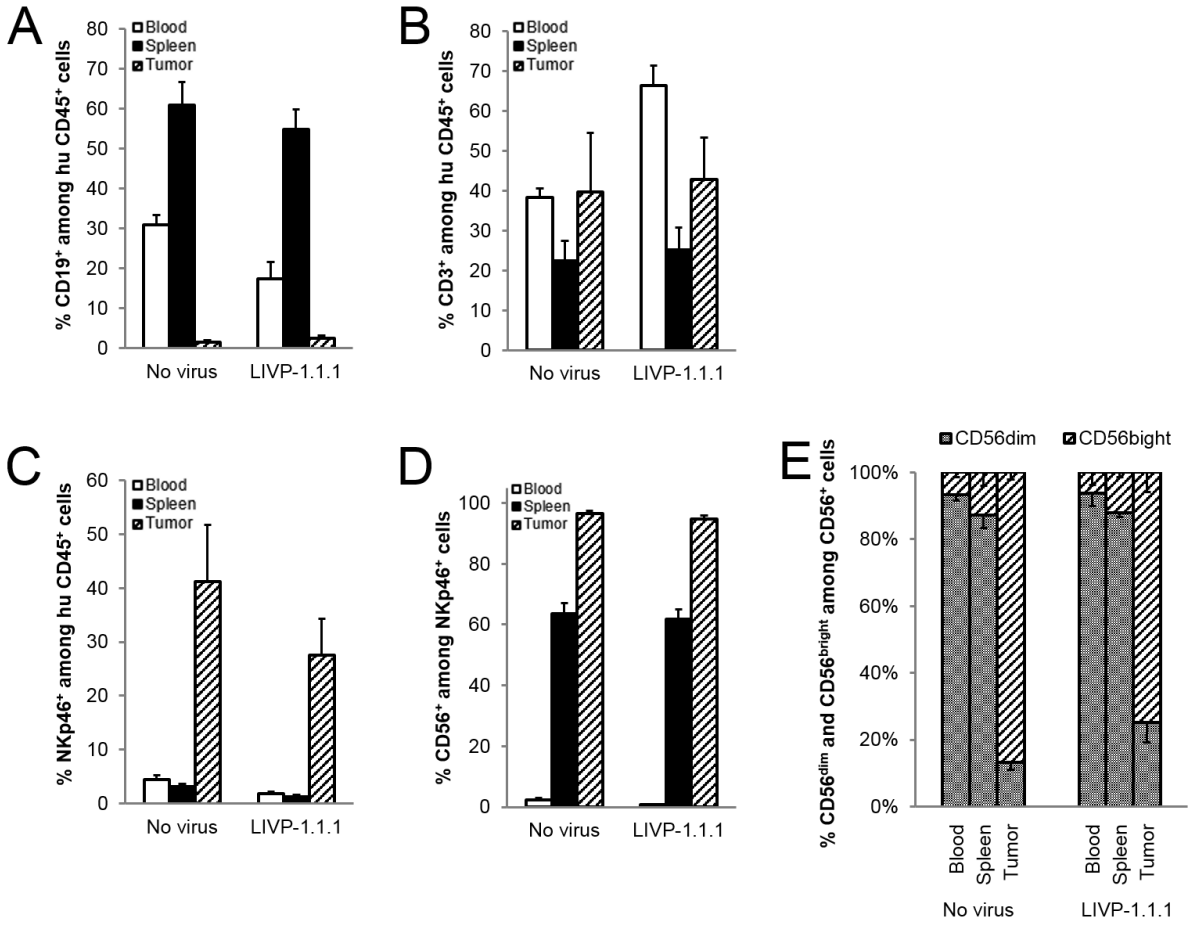

Figure 20. Human hematopoietic cells in tumor-bearing humanized NSG mice. Blood, spleen and tumor samples from untreated (n=5) or injected with LIVP-1.1.1 (n=9) A549 tumor-bearing humanized NSG mice were analyzed by flow cytometry for presence of human reconstitution. Analysis were performed 13 weeks post humanization and 8 days after virus administration to virus-treated mouse group. Human hematopoietic cells were stained with mouse anti-human monoclonal antibodies. B cell (A), T cell (B) and NK cell (C) subpopulations were first gated for human CD45 and then for the respective lineage-specific marker: CD19, CD3 and NKp46, respectively. Values are shown as percentage among the human $CD45^+$ cells. (D) $CD3^-NKp46^+$ subset was additionally examined for CD56 expression. (E) Percentage of $CD56^{dim}$ and $CD56^{bright}$ among $CD3^-NKp46^+CD56^+$ NK cells. Mean values and standard errors are plotted.

Further subset analysis of NKp46$^+$ NK cells revealed that CD56$^+$ as well as CD56$^-$ cells were present in the organs from both mouse groups. In tumors, 96.42 ± 1.07% and 94.63 ± 1.32% of the NKp46$^+$ cells in control and LIVP-1.1.1 group, respectively, were expressing CD56 (Figure 20D). Around 63% of the NK cells in spleens were also CD56$^+$. In contrast, only less than 2% of the NK cell in the blood were expressing CD56. No significant differences were observed between the mouse groups. Similarly to what was seen in the non-tumorous mice, majority of the NKp46$^+$CD56$^+$ NK cells, around 87 - 93 %, in blood and spleens of both mouse groups were CD56^{dim}, unlike the CD56^{bright} cells, which represented less than 13% of the total CD56$^+$ NK cells. In contrast, more than 75% of the human CD56$^+$ NK cells in tumors were NKp46$^+$CD56^{bright}. However, no major difference was observed between LIVP-1.1.1 treated and control mouse group.

4.1.10.2 Analyses of human CD4 and CD8 single positive T cell subsets

Human T cell population was further investigated. Percentages of different cell subtypes among the respective parental population are shown in Figure 21.

Figure 21A shows the percentages of differentiated CD4 (left panel) or CD8 (right panel) single-positive cells among the T cells in blood, spleen and tumor samples from both, LIVP-1.1.1 treated and untreated control, mouse groups. In blood, CD4$^+$ cells were the main T cell subpopulation representing 51 - 54% of the CD3$^+$ cells (Left panel). Compared to control mice, slightly smaller percentages of CD4$^+$ T cells were detected in spleens and tumors from virus-treated mice. In LIVP-1.1.1 group, CD8 single-positive cells represented slightly higher percentage of the T cells in all tested organs compared to the control group (right panel). Highest value of 52.01 ± 3.55%, compared to 43.11 ± 2.49%, was measured in spleen.

Further analysis revealed that 29 - 42% or 32 - 40% of the CD4$^+$ T cells presented in the blood or the spleens, respectively, were expressing CD25 (Figure 21B, left panel). Higher percentages of CD4$^+$CD25$^+$ T cells were observed in tumors. Surprisingly, highest portion, 69.25 ± 6.39%, of CD25 expressing cells among tumor-infiltrating

$CD4^+$ T cells were found in uninfected tumors of the control animals. No significant differences were observed between both groups.

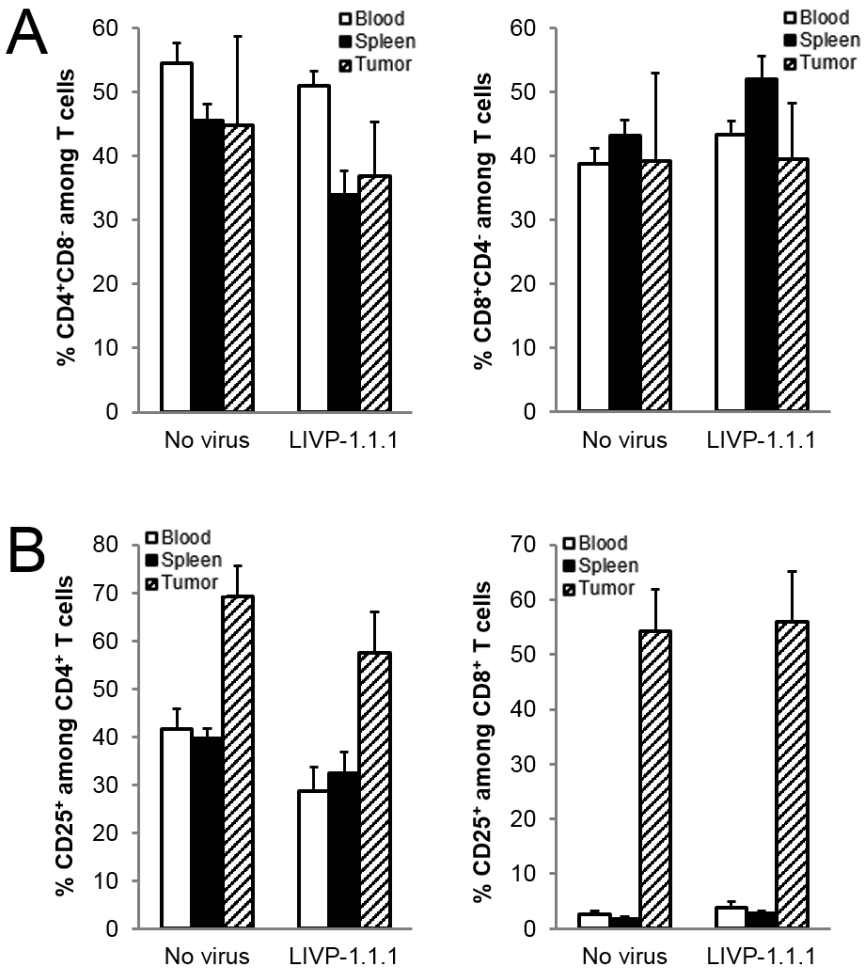

Figure 21. Flow cytometry analysis of T cell population in tumor-bearing humanized NSG mice. A549 tumor-bearing humanized NSG mice were left untreated (n=5) or injected with LIVP-1.1.1 (n=9) at 13 weeks post humanization. Eight days after virus administration the human T cell population in the blood, spleens and tumors of those mice were analyzed by flow cytometry. Cells were stained with mouse anti-human mAb and gated first for human CD45 and then for the respective lineage-specific marker. One mouse from each group did not show tumor colonization with T cells and were therefore excluded from the analysis of the tumor data. (A) CD4 (left panel) or CD8 (right panel) expression was determined following gating on all $CD3^+$ T cells. Gating strategy: $CD45^+ \rightarrow CD3^+ \rightarrow (CD4^+CD8^-$ or $CD8^+CD4^-)$. (B) CD4 (left panel) and CD8 (right panel) single positive cells were additionally examined for CD25 expression. Gating strategy: $CD45^+ \rightarrow CD3^+ \rightarrow (CD4^+CD8^-$ or $CD8^+CD4^-) \rightarrow CD25^+$. Mean values and standard errors are plotted.

Evaluation of the $CD8^+$ T cells revealed a significant activation of those cells in tumors (Figure 21B, right panel). Highest percentage (56.03 ± 9.13%) of activated $CD8^+$ T cells was found in LIVP-1.1.1 infected tumors. However, the difference in the tumor values between both groups was only 2%. In contrast, only 2 - 4% of the $CD8^+$ T cells were activated in the blood and spleens of both mouse groups. Again, no statistically significant differences were observed between the mouse groups.

4.2 Evaluation of new recombinant vaccinia virus strains, GLV-1h375, -1h376 and -1h377, encoding for human CTLA4-blocking single-chain antibody

Three new rVACV strains, GLV-1h375, -1h376 and -1h377, carrying the gene for CTLA4 scAb were initially evaluated *in vitro* and/or in cell culture. Next, in order to evaluate whether CTLA4 immune checkpoint blockade would have an effect on the activation status of tumor-infiltrating T lymphocytes could therefore increase the antitumor immunity, GLV-1h376 was used in animal studies.

4.2.1 Expression, secretion and purification of virus-mediated CTLA4 scAb

GLV-1h375, -1h376 and -1h377 carry the anti-human CTLA4 FLAG-tagged single-chain antibody encoding (*CTLA4*) gene under the control of VACV synthetic early (P_{SE}), early/late (P_{SEL}) and late (P_{SL}) promoters, respectively. Therefore, the strongest, a weaker and the weakest CTLA4 scAb expression and subsequent secretion into the growth media was expected to be found in GLV-1h376-, -1h377- and -1h375-infected cells, respectively. To test this hypothesis, A549 cells were infected with GLV-1h375, -1h376, -1h377 or the parental GLV-1h68 virus at an MOI of 1 or left untreated (Figure 22A and B).

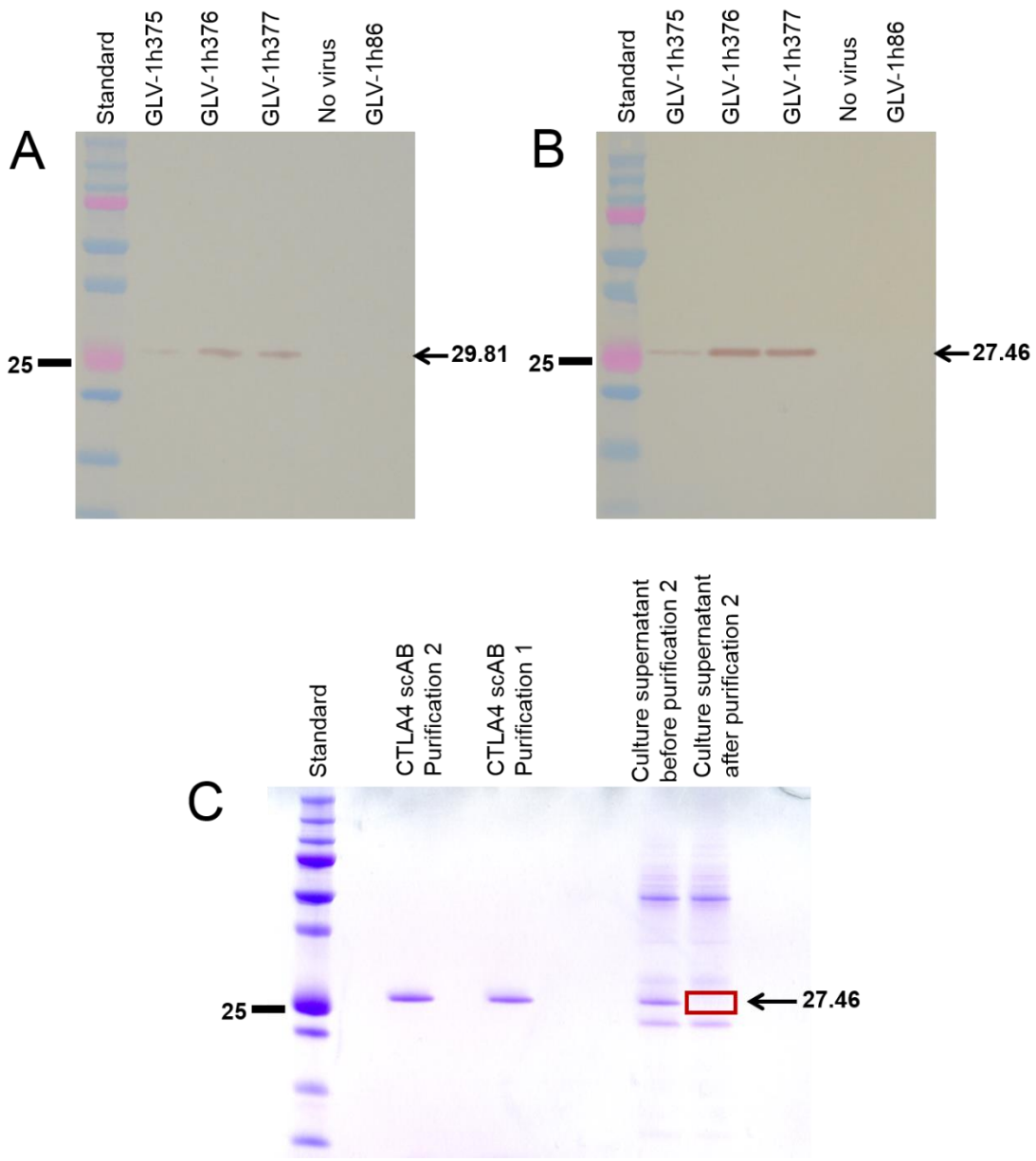

Figure 22. Expression, secretion and purification of virus mediated CTLA4 scAb. (A-B) Western blot analysis of CTLA4 scAb expression (A) and secretion (B) in A549 cell cultures. Cancer cells were infected with rVACV strains at an MOI of 1. Cell lysates (A) and supernatants (B) of infected cultures were collected 24 hours later and 4 and 10 µg of the samples, respectively, were separated by SDS-PAGE. Intracellular and secreted CTLA4 scAb with the expected size of 29.81 and 27.46 kDa, respectively, was detected in the Western blot analysis using an anti-DDDDK antibody. Line shows standard band, arrow shows the protein of expected size, both in kDa. (C) CV-1 cell cultures were infected with GLV-1h376 at an MOI of 2. Supernatant was harvested 24 hours later and concentrated. CTLA4 scAb was purified using affinity gel. To verify its purity, sample of the eluted scAb was separated by SDS-PAGE and stained with Coomassie brilliant blue. Coomassie-stained gel showing the purified CTLA4 scAb from two separate purifications, concentrated CTLA4 scAb containing culture supernatant before and after scAb purification.

Cells infected with the CTLA4 scAb encoding viruses showed a specific protein of the expected size of 29.81 or 27.46 kDa for cell lysates or supernatants, respectively. Ig kappa-chain leader sequence is available only in the intracellular protein and is removed upon secretion, responsible for the slightly smaller size of the secreted single-chain antibody. As expected highest expression levels of CTLA4 scAb were detected for GLV-1h376 followed by GLV-1h377 and -1h375. No protein of this size was observed in uninfected or GLV-1h68-infected cells.

Next, the virus-encoded CTLA4 scAb was purified from the supernatant of GLV-1h376-infected CV-1 cells using an affinity gel (Figure 22C). And its purity was confirmed in a Coomassie gel.

4.2.2 Affinity and functionality of virus-mediated CTLA4 scAb

Vaccinia virus-encoded anti-human CTLA4 scAb was purified from the supernatants of GLV-1h376-infected CV-1 cells. Thereafter, this isolated antibody was used in ELISA to evaluate its affinity to its human CTLA4 target molecule (Figure 23).

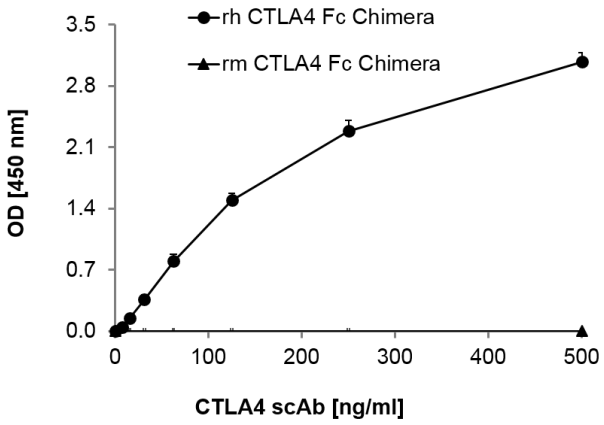

Figure 23. Affinity of virus-mediated CTLA4 scAb *in vitro*. Affinity of virus-encoded and purified CTLA4 scAb and its lack of cross-reactivity were demonstrated by ELISA. 96-well plates were coated with recombinant human CTLA4 (rhCTLA4) Fc Chimera (circles) or recombinant mouse CTLA4 (rmCTLA4) Fc Chimera (triangles). ODs obtained for various CTLA4 scAb concentrations against both human and mouse Fc Chimeras are plotted.

CTLA4 scAb proved to be functional and was able to bind to the recombinant human CTLA4 Fc Chimera. CTLA4 scAb is human specific and as expected a lack of cross-reactivity between the antibody and the recombinant mouse CTLA4 Fc Chimera was confirmed.

Next, the functionality of the CTLA4 scAb was tested in cell culture. The immortalized line of human T lymphocyte Jurkat cells were activated in two different ways. First a mix of PMA, Ionomycin, B7-1 and B7-2 were added to the cells (Figure 24A (b, c and d)). Alternatively, Jurkat cells were activated using a commercially available T cell activation beads (Figure 24A (e, f and g)). To evaluate whether mix or beads activation in these experimental settings could be fortified by adding anti-human CTLA4 antibody, monoclonal Ipilimumab (YERVOY®) was supplemented to the activation reagents in some of the wells (Figure 24A (c and f)). Next to test the ability of the VACV-encoded CTLA4 scAb to intensify the T cell activation, the purified single-chain antibody was supplemented to the activation reagents in other wells (Figure 24A (d and g)). Samples were analyzed 48 hours later by flow cytometry. For the analyses, gates were set up using a non-activated control cells (Figure 24A (a)). Images of representative dot lots are shown in Figure 24A. Activation levels were measured in duplicates and corresponding bar graphs with mean values of percentage $CD69^+$ or $CD25^+$ among Jurkat cells are presented in Figure 24B.

Because Jurkat cells are immortalized line of human T lymphocytes, which continuously proliferate, a relatively strong early CD69 activation marker expression (60% of the cells) and to a lesser extent a late CD25 activation marker expression (4% of the cells) were observed even in the non-treated control cells (Figure 24A (a) and B). Both mix- and beads-activated cells showed stronger expression of both activation markers (Figure 24A (b and e) and B). In both groups, approximately 89% and 23% of all activated Jurkat cells were CD69 or CD25 positive, respectively (Figure 24B). As expected Ipilimumab was able to further increase the activation of the mix-activated Jurkat cells (Figure 24A (b) and B (Mix)), almost 100% of the cells were $CD69^+$ and 71% were $CD25^+$ (Figure 24B (Mix)).

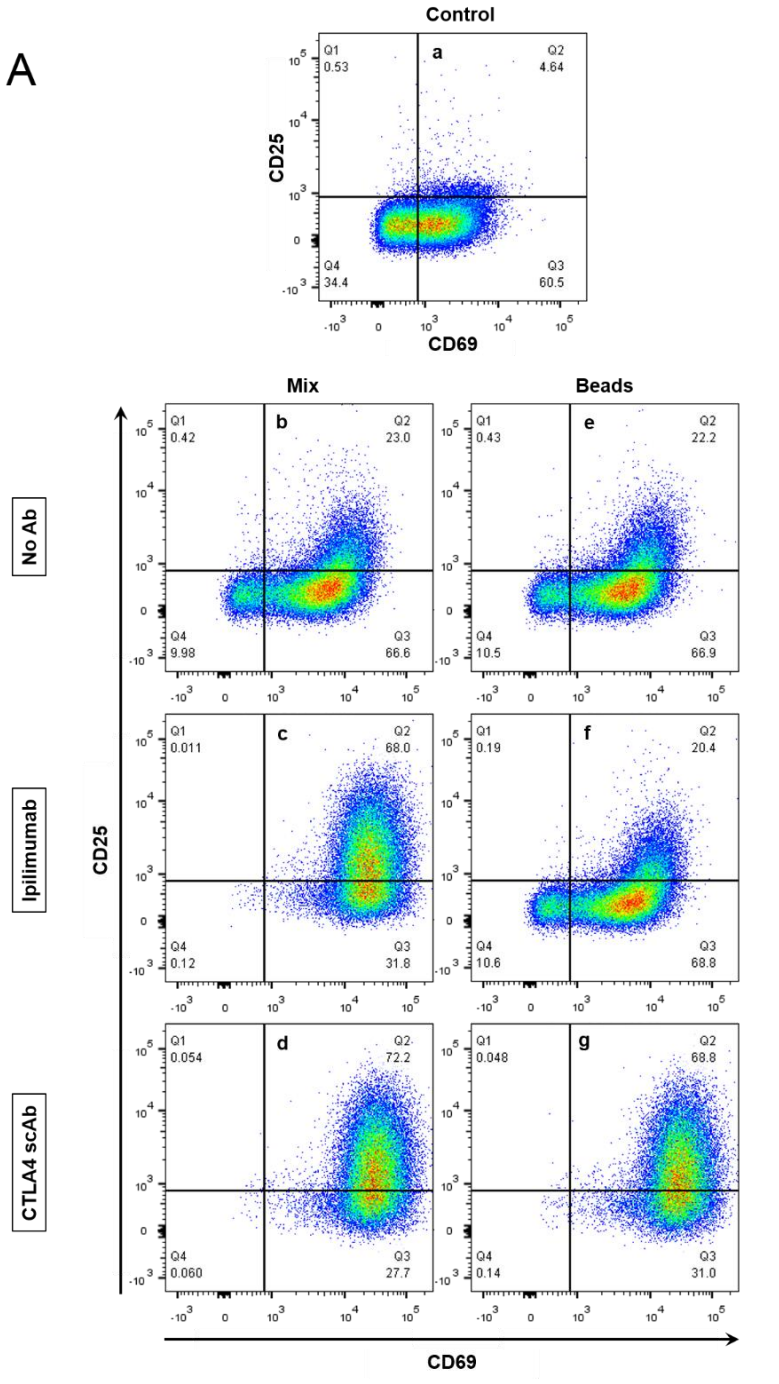
A
Control
a
Q1 0.53
Q2 4.64
Q4 34.4
Q3 60.5
CD25
CD69
Mix
Beads
No Ab
Ipilimumab
CTLA4 scAb
b
Q1 0.42
Q2 23.0
Q4 9.98
Q3 66.6
e
Q1 0.43
Q2 22.2
Q4 10.5
Q3 66.9
c
Q1 0.011
Q2 68.0
Q4 0.12
Q3 31.8
f
Q1 0.19
Q2 20.4
Q4 10.6
Q3 68.8
d
Q1 0.054
Q2 72.2
Q4 0.060
Q3 27.7
g
Q1 0.048
Q2 68.8
Q4 0.14
Q3 31.0
CD25
CD69

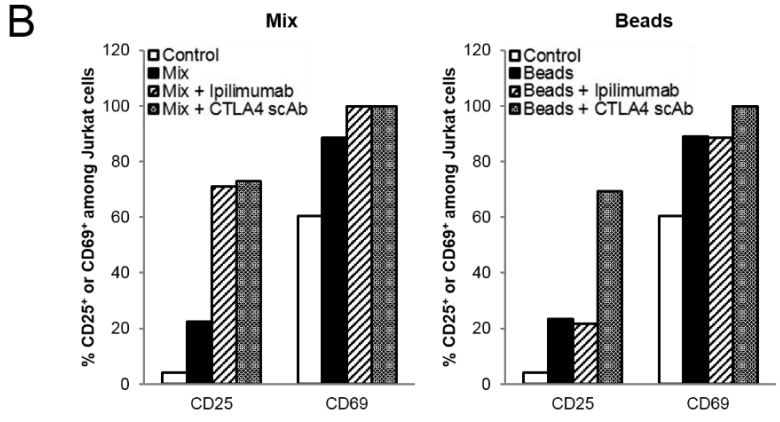
B
Mix
Beads
Control
Mix
Mix + Ipilimumab
Mix + CTLA4 scAb
Beads
Beads + Ipilimumab
Beads + CTLA4 scAb
% CD25+ or CD69+ among Jurkat cells
0
20
40
60
80
100
120
CD25
CD69

Figure 24. Functionality of virus mediated CTLA4 scAb in cell culture. Jurkat cells were activated with a mix of PMA, Ionomycin, B7-1 and B7-2 (b, c and d) or with commercially available T cell activation beads (e, f and g). Additionally to the mix and beads, cells were supplemented with anti-human CTLA4 antibodies, monoclonal Ipilimumab (YERVOY®) (c and f) or VACV-encoded single-chain CTLA4 scAb (d and g). An untreated sample of Jurkat cells was left as a control (a). Forty eight hours later all samples were analyzed in duplicates for early CD69 and late CD25 activation marker expression by flow cytometry. Images of representative dot lots (A) and corresponding bar graphs (B) are shown.

Unexpectedly, no effect of Ipilimumab was seen in the beads-activated cells in respect to the CD69 and CD25 expression, where same levels of activation marker expression as those in the beads only group were observed (Figure 24A (b and e) and B (Beads)). In contrast, purified CTLA4 scAb increased T cell activation in the mix- as well as in the beads-activated group, with almost 100% of the cells from both groups expressing CD69 and 73% or 69% of them expressing CD25, respectively (Figure 24A (d and g) and B). A possible explanation for that could be the smaller size of the single-chain antibody when compared to the monoclonal Ipilimumab, which allows the single-chain antibody to reach its CTLA4 target even in the presence of the large activation beads that are attached to the T cells.

4.2.3 Comparison of GLV-1h68, -1h375, -1h376 and -1h377 replication efficiencies in three different tumor cell lines

The replication efficiencies of the CTLA4 scAb-encoding GLV-1h375, -1h376 and -1h377 vaccinia virus strains as well as the parental GLV-1h68 was analyzed and compared in human A549, 1936-MEL and 888-MEL cell cultures. Tumor cells were infected with either one of the viruses at an MOI of 0.005 or 0.1. Supernatants and cells of infected cultures were collected separately and in triplicates at 24, 48, 72 and 96 hpi. Viral titers were determined in triplicates by standard plaque assay in CV-1 cell monolayers.

Figure 25 shows that all four recombinant vaccinia virus strains could replicate well in A549, better in 1936-MEL and most efficiently in 888-MEL cells. In A549 and 1936-MEL cells infected at an MOI of 0.005 (Figure 25A, left and middle panel) titer values

showed a constant increase during the whole course of the replication assay and no plateau was reached. In A549 cells, highest titers found in supernatant and cell lysate at 96 hpi were 2.80 x 10^4 and 9.00 x 10^5 pfu/ml for GLV-1h68 and GLV-1h376, respectively. Similar titers were observed in the 1936-MEL cell line. In contrast, viral replication in the human 888-MEL cell line resulted in a higher level of virus production, compared to the other two cell lines (Figure 25A, right panel). At 72 hpi viral titers in cell lysates peaked for all rVACVs. The highest viral titer value at this time point was 8.00 x 10^6 pfu/ml for GL-1h375. Afterwards, a decrease in cell lysate titers accompanied with increase of viral particles in the supernatant followed.

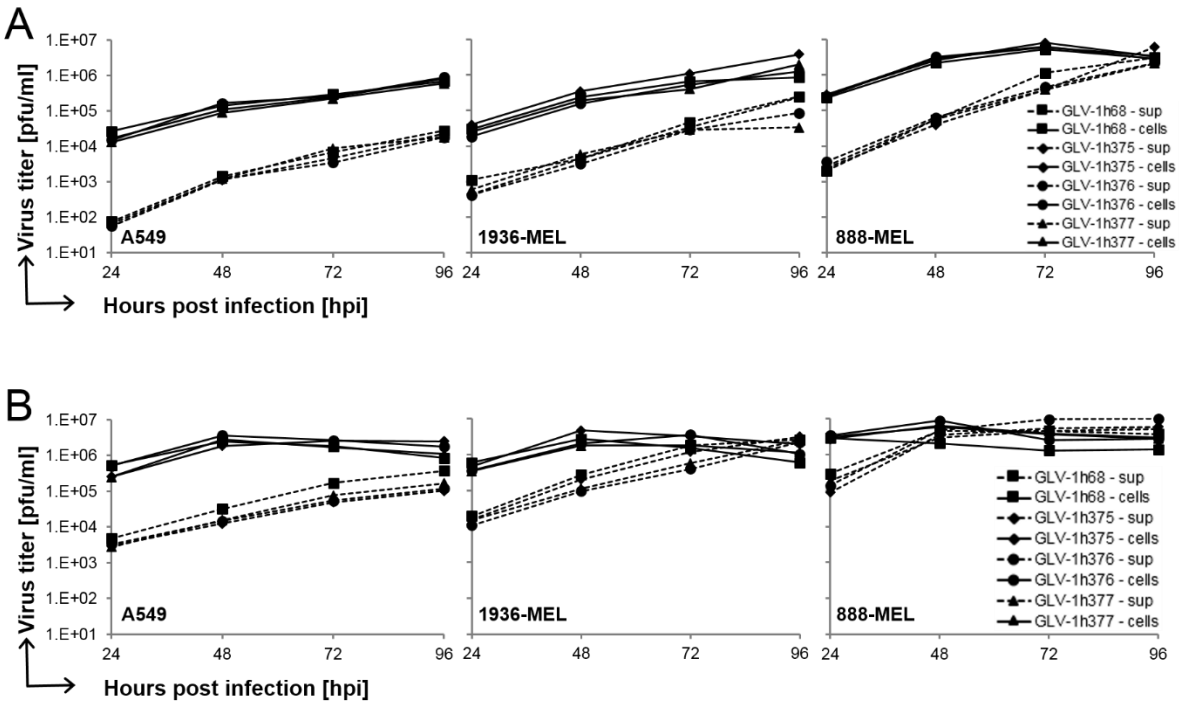

Figure 25. Replication of different rVACVs in human tumor cell cultures. Human A549, 1936-MEL and 888-MEL cell cultures were infected with GLV-1h68 (squares), -1h375 (diamonds), -1h376 (circles) and -1h377 (triangles) vaccinia viruses at an MOI of 0.005 (A) and 0.1 (B). To determine replication efficiency, supernatants and cells of infected cells were collected separately and in triplicates at 24, 48, 72 and 96 hpi. Viral titers were determined in triplicates as pfu per ml of medium by standard plaque assay in CV-1 cell monolayers and plotted against the course of time. Mean values (n=3) and standard errors are plotted.

After infection with an MOI of 0.1 (Figure 25B) viral loads in most cell lysates peaked at 48 hpi, followed by slow decrease. Only exception were the GLV-1h68-infected 888-

MEL cells, which highest titer was observed 24 hours after infection (Figure 25B, right panel). Again highest viral loads were observed in the 888-MEL cell line. Highest titer found in cell lysates at 48 hpi was 8.83 x 10^6 pfu/ml for GLV-1h376.

GLV-1h375, -1h376 and -1h377 viruses replicated in all three tested cancer cell lines in a dose- and time-dependent fashion and in a similar manner to the parental GLV-1h68. Comparable viral titers were reached at each time point, indicating that CTLA4 scAb expression did not altered their replication capabilities in cells.

4.2.4 GLV-1h68-, -1h375-, -1h376- and -1h377-mediated cytotoxicity in different tumor cell lines

To evaluate whether the CTLA4 scAb expression affects the cytotoxic potential of GLV-1h375, -1h376 and -1h377 on A549, 1936-MEL and 888-MEL cells in comparison to the parental GLV-1h68, cells were infected with either one of the viruses at an MOI of 0.005 or 0.1 and MTT assay was performed (Figure 26). Tumor cell viability was monitored in triplicates at 0, 24, 48, 72 and 96 hpi. Viable cells were calculated as percentage from the mock-infected control cells for each time point, which were considered to be 100% viable.

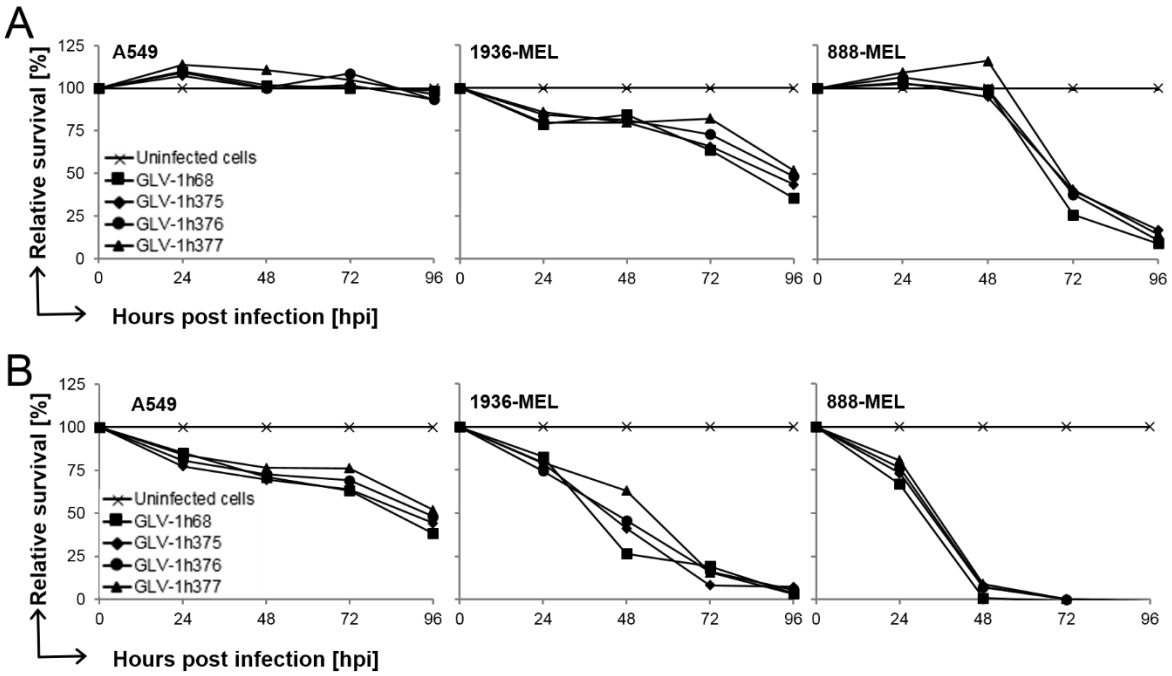

Figure 26. Vaccinia virus-mediated cytotoxicity in human tumor cell cultures. Human A549, 1936-MEL and 888-MEL cell cultures were infected with GLV-1h68 (squares), -1h375 (diamonds), -1h376 (circles) and -1h377 (triangles) vaccinia viruses at an MOI of 0.005 (A) and 0.1 (B). Viability of virus-infected cancer cells was monitored in triplicates over 96 hours using an MTT assay. Viable cells were calculated as percentage from the uninfected control cells for each time point, which were considered to be 100% viable. Mean values (n=3) and standard errors are plotted.

Tumor cells were first infected at an MOI of 0.005 (Figure 26, A). This resulted in an inefficient killing of A549 cells by all four viruses used during the course of the assay (Figure 26A, left panel). Better cytotoxic effect was observed in the 1936-MEL cell line (Figure 26A, middle panel). GLV-1h68 showed a slightly better killing potential compared to the other three viruses but the cytotoxic effect of all four viruses followed a very similar path. At 96 hpi only 35.68 ± 0.03% GLV-1h68-infected cells were still viable. Worst killing potential was observed for GLV-1h377 with 51.69 ± 0.06% viable tumor cells left after 96 of infection. Due to the high susceptibility of the human 888-MEL cells to vaccinia infection the increasing viral load led to a faster tumor cell destruction, compared to the other two cell lines (Figure 26A, right panel). At the final time point, only 17% or less of the infected tumor cells were viable.

Much stronger cytotoxic effect was observed with an MOI of 0.1 (Figure 26B). The cytotoxicity of all viruses followed a similar path. In contrast to the infection with an

MOI of 0.005, 48% or more of the A549 tumor cells infected at an MOI of 0.1 were killed by all viruses at 96 hpi (Figure 26B, left panel). A better cytotoxic activity was observed in the middle and right panels of Figure 26B. More than 93% of the 1936-MEL and more than 91% of the 888-MEL cells were killed by all viruses at 96 and 48 hpi, respectively.

GLV-1h375, -1h376 and -1h377 viruses killed the cancer cell lines in a dose- and time-dependent fashion and in a similar manner to the parental control virus GLV-1h68. The performed MTT assay demonstrated that the CTLA4 scAb expression in those viruses have not compromised their ability to efficiently kill tumor cells.

4.2.5 Comparison of GLV-1h68- and -1h376-mediated GFP expression in A549 cells

To evaluate the expression of the reporter protein GFP in cell culture, A549 human lung carcinoma cells were infected with GLV-1h68 or GLV-1h376 at an MOI of 0.005 (Figure 27A) or 0.1 (Figure 27B). GFP expression was assessed daily at 24, 48, 72 and 96 hpi by fluorescence microscopy.

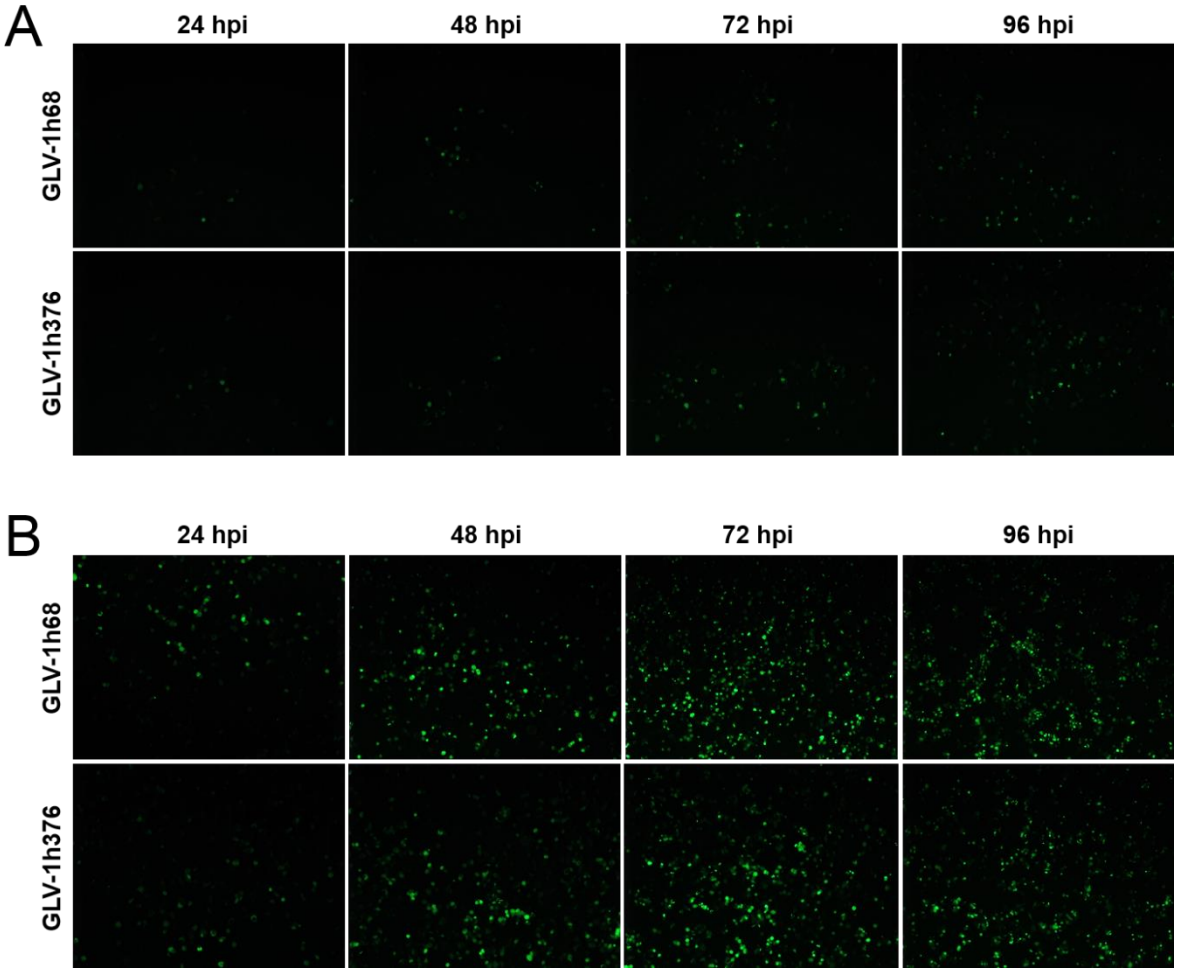

Figure 27. Fluorescence microscopy of virus-mediated green fluorescent protein expression. (A) A549 lung carcinoma cells were infected with GLV-1h68 or -1h376 vaccinia viruses at an MOI of 0.005 (A) or 0.1 (B) and monitored over 96 hours. All the pictures of the set were taken at the same magnification and modified equally by increasing brightness and contrast by 20%. GFP expression in infected cell cultures was visualized by direct fluorescent microscopy. No fluorescent signal was observed in the PBS treated control cells (data not shown).

The replication of both viruses resulted in a very slow increase of marker gene expression during the whole course of the infection for the lower MOI (Figure 27A). In contrast, much stronger GFP expression was observed in the cells infected at an MOI of 0.1 (Figure 27B). Fluorescent signal increased over the first 72 hours after the infection followed by a decline due to viral cytotoxicity and subsequent virus-mediated cancer cell killing.

GFP expression levels in GLV-1h376-infected cells changed in a time- and dose-dependent fashion and in a similar manner to those in cells infected with the control GLV-1h68 virus. The results from the fluorescent microscopy correlate well with the virus replication and cytotoxicity data obtained in 5.2.3 and 5.2.4.

4.2.6 GLV-1h376 virus-mediated GusA and CTLA4 scAb expression and viral titers in cell culture samples

Expression of CTLA-4 scAb and/or GusA and their correlation with viral titers were analyzed and compared in A549 culture samples infected with GLV-1h376 or the control GLV-1h68 virus. This experiment would provide better understanding for the expression patterns of the virus-encoded proteins in the following studies with A549 tumor-bearing humanized mice treated with these two rVACVs. A549 cells were infected with either one of the viruses at an MOI of 0.005 (Figure 28) for up to 96 hours. Collected supernatants and cell lysates from each time point were assayed separately for CTLA4 scAb, GusA and plaque forming units by ELISA, β-glucuronidase assay and standard plaque assay, respectively, and the sum values were presented per milliliter.

First, to evaluate whether the CTLA4 scAb expression affects the expression of the reporter protein GusA, GusA levels and viral titers in A549 cells infected with GLV-1h376 or the parental GLV-1h68 virus were compared (Figure 28A). Both vaccinia virus strains could efficiently replicate in A549 cells in culture and reached comparable viral titers at each time point. Viral titers showed a slight but constant increase during the whole course of the replication assay and no plateau was reached. Although GLV-1h68 titer (4.62×10^3 pfu/ml) at 24 hpi was slightly lower when compared to the GLV-1h376 titer (7.69×10^3 pfu/ml), viral loads for both strains reached similar levels by 48 hours. Highest viral loads reached at 96 hpi were 5.00×10^4 and 3.50×10^4 pfu/ml for GLV-1h376 and GLV-1h68, respectively. Increasing viral titers in the culture samples resulted also in increasing GusA levels throughout the whole assay. Although GLV-1h376 replication during the first 24 hours was slightly more efficient than this of GLV-1h68, GusA concentration in GLV-1h68-infected cells (4.08×10^1 ng/ml) at 24 hpi was slightly higher compared to this in GLV-1h376 treated cells (2.12×10^1 ng/ml). This

difference in the GusA concentrations for both virus strains decreased and they reached similar levels at 72 hpi. Highest GusA concentrations reached at 96 hpi were 5.48 x 10^2 and 4.73 x 10^2 ng/ml for GLV-1h376 and GLV-1h68, respectively. As a conclusion it could be said that this difference in the GusA concentrations between both viruses was observed only in the early stage of the virus infection and was overcome as the infection progressed.

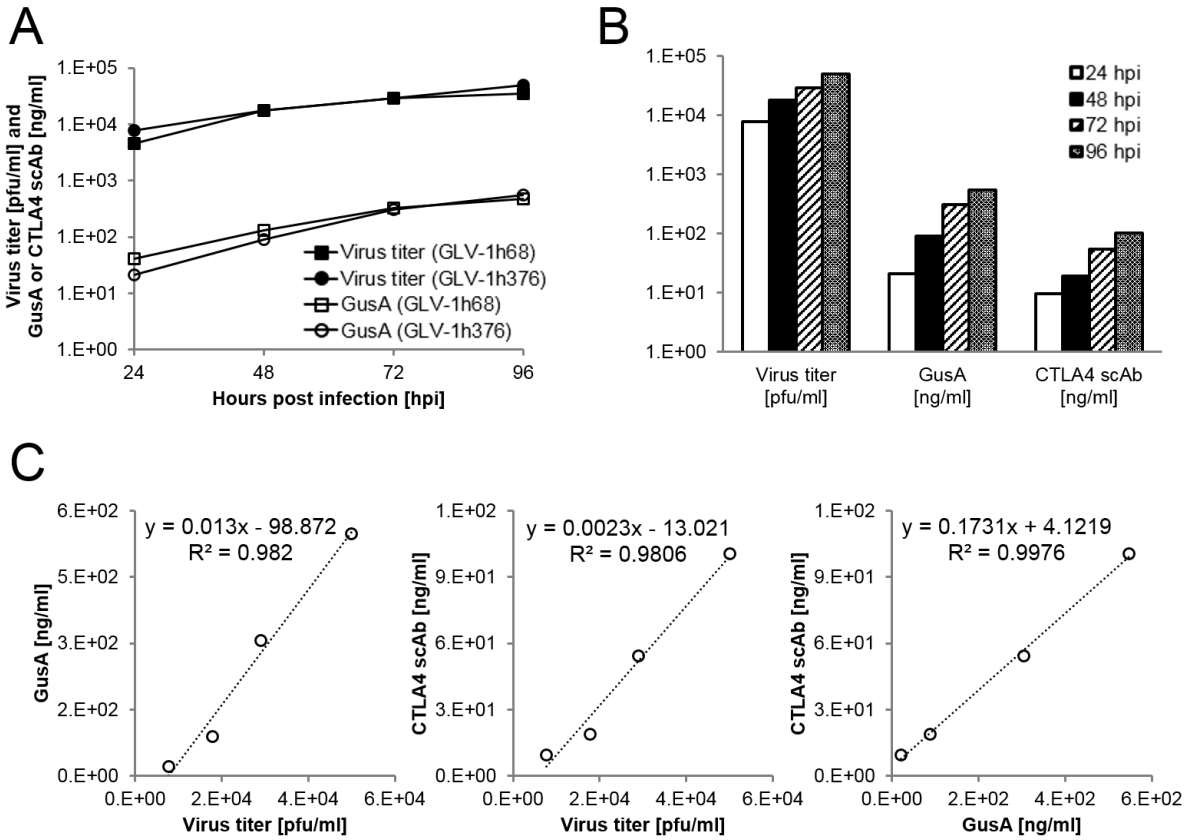

Figure 28. CTLA4 scAb and *E.coli* β-glucuronidase (GusA) expression in GLV-1h376-infected cells. A549 cell cultures were infected with GLV-1h376 or the control GLV-1h68 (CTLA4 scAb^{neg}) strain at an MOI of 0.005. Supernatants and cell lysates of infected cells were harvested separately and in triplicates at 24, 48, 72 and 96 hpi. After collecting all time points, samples were assayed for CTLA4 scAb, GusA and plaque forming units by ELISA, β-glucuronidase assay and standard plaque assay, respectively. Shown values per milliliter are sum of the supernatant and cell lysate values. (A) GLV-1h376-infected cells (circles) showed similar virus replication efficiency (solid fill) resulting in comparable GusA expression pattern (no fill) when compared to those in cells infected with parental GLV-1h68 strain (triangles). (B) The increase in the GusA and CTLA4 scAb levels in GLV-1h376 treated cells resembled the pattern of viral titer increase during the time of the infection. (C) Excellent correlation with correlation coefficients R^2>0.9806 were observed between virus titer, GusA and CTLA4 scAb in GLV-1h376-infected cells.

Next, Figure 28B illustrates the viral titers and GusA and CTLA4 scAb concentrations obtained from GLV-1h376-infected A549 cells at 24, 48, 72 and 96 hpi. Viral replication resulted in increasing virus-mediated protein expression throughout the course of the assay. Correlations between those three parameters are shown in Figure 28C. An excellent correlation with correlation coefficients R^2>0.9820 or R^2>0.9806 were observed between GusA or CTLA4 scAb concentration and viral titer, respectively. Because both proteins correlated with viral replication, a good correlation between them was expected too. Indeed, the correlation coefficient between GusA and CTLA4 scAb was R^2>0.9976. The excellent correlations indicate that each of the three parameters could be used to estimate the amount of the other two when tested in cell culture samples. This also means that only the least time-consuming and labor-intensive of the three assay would be necessary to perform to calculate all variables.

4.2.7 Flow cytometric analyses of blood, spleen and tumor samples derived from GLV-1h376- or GLV-1h68-injected or control humanized A549 tumor-bearing NSG mice

Aim of this mouse study was to evaluate the proportion of B, T and NK cells subsets among the human $CD45^+$ cell population in blood, spleens and tumors of humanized A549 tumor-bearing NSG mice and even more importantly to investigate the main two T cell subsets and their activation status in the presence or absence of the CTLA4 scAb encoding GLV-1h376 or the parental GLV-1h68 rVACV *in vivo*. To start with, newborn NSG mice were humanized and 11 weeks later implanted subcutaneously with A549 cells. In three weeks the tumor volume reached an average of 300 mm^3 and mice were either injected retroorbitally with 6 x 10^6 pfu of GLV-1h68 or -1h376, or left untreated as a control group. All three mouse groups before virus injection had an average of 62 - 64% $CD19^+$ B cells and 21 - 23% $CD3^+$ T cells among their human $CD45^+$ cells in blood, which allowed direct comparison of immune cell subsets between the groups. Ten days after virus administration was performed flow cytometric analysis of blood, spleen and tumor samples (Figure 29 and 30).

4.2.8.1 Flow cytometric analyses of human B, T and NK cell subsets

Percentages of $CD19^+$ B cells, $CD3^+$ T cells and $CD3^-NKp46^+$ NK cells among the human $CD45^+$ cells as well as percentage of $CD56^+$ NK cells among $CD3^-NKp46^+$ NK cells are presented in Figure 29.

Spleens of the humanized mice were reconstituted mainly with B cells (Figure 29A). Highest percentages of B cells were observed for the GLV-1h68 group, where 56.64 ± 9.26 % of the $CD45^+$ cells were $CD19^+$. In blood, B cells represented 33 - 40% of the human hematopoietic cells. In contrast, only 3 - 5 % of the tumor-infiltrating $CD45^+$ cells were $CD19^+$ cells. Generally, no major differences were observed between the three groups.

Figure 29B illustrates the $CD3^+$ T cell portion among the total human hematopoietic cells. The smallest percentage of T cells, about 26%, was observed in the spleens followed by the blood samples, about 40%. In the tumor, $CD3^+$ cells represented the main population with highest values of 56.62 ± 13.60% for GLV-1h376 group, followed by 41.36 ± 20.94% and 39.52 ± 18.13% for non-virus and GLV-1h68-infected groups, respectively.

Second largest population of $CD45^+$ cells infiltrating the tumors after the T cells were $NKp46^+$ NK cells (Figure 29C). Again highest value of 12.34 ± 5.75% was observed in GLV-1h376-infected tumors, this time followed by 11.11 ± 4.07% and 9.95 ± 4.55% for GLV-1h68 and non-virus group, respectively. In contrast, only 1 - 3% and 2 - 6% of the human hematopoietic cells in spleen and blood, respectively, were NKp46 positive.

Further subset analysis of $NKp46^+$ NK cells revealed that $CD56^+$ as well as $CD56^-$ cells were present in the organs from all three groups. In tumors, 89 - 95% of the $NKp46^+$ cells were expressing CD56 (Figure 29D). In contrast, only around 50% and 40% of the NK cells in spleens and blood, respectively, were $CD56^+$. No significant differences were observed between the mouse groups. Majority of the $NKp46^+CD56^+$ NK cells, around 81 - 92 %, in blood and spleens of the three mouse groups were $CD56^{dim}$, unlike the $CD56^{bright}$ cells, which represented less than 19% of the total $CD56^+$ NK cells. In contrast, most of the human $CD56^+$ NK cells in tumors were $NKp46^+CD56^{bright}$, 64 - 80%. Although, no major difference was observed between virus-treated and

control mouse groups, highest percentage of CD56^{bright} NK cells was observed in the GLV-1h376-infected tumors.

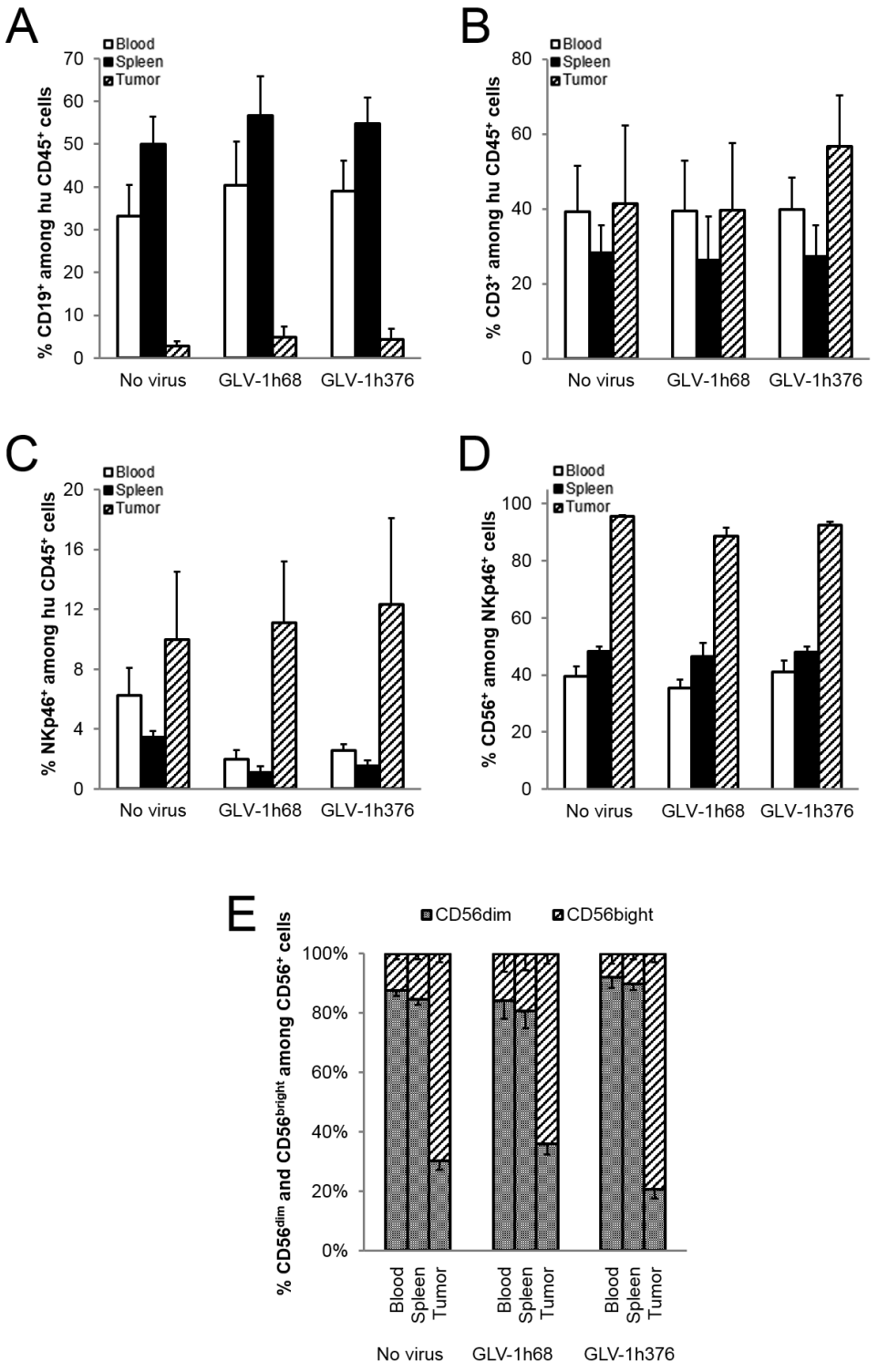

Figure 29. Human hematopoietic cells in tumor-bearing humanized NSG mice. Blood (no fill), spleen (solid fill) and tumor (pattern fill) samples from non-treated (n=4) or GLV-1h68- (n=5) or -1h376- (n=5) injected A549 tumor-bearing humanized NSG mice were analyzed by flow cytometry for presence

of human reconstitution. Analysis were performed 15 weeks post humanization and 10 days after virus administration to virus-treated mouse groups. Human hematopoietic cells were stained with mouse anti-human monoclonal antibodies. B cell (A), T cell (B) and NK cell (C) subpopulations were first gated for human CD45 and then for the respective lineage-specific marker: CD19, CD3 and NKp46, respectively. Values were shown as percentage among the human $CD45^+$ cells. (D) $CD3^-$ $NKp46^+$ subset was additionally examined for CD56 expression. (E) Percentage of $CD56^{dim}$ and $CD56^{bright}$ among $CD3^-$ $NKp46^+C56^+$ NK cells. Mean values and standard errors are plotted.

4.2.8.2 Analyses of human CD4 and CD8 single positive T cell subsets

T cell population in A549 tumor-bearing humanized NSG mice was further investigated. Percentages of $CD4^+CD8^-$ and $CD8^+CD4^-$ cells among the human $CD3^+$ T cells as well as $CD4^+CD25^+$ and $CD8^+CD25^+$ among $CD4^+$ and $CD8^+$ T cells, respectively, are shown in Figure 30.

Figure 30A shows the percentages of differentiated CD4 (left panel) or CD8 (right panel) single-positive cells among the T cells in blood, spleen and tumor samples from all three mouse groups. In blood, $CD4^+$ cells were the main T cell subset representing 51 - 55% of the $CD3^+$ cells (Left panel). $CD4^+$ cells were also the predominant T cell subset in the spleens of all mouse groups. In contrast, only 14 - 25% of the tumor-infiltrating T cells were $CD4^+$. Intriguingly, CD8 single-positive cells were the predominant T cell subpopulation only in both rVACV infected tumors but not in the non-treated tumors or any of the other tested organs (right panel). More interestingly, highest percentage of $CD8^+$ cells (31.39 ± 8.47%) in tumors was observed in the GLV-1h376 treated animals. Similarly, higher percentage of $CD8^+$ cells were detected in spleens of rVACV treated animals compared to the non-treated controls. However, no statistically significant differences were observed between the groups.

Further analysis revealed that 23 - 32% or 33 - 41% of the $CD4^+$ T cells presented in the blood or the spleens, respectively, were expressing CD25 (Figure 30B, left panel). Higher percentages of $CD4^+CD25^+$ T cells were observed in tumors. Surprisingly, highest portion of CD25 expressing cells among tumor-infiltrating $CD4^+$ T cells was found in uninfected tumors of the control animals.

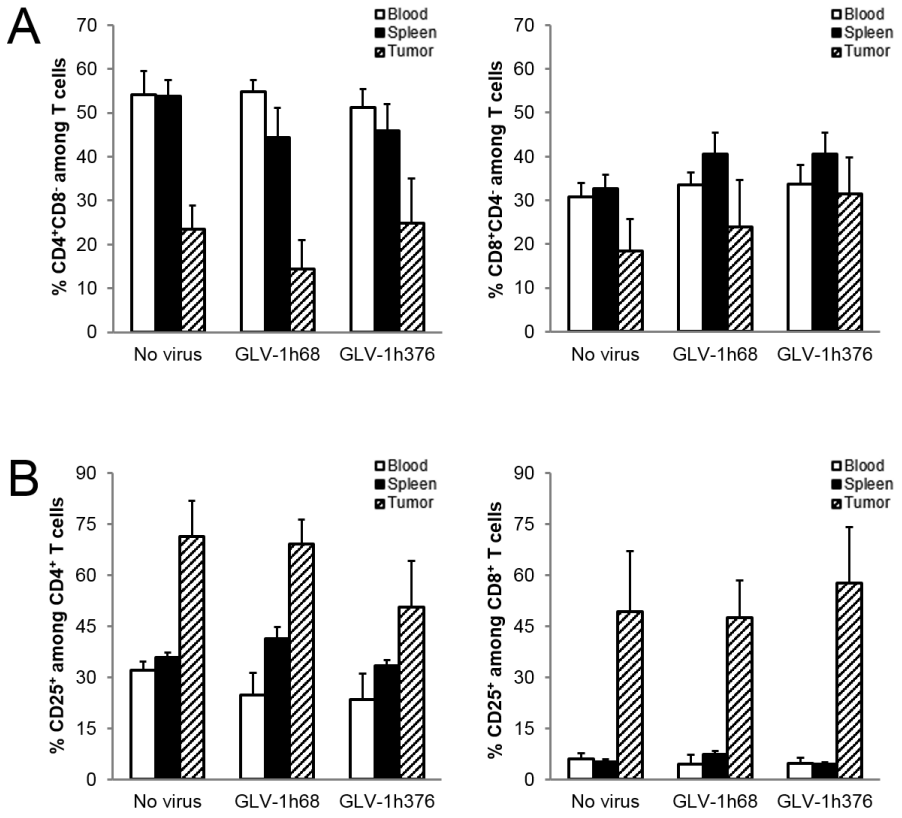

Figure 30. Flow cytometry analysis of T cell population in tumor-bearing humanized NSG mice. A549 tumor-bearing humanized NSG mice were left untreated (n=4) or injected with GLV-1h68 (n=5), -1h376 (n=5) at 14 weeks post humanization. Ten days after virus administration the human T cell population in the blood (no fill), spleens (solid fill) and tumors (pattern fill) of those mice were analyzed by flow cytometry. Cells were stained with mouse anti-human mAb and gated first for human CD45 and then for the respective lineage-specific marker. (A) CD4 (left panel) or CD8 (right panel) expression was determined following gating on all CD3+ T cells. Gating strategy: $CD45^+ \rightarrow CD3^+ \rightarrow (CD4^+$ or $CD8^+)$. (B) $CD4^+CD8^-$ (left panel) and $CD4^-CD8^+$ (right panel) single positive cells were additionally examined for CD25 expression. Gating strategy: $CD45^+ \rightarrow CD3^+ \rightarrow (CD4^+$ or $CD8^+) \rightarrow CD25^+$. Mean values and standard errors are plotted.

Evaluation of the $CD8^+$ T cells revealed a significant activation of those cells in tumor samples (Figure 30B, right panel). Interestingly, in GLV-1h376-infected tumors was found the highest percentage (57.56 ± 16.62%) of activated $CD8^+$ T cells. In contrast only 4 - 7% of those cells were activated in the blood and spleens of all three mouse groups. Again, no statistically significant differences were observed between the mouse groups.

4.2.9 Activation of T cells from control or GLV-1h68- or -1h376-injected A549 tumor-bearing NSG mouse-derived splenic tissue

Single cell suspensions were prepared from spleens excited from non-treated or GLV-1h68- or -1h376-injected A549 tumor-bearing humanized NSG mice about 15 weeks after reconstitution with human hematopoietic cells and 10 days after virus administration. First, it was evaluated whether the T cells among those splenocytes could be activated with commercially available beads, loaded with anti-human CD2, CD3 and CD28 antibodies, designed to activate specifically human T cells. Another objective of this experiment was to investigate the ability of the T cells among the splenocytes to recognize A549 cells in culture and therefore be activated. Furthermore, the activation patterns between all three mouse groups were evaluated for any differences. To do so, equal number of splenocytes from each mouse were separated into three wells with equal volume of culture media. The cells from the first well were left untreated as a control and used to set up the gates in the consequent flow cytometric analyses. Activation beads or irradiated A549 cells were added to the other two wells.

After 48 hours in culture splenocytes were studied under a light microscope (Figure 31A). Typical clumps of activated T cells and beads could be observed in the beads-activated wells (middle panel). Some of the clumps were of larger size and could be seen even with a bare eye. These clumps could not easily be disrupted by simply agitating the plates. In contrast, some much smaller groups of splenocytes, that looked slightly different and could be disrupted easier, have built around rounded, dying A549 cells (right panel). As expected, very few to none grouped splenocytes were found in the control wells (left panel).

Next, the expression of the late activation marker CD25 on the cell surface was analyzed by flow cytometry (Figure 31B). Percentages of CD25 expressing cells among the respective parental population are shown. After activation with beads, significantly more CD25 expressing cells were observed among $CD4^+$ and $CD8^+$ T cells when compared to the respective control samples. The highest 78.70 ± 8.63% of $CD4^+CD25^+$ T cells was found in the GLV-1h376 group. For the $CD8^+$ T cells, highest

percentages of activated cells were observed in the GLV-1h68 and -1h376 groups with values of 95.32 ± 1.44% and 95.29 ± 3.16%, respectively. In contrast, incubation with A549 cells did not increased CD25 expression on $CD4^+$ T cells. Respectively, no statistically significant differences were observed between the $CD4^+$ T cells incubated with A549 cells and the control samples (Figure 31B, left panel). No increase in CD25 expression on $CD8^+$ T cells was found either (Figure 31B, right panel). Interestingly, a p-value <0.01 was calculated when comparing percentages of $CD8^+CD25^+$ T cells between control and A549 cell-treated samples in the GLV-1h376 group. The reason for that was a slight but present in all samples reduction in $CD8^+CD25^+$ T cells after incubation with the A549 cells in combination with a very small standard deviation. The p-value from this t-test might be mathematically significant, but has no biological importance.

Figure 31C illustrates the flow cytometric analyses of the intracellular IFN-ɣ synthesis in the $CD4^+$ and $CD8^+$ T cells. Percentages of cytokine expressing cells among the respective parental population are shown. Beads activated $CD4^+$ T cells showed significant increase in IFN-ɣ expression compared to the respective control samples (Figure 31C, left panel). The highest 32.80 ± 4.34% of $CD4^+$ IFN-ɣ $^+$ T cells was found in the GLV-1h376 group. Statistically significant increase in IFN-ɣ expression was observed also among the beads activated $CD8^+$ T cells derived from non-virus or GLV-1h376 treated mice, but again, in GLV-1h376 group, the increase of IFN-ɣ expressing $CD8^+$ T cells was most prominent, with 56.96 ± 3.98% of the cells producing the cytokine (Figure 31C, right panel). Although the number of IFN-ɣ expressing cells among beats activated $CD8^+$ T cells in the GLV-1h68 group also increased dramatically, there was no statistically significant difference between the beads activated and the control wells, due to higher standard error.

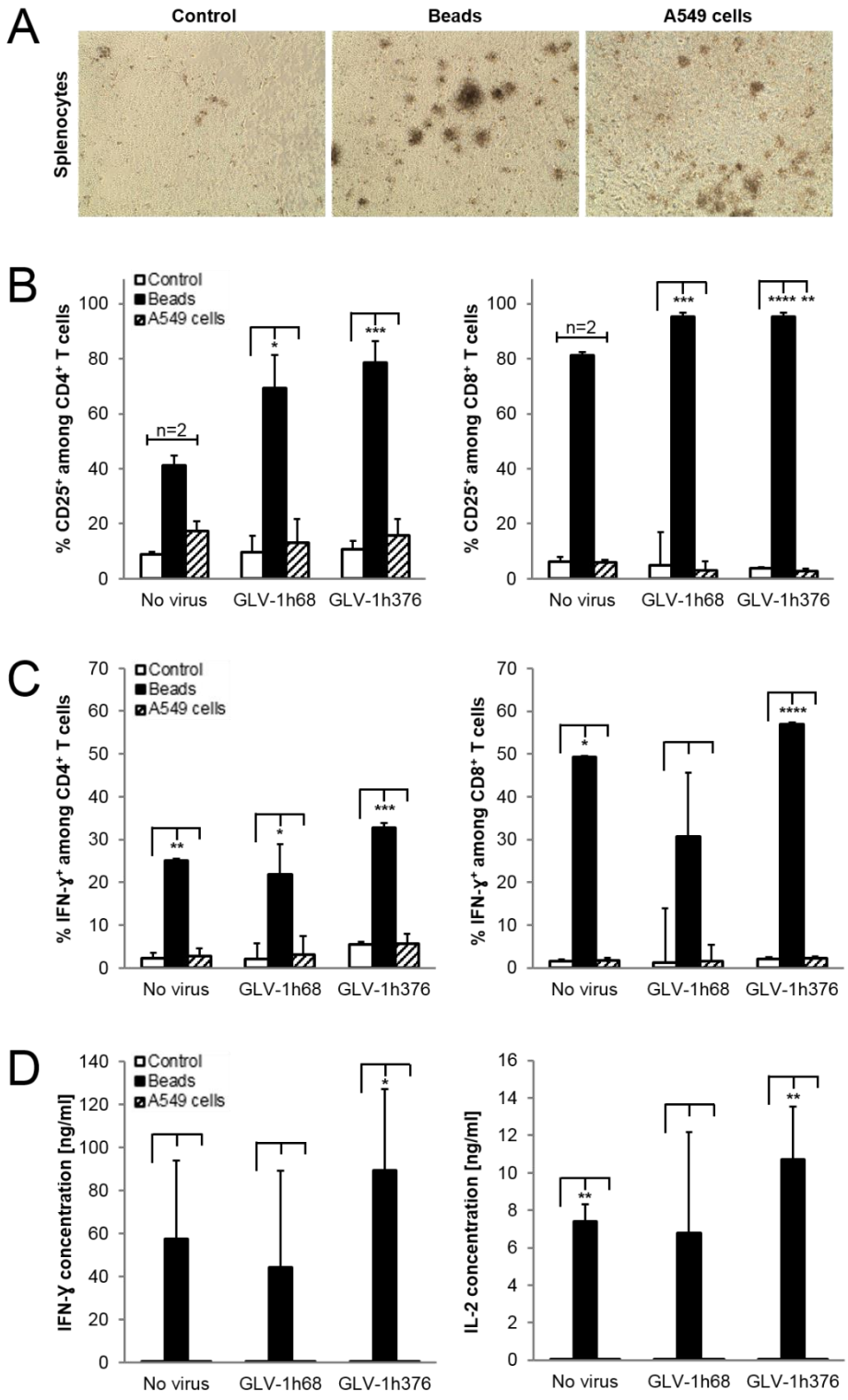

Figure 31. Splenocytes activation assay. A549 tumor-bearing humanized NSG mice were left untreated or injected with GLV-1h376 or -1h68 at 14 weeks post humanization. Ten days after vaccinia virus administration spleens from all three mouse groups were collected. Single cell suspension from each spleen was separated into three groups, in 2 ml culture medium each, and treated with PBS (no fill), anti-biotin beads loaded with biotinylated CD2, CD3 and CD28 antibodies from Miltenyi Biotech (solid fill) or irradiated A549 (pattern fill). (A) Light microscopy of splenocytes after treatment. (B) Cells

were stained with mouse anti-human mAb against surface markers and subjected to flow cytometric analysis. CD25 expressing $CD4^+$ (left panel) and $CD8^+$ (right panel) subpopulations were first gated for human CD45 and then for the respective lineage-specific marker. Gating strategy: $CD45^+ \rightarrow CD3^+ \rightarrow (CD4^+ \text{ or } CD8^+) \rightarrow CD25^+$. Bar graph shows mean values in percentage and standard errors of no virus (n=2), GLV-1h68 (n=3) and GLV-1h376 (n=4) groups. (C) Human interferon-gamma (IFN-ɣ) expression in $CD4^+$ (left panel) and $CD8^+$ (right panel) T cells was determined by intracellular staining using a mouse anti-human IFN-ɣ mAb. Gating strategy: $CD45^+ \rightarrow CD3^+ \rightarrow (CD4^+ \text{ or } CD8^+) \rightarrow IFN\text{-}ɣ^+$. Mean values in percentage and standard errors for no virus (n=3), GLV-1h68 (n=4) and GLV-1h376 (n=5) groups are plotted. (D) Human IFN-ɣ (left panel) and IL-2 (interleukin-2, right panel) levels in splenocytes culture supernatant samples were assayed by ELISA. Mean values in nanogram per milliliter and standard errors for no virus (n=3), GLV-1h68 (n=4) and GLV-1h376 (n=5) groups are plotted.

Finally, IFN-ɣ as well as Il-2 levels in collected culture supernatants from the analyzed splenocytes were measured by ELISA (Figure 31D). Dramatic increase in IFN-ɣ expression levels was observed in all three groups when activated with beads (Figure 31D, left panel). However, significant increase in the cytokine levels was detected only in the GLV-1h376 group, due to very high variations in the other two groups. Highest IFN-ɣ concentration, with value of 89.25 ± 37.76 ng/ml, was detected in the GLV-1h376 group. In addition to the high IFN-ɣ concentration, supernatants of beads activated cells showed evaluated IL-2 levels as well (Figure 31D, right panel). Compared to control samples, significant differences were observed in non-virus and GLV-1h376 groups. Again, highest IL-2 concentration with value of 10.72 ± 2.80 ng/ml was measured in the GLV-1h376 group. The incubation of the splenocytes with A549 cells has not increased cytokine production in any of the tested samples. No significant differences between groups were found.

4.2.10 Visualization of virus-mediated GFP expression in tumors

Successful colonization of subcutaneous A549 tumors with GFP-encoding GLV-1h68 and -1h376 viruses was visualized by direct fluorescent microscopy (Figure 32). A549 tumor-bearing humanized NSG mice were injected with GLV-1h68 (n=5) or -1h376

(n=5) at 14 weeks post humanization, or left untreated (n=4) as a control mice. Ten days after virus administration tumors were excised and monitored. All virus-infected tumors were expressing GFP. Representative pictures for both viruses are shown in Figure 32. No fluorescent signal was observed in the untreated control tumors (data not shown).

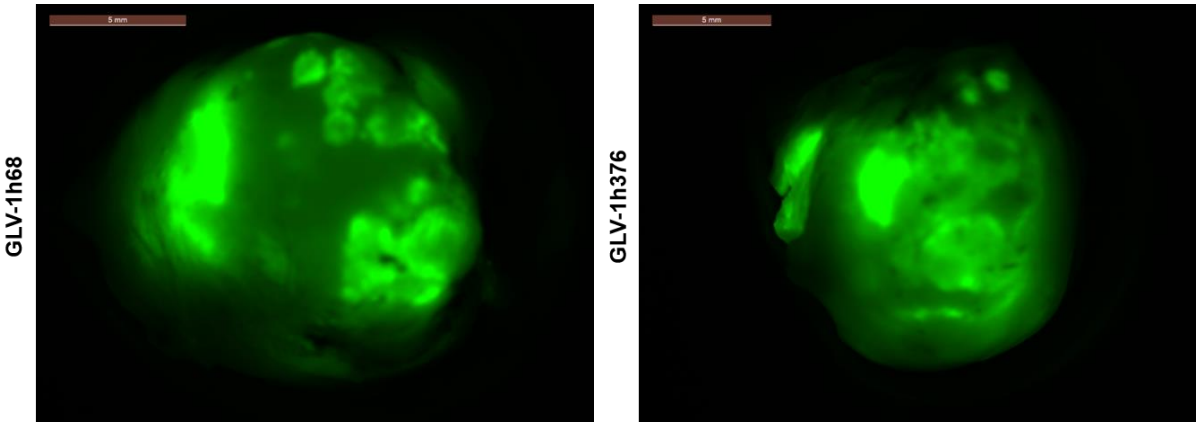

Figure 32. Fluorescence microscopy of virus-mediated green fluorescent protein (GFP) expression in tumors. A549 tumor-bearing humanized NSG mice were injected r.o. with 6 x 10^6 viral particles of GLV-1h68 or -1h376. Ten days post infection tumors were excised and examined for GFP expression. Representative, non-modified pictures from both virus groups are shown. GFP expression in infected tumors was visualized by direct fluorescent microscopy.

4.2.11 Virus-mediated GusA and CTLA4 scAb expression and viral titers in humanized mice-derived A549 tumors

Expression of CTLA-4 scAb and/or GusA and their correlation with viral titers were analyzed and compared in A549 tumor samples infected with GLV-1h376 or the control GLV-1h68 virus (Figure 33). A549 tumor-bearing humanized mice were treated with either one of the viruses by r.o. administration of 6 x 10^6 pfu. Ten days after virus administration single cell suspension from excited tumors were prepared and assayed for CTLA4 scAb, GusA and plaque forming units by ELISA, β-glucuronidase assay and standard plaque assay, respectively, and the values were calculated per 1 g of tumor tissue. Tumors from untreated control animals were used to confirm lack of any of the tested three parameters (data not shown).

First, to evaluate whether the CTLA4 scAb expression affects the expression of the reporter protein GusA, GusA levels and viral titers in A549 tumors infected with GLV-1h376 or the parental GLV-1h68 virus were compared (Figure 33A). Both vaccinia virus strains could efficiently replicate in A549 tumors *in vivo* and reached comparable viral loads at day 10 after the infection. Viral titers of 3.56 x 10^8 and 5.74 x 10^8 pfu/1g tumor and corresponding GusA concentrations of 1.43 x 10^6 and 1.94 x 10^6 ng/1g tumor were observed for GLV-1h68 and GLV-1h376, respectively.

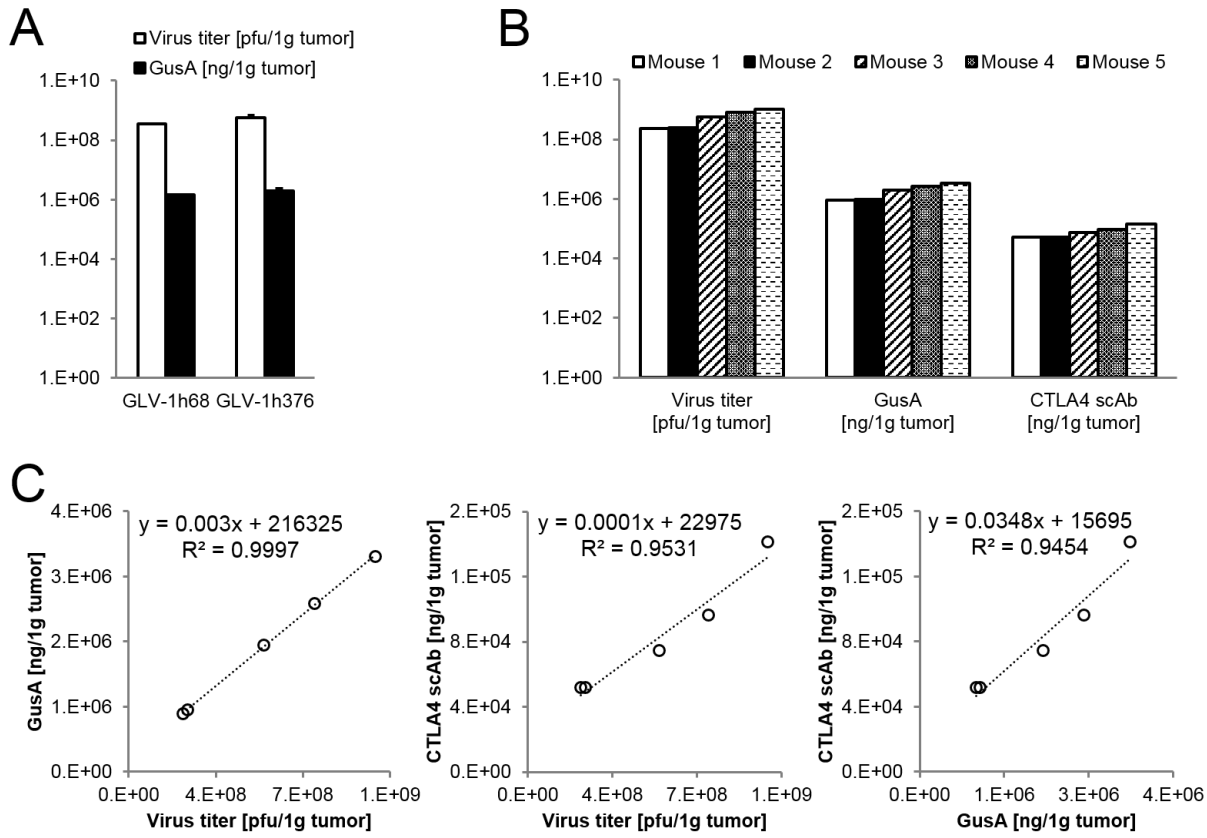

Figure 33. CTLA4 scAb and *E.coli* β-glucuronidase (GusA) expression in GLV-1h376-infected tumors in mice. A549 tumor-bearing humanized NSG mice were injected with GLV-1h68 (n=5), -1h376 (n=5) at 14 weeks post humanization, or left untreated as control mice. Ten days after virus administration tumors were excised. Prepared single cell suspensions were assayed for plaque forming units, GusA and CTLA4 scAb by standard plaque assay, β-glucuronidase assay and ELISA, respectively. Values are shown per 1 g of tumor tissue. (A) Similar virus titer (no fill) and GusA concentrations (solid fill) were detected in tumors infected with GLV-1h376 as well as the parental GLV-1h68 strain. Mean values and standard errors are plotted. (B) Viral titer and GusA and CTLA4 scAb concentration in tumors from five GLV-1h376 treated mice. (C) Excellent correlation with correlation coefficients R^2>0.9454 were observed between virus titer, GusA and CTLA4 scAb in GLV-1h376-infected tumors.

Next, Figure 33B illustrates the viral titers and GusA and CTLA4 scAb concentrations obtained from five GLV-1h376-infected A549 tumors. Higher viral loads corresponded to higher protein concentrations. Correlations between those three parameters are shown in Figure 33C. An excellent correlation with correlation coefficients R^2>0.9997 or R^2>0.9531 were observed between GusA or CTLA4 scAb concentration and viral titer, respectively. Because both proteins correlated with viral replication, a good correlation between them was expected too. Indeed, the correlation coefficient between GusA and CTLA4 scAb was R^2>0.9454. The excellent correlations indicate that each of the three parameters could be used to estimate the amount of the other two when tested in tumor samples. This also means that β-glucuronidase assay as the least time-consuming and labor-intensive of the three assay would be sufficient to perform to calculate all variables.

5 Discussion

According to the World Health Organization cancer remains responsible for millions of deaths worldwide with approximately 90% of the cancer deaths caused by metastatic recurrence. The inability of conventional cancer treatment modalities such as surgery, chemotherapy and radiation therapy to always lead to a complete cure or even to prolong the life of all cancer patients, requires finding new less invasive and more effective cancer treatment options, which can be used alone or in combination with the conventional therapies. One promising new approach for the treatment of human cancer is the use of oncolytic viruses, which exhibit a natural or genetically engineered tumor tropism. Ones of the top candidates in this area are the oncolytic vaccinia viruses. The use of vaccinia virus for the smallpox vaccination provided important information on its behavior in humans [12] making it the virus with the longest and the most extensive history of use in humans. The injection of the virus into the bloodstream of cancer patients and its systemic delivery through the leaky tumor vasculature into solid tumors and their metastases in mouse models and clinical trials has already shown promising results [18-20] (www.clinicaltrials.gov; keywords: GL-ONC1 and vaccinia). However, due to discrepancies in both innate and adaptive immunity between mice and men [72] the evaluation of the vaccinia virus' interactions with the host immune system in mice are not fully conclusive of what is actually happening in human cancer patient after VACV systemic administration. Further, ethical and legal concerns as well as risk of potential toxicity limit research involving human patients. Therefore, a good *in vivo* model for testing interactions between VACV and human immune cells, avoiding the numerous limitations and risks associated with human studies, is the humanized mouse model. It is an excellent small animal model that could improve our understanding of the physiology of the human immune system and the immune responses to diseases and pathogen agents. The advances in mammalian genetics during the last 30 years led to the development of new immunodeficient mouse models that allowed successful engraftment with human hematopoietic stem cells. The highest levels of human immune system reconstitution after human $CD34^+$ stem cell transplantation in newborn mice [63, 66] were observed in the highly immunodeficient NOD/SCID/IL2rγ^{null} (NSG) mouse strain [65]. In 2011, Wege *et al*. reported the first humanized tumor mouse model [67]. This model involves

a co-transplantation of human umbilical cord blood-derived $CD34^+$ cells and human cancer cells into the liver of newborn NSG mice resulting in a stable, long-term, multilineage reconstitution of a functional human immune system and at the same time development of solid tumors and tumor metastases without sign of rejection. The humanized tumor mouse model was utilized at the end of my Master Thesis [73]. However, a major drawback of this model was the injection of tumor cells at this early stage of mouse development in the liver. Not all of the injected tumor cells remained in the liver but reached other organs in the abdominal cavity and built tumors there. Therefore, before the age of 10 weeks or older, when multilineage human hematopoietic reconstitution with developed T cells could be detected also in peripheral mouse blood, multiple large tumors have developed in multiple mouse organs. Because these tumors developed in the abdominal cavity, a precise caliper measurements of their size was impossible. As a result, deteriorated health status of the mice and early mouse death was observed. Therefore, a major part of this thesis focused on the establishment of a new humanized mouse model with subcutaneous human tumor (Figure 34).

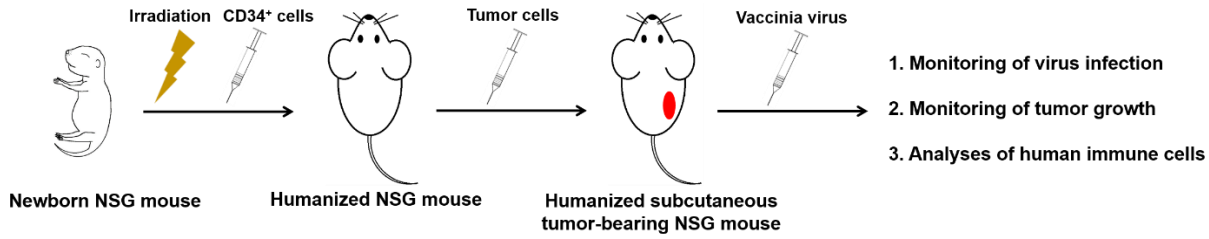

Figure 34. Schematic overview of the generation of the humanized subcutaneous tumor-bearing NSG mouse model for evaluation of VACV-mediated oncolytic therapy in the context of the human immune system.

Such small animal model would allow the evaluation of the oncolytic properties of vaccinia virus and at the same time the interactions of the virus with the host immune cells in the context of the human immune system. Indeed, implantation of human A549 lung cancer cells under the skin of humanized NSG mice resulted in a progressive tumor growth. These tumor-bearing humanized mice were treated with different oncolytic VACV strains and immune cells in tumors and other organs were analyzed by flow cytometry for any marked changes when compared to non-virus-treated control

animals. To my knowledge, this work describes for the first time that NSG mice engrafted with human cord blood-derived $CD34^+$ stem cells could successfully be subcutaneously implanted with human tumor cells at 10 - 13 weeks post humanization without any sign of rejection.

5.1 Studying the human immune system response to LIVP-1.1.1 vaccinia virus in a novel humanized NSG mouse model with subcutaneous human tumors.

The development of malignant tumors might be seen as a failure of the host antitumor immunosurveillance. During the multistep process of tumorigenesis tumors adopt mechanisms allowing them to attract excessive levels of immune tolerance-inducing components of the host immune system [35] and damp antitumor immune responses [36]. Although, the oncolytic vaccinia virus itself possesses a large panel of immunosuppressive gene products [10] its selective and highly efficient VACV replication in tumor cells overwhelms the translational machinery of the host cells inducing ICD through the released DAMPs [35], which subsequently activate the immune system. Additionally, the lysis of infected tumor cells leads to release of large amounts of PAMPs. DCs activate T cells by presenting them the released VAAs and TAAs, recruiting effector T cells to the site of infection. In the current study it was investigated whether infection with VACV can indeed overcome the localized tumor-mediated immune suppression and to increase antitumor immunity by attracting tumor-infiltrating effector lymphocytes to the tumor site in the here established humanized subcutaneous tumor-bearing NSG mouse model (Figure 34).

In initial cell culture experiments, two vaccinia viruses, LIVP-1.1.1 and GLV-2b372, were investigated for their potential to infect, replicate in and kill human A549 lung cancer cells. LIVP-1.1.1 was chosen as a test virus, because it is an attenuated isolate from the wt LIVP with naturally disrupted *J2R* locus and allowed investigation of the VACV effect on the immune system in animals without addition of any potentially immunogenic transgenes' products. The second test virus, GLV-2b372, was delivered from LIVP-1.1.1 by inserting the TurboFP635 expression cassette at the *J2R* locus.

Therefore, unlike its parental virus, GLV-2b372 provide a monitoring option. The performed replication and cytotoxicity assays demonstrated that both viruses were able successfully and in a similar manner to infect, replicate in and destroy the tumor cell cultures. The replication capability of the GLV-2b372 virus was not altered by the insertion of the TurboFP635 expression cassette into the viral genome. The results also evidently showed, that both, virus replication and virus-mediated cell killing, were dose- and time-dependent for both viruses.

The expression of the reporter protein TurboFP635 in GLV-2b372-infected A549 cell culture correlated very well with the replication and cytotoxicity data and increased with the time in viral dose-dependent fashion. The results demonstrated that measurement of the increasing TurboFP635 expression correctly represent increasing viral titers in cells, suggesting that GLV-2b372 could be used instead of LIVP-1.1.1, when *in vivo* monitoring of the infection in cell culture or in animal studies is desired.

After it was shown that the A549 cells could be successfully infected and killed by the LIVP-1.1.1 and GLV-2b372 viruses in culture, the human lung carcinoma cell line was used to establish the humanized subcutaneous tumor-bearing NSG mouse model. For this model preconditioned newborn NSG mice were injected into the liver with human cord blood-derived $CD34^+$ cells and 10 - 13 weeks later s.c. implanted with A549 cells into the right hind leg (Figure 34). In contrast to previous report [67], which suggest that the tumor cells must be implanted together with the human hematopoietic stem cells, in order to prevent their rejection by the developed human immune system, the A549 cells successfully formed tumors. At 3 - 4 weeks after implantation, tumors reached an average size of 300 - 400 mm^3. Multiple blood vessels and hemorrhagic regions were observed in tumors obtained from non-humanized and humanized animals, which did not receive a VACV treatment. The finding was in line with the knowledge that growing tumors are able to induce and sustain angiogenesis, via activation of an “angiogenic switch” [3, 5]. The tumor-associated neovasculature provides oxygen and nutrients supply for the growing tumor tissue. In contrast, the majority of tumors excited from VACV-treated tumors had more compact structure with very little to none visible blood vessels. This result was expected, due to the fact that many oncolytic viruses have the natural antiangiogenic properties to target, infect and destroy developing and established tumor vasculature without harming normal blood vessels of the host [74]. More specifically, VACV infects CD31 positive tumor

endothelial cells and thus reducing the vasculature density of the blood vessels, which together with the direct tumor cell lysis ultimately leads to the virus-mediated eradication of the tumor.

Macroscopic examination of the spleens showed detectable increase in splenic cellularity in most humanized animals compared to non-humanized control mice. Reason for this expected increase was the reconstitution of the mouse spleens with human immune cells [62]. Additionally, mild splenomegaly was observed in VACV-injected humanized animals when compared to non-treated humanized mice.

Successful *in vivo* infection of the tumors after systemic administration of the vaccinia virus was demonstrated by treating a small group of humanized A549 tumor-bearing NSG mice with GLV-2b372. The virus selectively infected and replicated in the tumors, which were therefore expressing TurboFP635. Imaging of the live animals at different time points after the virus injection showed initial 22-fold increase of fluorescent signal in tumors during the first 8 days of the infection. Afterwards, TurboFP635-mediated fluorescence declined, suggesting that most tumor cells were already lysed or that the virus got cleared by the immune system. Indeed, immunohistochemical analyses of GLV-2b372-infected tumors revealed that 15 dpi virtually the whole sections were positive for vaccinia virus. At that late time point, the majority of tumor cells were lysed and extensive necrotic regions and lesions were observed, which explain the decreased TurboFP635-mediated fluorescent signal. Similar infection progression with significantly increasing areas of virus infection were observed also in paraffin slides from tumors treated with the parental LIVP-1.1.1 virus.

Regarding the humanization process, the intrahepatic transplantation of preconditioned newborn NSG mice with human cord blood-derived $CD34^+$ stem cells resulted in a successful systemic reconstitution with human immune cells. As previously reported, cells from lymphoid and myeloid lineage developed [65, 67]. $CD19^+$ B cells, $CD3^+$ T cell, $NKp46^+$ NK cells as well as $CD33^+$ myeloid cells were detected among the human $CD45^+$ cells in blood and spleens of non-tumorous and tumor-bearing humanized mice in very close proportions comparing the both mouse groups. At early time points after engraftment, the majority of the human hematopoietic cells detected in the mouse blood were $CD19^+$ B cells and only a small portion were $CD3^+$ T cells. With time a significant change in $CD19^+/CD3^+$ ratio was reported with a

decrease of B cells and an increase of T cells. These results suggested that for experiments focusing on the T cell population it would be necessary to use mice which are at least 10 weeks post humanization.

Before investigating the human reconstitution levels in the humanized tumor-bearing model, the presence of human B, T and NK cells were first evaluated in blood and spleen of control and LIVP-1.1.1 vaccinia virus-injected non-tumorous humanized NSG mice. At 8 weeks post humanization, flow cytometric analysis of the samples showed that the majority of the human $CD45^+$ cells in blood of both mouse groups were B cells. Even higher percentage of B cells were observed in spleens of those animals. Respectively, T cells represented higher percentage of the human hematopoietic cells in the blood when compared to spleens. The higher observed B to T cells 3.5:1 ratio in splenocytes differs from the previously reported 2:1 because of the earlier time point of 8 weeks compared to the reported >4 months after engraftment to perform the flow cytometric analysis [75]. This result is in line with what has been said above, that T cells increased with time in this mouse model, explaining the higher T cell percentages observed by Strowig *et al.*.

Further evaluation of the T cell population showed that both CD4 as well as CD8 single positive T cells were present in blood and spleens of the humanized mice. The T cells are an important immune cell subset during oncolytic virotherapy. For successful immune response during oncolytic virotherapy is essential that activation and proliferation of tumor- and virus- specific T cells occur. Activated cytotoxic $CD8^+$ T cells with developed effector properties are then able to move to the tumor site, which represents also the site of viral infection, and to destroy tumor cells and kill the pathogen [35, 36]. Also, activated $CD4^+$ helper T cells provide essential additional signals necessary to promote and maintain cytotoxic T cell, macrophage and other immune cell functions [76]. Before evaluating the CD25 late activation marker expression [77, 78] on $CD4^+$ and $CD8^+$ T cells in tumor-bearing mice, CD25 expression was first studied in non-tumorous mice in absence or presence of vaccinia virus. However, the introduction of virus in the LIVP-1.1.1-injected mouse group did not significantly changed the activation status of these two T cell subsets when compared to the control group. Very few $CD8^+CD25^+$ and much more $CD4^+CD25^+$ T cells were found in blood and spleen of both mouse groups. Some of the CD25 expressing $CD4^+$ T cells are regulatory T cells, which central role is to protect the individual from

excessive immune responses and autoimmunity [67, 79, 80]. However, because of small blood sample volume, limited number of mice as well as limitation in total sample number for acquisition on flow cytometer it was not possible to examine additional cell surface markers to further phenotype the $CD4^+$ T cell subset to be able to differentiate the Treg cells.

Beside B and T cells, the $CD3^-NKp46^+$ NK cell population was also evaluated. In humans, NKp46 is a NK-specific marker, which is exclusively expressed only on resting and activated NK cells [81]. In the performed study, NK cells represented as little as 1 - 2% of the $CD45^+$ cells in blood and in spleens in both mouse groups. Further subset analysis of $NKp46^+$ NK cells revealed that $CD56^-$ as well as $CD56^+$ cells were present in the organs from both groups. The presence of $NKp46^+CD56^+$ as well as $NKp46^+CD56^-$ cells in humanized mice was initially reported by Strowig *et al.* and later confirmed by Wege *et al.* [67, 82]. Except in humanized mice, $NKp46^+CD56^-$ cells could also be found in human cord blood and in blood from human healthy donor [82]. However, although in CB they represent 30% of the NK cells, in adult blood only around 3% of the NK cells are $NKp46^+CD56^-$, suggesting that this phenotype might correspond to resting NK cells prior to history of pathogen exposure. Indeed, it has been demonstrated that activation of humanized mouse-derived $NKp46^+CD56^-$ NK cells leads to up-regulation of CD56 expression [82, 83]. As previously reported [82], around 50% of the human NK cells among the humanized mouse-derived splenocytes in this study were $NKp46^+CD56^+$. In contrast, only less than 2% of the NK cell in the blood were expressing CD56. However, no difference in CD56 expression levels among NK cells was observed between virus-treated and control groups. In human blood, NK cells could be additionally divided into two groups on the basis of the CD56 marker expression strength, abundant cytokines producers $CD56^{brigh}$ and cytotoxic $CD56^{dim}$ NK cells [84]. Produced cytokines are a variety of proinflammatory, such as IFN-ɣ, IL-2 etc., or immunosuppressive molecules, such as IL-4, IL-10 etc., [84, 85]. In humans, $CD56^+$ NK cells in blood, lymph nodes or various peripheral tissues consist of different rates of the $CD56^{bright}$ and $CD56^{dim}$ phenotypes. Also, the abundant cytokines producers $CD56^{brigh}$ could be producing proinflammatory or inhibitory molecules depending on the tissues they are residing in. Although, NK cells have traditionally been seen as effector lymphocytes capable of spontaneous cytotoxicity against body's foreign, transformed or infected cells without the need of preactivation

or prior exposure to antigen [82, 86, 87], the concept of regulatory NK (NKreg) immerged too [84, 86]. In blood and spleens of the tested mice, the majority of the NK cells expressing CD56 were NKp46^{+}CD56^{dim}. However, further characterization on those CD56^{dim} and CD56^{bright} cells, in terms of type of cytokine expression as well as identification of other surface markers, to determine their cytotoxic, immunosuppressive or immunostimulatory function in the different organs of the humanized mice was not possible due to limitations in number of mice and volume of samples.

After evaluating the reconstituted human immune system components in non-tumorous humanized mice, human immune cell subsets were studied in humanized NSG mice with subcutaneously implanted A549 tumors in the presence or absence of the LIVP-1.1.1 vaccinia virus. The percentages of B, T and NK cells among the human CD45^{+} cells in blood and spleens of tumor-bearing mice were very close to those seen in the non-tumorous humanized mice. Interestingly, almost no B but plenty of T and NK cells were detected in tumors. An increased NK cell percentages among tumor-infiltrating human CD45^{+} cells were expected because NK cells are part of the innate immune system serving as a first-line defense against malignant and virus-infected cells [85-89]. However, presence of virus in the LIVP-1.1.1-infected tumors did not additionally increased NK cell percentages but even the contrary, a slightly higher percentage of those cells were observed in the non-virus group. More interestingly, further examination of the NKp46^{+} NK cell population in the tumors revealed that almost 100% of those cells were CD56^{+}, but again, no difference was observed between the LIVP-1.1.1-treated and the control mouse group. Even more, 86.74 ± 2.19% and 74.80 ± 5.91% from the CD56^{+} NK cells in non-treated and LIVP-1.1.1-infected tumors, respectively, were CD56^{bright}. This observation significantly differed from what was seen in the blood and spleens of those mice, where CD56^{bright} cells represented only less than 13% of all NKp46^{+}CD56^{+} NK cells. Because the increased numbers of NK cells among the tumor-infiltrating human CD45^{+} cells and the increased rate of CD56^{bright} cells among those NK cells were observed not only in the VACV-infected but also in the non-treated tumors, it was suggested that the reason for that were the implanted human A549 tumor cells and not the subsequent infection of those tumors with the virus. Unlike previous report [67], where tumor cells were implanted together with the human cord blood-derived CD34^{+} stem cells into newborn

NSG mice in order to avoid allograft rejection of eventually human leukocyte antigen (HLA) mismatched human A549 cells, in the here present humanized tumor mouse model, tumor cells were implanted 10 weeks or later after humanization. Therefore, developed human immune cells responded eventually in some way to the growing most probably mismatched A549 tumors. However, implanted tumor cells were able to form growing tumors, indicating that the human immune system in the humanized mice did not reject them. NK cells have already been shown to be able to promote allograft tolerance [86, 90-92]. More interestingly, a high number of NK cells in the uterine endometrium that were almost exclusively $CD56^{bright}$ and produced IL-4 and IL-10 have been shown to play an important role in trophoblast invasion, development of placenta, angiogenesis and maintenance of the early pregnancy [84, 85]. Immunoregulatory $CD56^{bright}$ cells, which downregulate the immune responses and reduce inflammation by producing the immunosuppressive cytokine IL-10, were observed also in context of different diseases [84]. Therefore, it was suggested that a large percent of the $CD56^{bright}$ cells found in the tumors of the humanized mice were NKregs, which deliver immunosuppressive cytokines and alter T cell responses allowing the A549 cell graft and tumor development. However, further characterization on those $CD56^{bright}$ and $CD56^{dim}$ cells would be necessary to determine their cytotoxic, immunosuppressive or immunostimulatory function in the tumors of this mouse model.

In regard to the human T cells found in tumors, approximately half of them were $CD4^+$ and the other half were $CD8^+$, and the majority of them were expressing CD25 on their surface. Nevertheless, greatest activation of the cytotoxic $CD8^+$ cells was again not caused by the virus, because even in the absence of virus, they showed up-regulated CD25 expression. Therefore, this finding suggested that some of the $CD56^{bright}$ cells found in tumors might be performing also immunostimulatory functions, or that the recognition of the tumor antigens presented to the T cells might have attracted them to the tumor site. However, despite the presence of activated cytotoxic T cells in the tumors, no sight of tumor rejection was observed, and implanted tumors were able to continue growing. Additionally, further characterization of the $CD4^+CD25^+$ T cell subset would be necessary to evaluate whether the increased rate of CD25 expressing $CD4^+$ T cells in tumors is not in fact due to increased percentage of Treg, which perform immunosuppressive functions and therefore inhibit effector T cell function.

The administration of LIVP-1.1.1 virus into the newly established humanized subcutaneous tumor-bearing NSG mouse model did not result in a difference in the activation of the tumor-infiltrating effector lymphocytes compared to control mice. Also, the implanted tumors alone attracted plenty of NK and T cells, but further characterization of those tumor-infiltrating lymphocytes is required in order to determine their immunosuppressive or effector functions in greater detail. In the event that attracted NK cells are immunoregulatory and suppress effector cell function in order to help implantation of eventually HLA mismatch tumor cells, it might be recommended to implant tumor cells, which are HLA matched with the engrafted human hematopoietic stem cells, at earlier time point after reconstitution than the here tested 10 weeks. This would prevent the recognition of the tumor cells as something foreign by the developing human immune system and would represent more accurately the situation and the immune responses in human cancer patient.

5.2 Effect of CTLA4 immune checkpoint blockade on the activation status of tumor-infiltrating T lymphocytes in humanized subcutaneous tumor-bearing NSG mouse treated with GLV-1h376 vaccinia virus

In order to evaluate whether CTLA4 immune checkpoint blockade could help overcome the localized immune suppression, that is typically found within the tumor and in this model possibly further enhanced by regulatory NK cells, and therefore to increase the antitumor immunity, a new recombinant vaccinia virus encoding for human CTLA4-blocking single-chain antibody was used.

In initial experiments, three rVACV strains ,GLV-1h375, -1h376 and -1h377, carrying the gene for a FLAG-tagged anti-human CTLA4 scAb under the control of three different VACV synthetic early (P_{SE}), early/late (P_{SEL}) and late (P_{SL}) promoters, respectively, were evaluated in cell culture for expression of the transgene and the secretion of the CTLA4 scAb into the growth media. As expected highest expression

levels of CTLA4 scAb were detected for GLV-1h376 with the strongest P_{SEL} promoter, followed by GLV-1h377 and -1h375. CTLA4 scAb was successfully secreted into the growth media of GLV-1h376-infected CV-1 cells and could be efficiently purified from there. This purified single-chain antibody was human-specific and able to bind to recombinant human CTLA4 Fc Chimera. Lack of cross-reactivity between the antibody and the recombinant mouse CTLA4 Fc Chimera was confirmed. The functionality of CTLA4 scAb was demonstrated in a proof of principle experiment in Jurkat cell culture and compared to that of the clinical CTLA4-blocking monoclonal antibody Ipilimumab. Both antibodies successfully enhanced the CD25 late activation marker expression on Jurkat cells activated with a mixture of PMA, Ionomycin, B7-1 and B7-2, demonstrating that virus-encoded CTLA4 scAb was able to activate the cells in a similar manner, but even more powerful than Ipilimumab. However, in beads-activated Jurkat cells CTLA4 scAb was the only antibody capable of increasing the activation of the human T lymphocytes. A possible explanation for the lack of function of Ipilimumab in these experimental settings could be the larger size of the monoclonal Ipilimumab when compared to the single-chain antibody, which did not allow the monoclonal antibody to reach its CTLA4 target in the presence of the large activation beads that are attached to the T cells. This result reinforces the proposal that a replacement of the monoclonal Ab used in the clinic with a smaller single-chain one could facilitate its distribution within the tumorous tissue *in vivo*.

Next, analysis of the replication and cytotoxic potential of GLV-1h375, -1h376 and -1h377 and the parental GLV-1h68 in human A549, 1936-Mel and 888-MEL cancer cell cultures showed that CTLA4 scAb-encoding viruses replicated in and killed all three tested cancer cell lines in a dose- and time-dependent fashion and in a similar manner to the parental GLV-1h68. All four rVACVs have the *Renilla* luciferase-Aequorea green fluorescent protein fusion (*ruc-gfp*) expression cassette in the *F14.5L* locus and under the control of VACV synthetic early/late (P_{SEL}) promoter. The expression of the reporter protein GFP in GLV-1h68-, -1h375-, -1h376- and -1h377-infected A549 cell cultures correlated very well with the replication and cytotoxicity data and increased with the time in viral dose-dependent fashion. The results demonstrated that measurement of the increasing GFP expression correctly represent increasing viral titers in cells, suggesting that monitoring of the fluorescent signal could be used, when monitoring of the infection in cell culture or in animal studies is desired.

As GLV-1h376 exhibited the same replication and killing potential against tumor cells in culture as the other two CTLA4 scAb-encoding rVACVs, but its replication let to production of larger amount of CTLA4 scAb, it was decided this virus to be used in animal studies. But before being studied in humanized mice, an additional experiment was performed in A549 cell culture. Beside CTLA4 scAb and the *Renilla* luciferase-GFP fusion protein expression cassettes, GLV-1h376 also carries the *E. coli* β-glucuronidase-encoding (*gusA*) gene in the *A56R* locus. The quantitative β-glucuronidase assay using this GusA enzyme is a very promising reporter system [24] (Tsoneva, Stritzker 2015, unpublished data). It is very accurate, requires very small sample volume, uses relatively cheap substrates and could be carried out in a very short time. Because high sensitivity of the assay even with small sample volumes would be very useful feature especially in humanized mouse studies, this assay was of particular interest to this work. A small blood volume needed for monitoring of successful virus replication in the tumor of these mice during oncolytic viral therapy would be very helpful to reduce the volume of blood withdraws. Therefore, correlation of CTLA4 scAb, GusA and viral titers, assayed separately by ELISA, β-glucuronidase assay and standard plaque assay, respectively, in A549 cultures infected with GLV-1h376 were analyzed and compared. Indeed, an excellent correlations with correlation coefficients R^2>0.9806 were observed, indicating that each of the three parameters could be used to estimate the amount of the other two when tested in cell culture and presumably also in mouse blood or tumor samples. Therefore, next it was studied the relationship of those three parameters in single cell suspensions from tumors excited from GLV-1h376-treated mice. Again, an excellent correlation with correlation coefficients R^2>0.9454 was observed. The excellent correlations indicate that each of the three parameters could be used to estimate the amount of the other two when tested in tumor samples, as well. This also means that only the assay using the smallest sample volume of the three assays would be sufficient to calculate all variables. The required sample volume is of crucial importance when working with scarce resources of humanized mice because of the high costs involved in the generation of this mouse model and the small number of animals available to work with. Therefore, β-glucuronidase assay, which is the least time- and sample-consuming as well as the least labor-intensive of the three assay, will be the assay of choice to be perform when testing viral titers, GusA and CTLA4 scAb concentrations in tumor-bearing humanized mice-derived samples after treatment with GLV-1h376.

After establishing the regression lines for all three parameters, the measurement of the GusA amounts in mouse samples would be enough to calculate viral loads and the CTLA4 scAb concentration. The low test volume of 5 µl or less needed for the β-glucuronidase assay would allow saving the precious mouse samples, such as blood serum samples, tumor samples etc., so they can be used for testing others than the mentioned three parameters.

After it was shown that the A549 cells could be successfully infected and killed by the GLV-1h376 virus in culture, the human lung carcinoma cell line was used in the above described tumorous humanized mouse model. The potential of GLV-1h376 to increase levels of activated tumor-infiltrating lymphocytes in A549 tumors was evaluated and compared to the parental GLV-1h68 virus. Successful infection of the subcutaneous tumors after systemic administration of the VACV strains was verified and confirmed by fluorescent microscopy of virus-mediated GFP expression. However, no significant difference was observed in the ratios of B, T and NK cells in blood, spleen and tumors of control and GLV-1h68- or -1h376-injected mice. Again, highest percentages of $NKp46^+$ NK cells, the majority of which were $CD56^{bight}$, were detected in tumors. Also, activated cytotoxic $CD8^+CD25^+$ T cells were found almost exclusively in tumors but no other organs. Interestingly, in GLV-1h376-infected tumors, a slight increase of T, $NKp46^+$ NK, $CD56^{bright}$ NK and cytotoxic $CD8^+$ T cell percentages accompanied with a slight decrease of $CD4^+CD25^+$ T cell percentage were detected. However, no significant differences were observed between control and VACV-infected tumors. Thus, these results suggested that the recruitment of NK and activated T cells were more tumor tissue specific than virus-dependent. The virus-mediated CTLA4 scAb in the GLV-1h376-infected tumors was not able to significantly increase activation of tumor-infiltrating T cells.

Human T cells among splenocytes from untreated and GLV-1h68 or -1h376-treated humanized A549 tumor-bearing mice were additionally evaluated and compared for their ability to be activated by T cell activation beads and to recognize A549 tumor cells *ex vivo*. These T cells were functional and could successfully be activated with commercially available beads designed to mimic dendritic cells and to specifically activate human T cells. As a result, significantly increased late activation marker CD25 expression and intracellular IFN-ɣ production were detected for the $CD4^+$ and $CD8^+$ T cells of all three mouse groups when compared to the respective cells before

activation. Activation of the T cells was also accompanied with IL-2 and IFN-ɣ increase in the culture supernatants of those cells. Interestingly, $CD4^+$ as well as $CD8^+$ T cells delivered from GLV-1h376-treated mice always showed more significant increase of the tested markers, suggesting that these cells might have been preactivated due to the CTLA4 blockade by the virus-encoded CTLA4 scAb in the GLV-1h376-treated mice. However, no significant differences were observed between the three mouse groups. In contrast to the activation with beads, T cells from all three mouse groups were not able to recognize and to be activated by A549 tumor cells. A possible explanation for the lack of activation could be that very little to none tumor-specific T cells were residing in the spleens. But because of the fact that absolutely no increase in activation markers was detected, a more plausible explanation could be that T cells have not had the opportunity to meet TAAs due to missing or dysfunctional antigen-presenting cells in the humanized mouse model. This assumption was supported by a previous report [93] showing that although few myeloid cells could be found in the circulation of such humanized mice [94] they are phenotypically immature and functionally impaired [95]. Immature and functionally impaired dendritic cells would not be able to present viral- or tumor-associated antigens to T cells thereby would prevent development of viral- and tumor-specific T cell response and activation, which could then be further enhanced by the CTLA4-blocking antibody. Therefore, even though $CD33^+$ myeloid cells were detected in blood and different organs of the here presented humanized tumor mouse model, a more detailed characterization would be necessary to determine the presence and the functionality of the dendritic cells. Additionally, another possible reason for improper antigen-presenting-T cell HLA-restricted interaction could be the fact that the human T cells in this model develop in the mouse thymus and are therefore mainly mouse MHC (H2)-restricted [93, 96].

As a conclusion it could be said that, although GLV-1h376-encoded human CTLA4 single-chain blocking antibody successfully bound to its human CTLA4 target *in vitro* and proved its functionality in Jurkat cell culture, the use of CTLA4 scAb-VACV could not significantly increase the activation of the tumor-infiltrating effector lymphocytes in humanized NSG mice with subcutaneous A549 tumors compared to such mice treated with its parental GLV-1h68 virus or non-treated control mice. A possible reason for apparent lack of CTLA4 scAb functionality in tumorous humanized mice could be imperfections in the reconstituted human immune system. Therefore, further

examination of the individual human immune cell populations developed in this mouse model as well as testing of their functionality will be necessary to enable a better interpretation of the observed interactions between the virus, the tumor and the developing human immune cells.

5.3 Humanized mouse model – conclusion and options for improvement

The use of the oncolytic vaccinia viruses is proving so far in animal studies [18-20] and in several Phase I and II clinical trials (www.clinicaltrials.gov; keywords: GL-ONC1 and vaccinia) to be a very promising new approach in the fight with the growing threat of human cancer, which can be used alone or in combination with the conventional cancer treatment modalities. However, due to species-specific differences between mouse and human [72] as well as ethical limitations of experimentation in humans, a development of a new experimental model is required. An example for such a model, which combine the advantages of the small animal mouse model with the ability to study the VACV-mediated oncolytic therapy in the context of the human immune system, is the humanized mouse model. This study describes for the first time the successful subcutaneous implantation of human tumor cells in human cord blood-derived $CD34^+$ stem cells-engrafted NSG mice, 10 - 13 weeks post humanization. The development of subcutaneous tumors in this model was crucial because it allows precise caliper measurements of tumor size and therefore much more accurate monitoring of tumor growth and tracking of the oncolytic virotherapeutical treatment, when compared to the previously reported humanized tumor mouse model, where tumors developed in the abdominal cavity [67]. However, treatment with LIVP-1.1.1, GLV-1h68 or human CTLA4-blocking antibody-encoding GLV-1h376 vaccinia viruses in the here presented humanized tumor mouse model did not result in a significantly increased activation of the tumor infiltrated effector lymphocytes compared to control tumorous mice, suggesting that functionality impairments of the developing human immune system and/or late implantation of HLA mismatch humor cells might be to blame. To be able to understand and to more precisely interpret these results in the model system being used in the particular study however further characterization of

the developed immune cell types and proof of their functionality will be necessary. Although, many humanized mouse models have already been developed, each of them has its strengths and limitations [93], and previous reports have demonstrated that even in the promising human $CD34^+$ stem cell-engrafted humanized mouse model further improvements are necessary before such mice with a functional human immune system are achieved [93, 96, 97]. Deficiencies in human growth factors and cytokines necessary for the hematopoietic and immune cell development, poorly developed lymph nodes and remaining functional host innate immune system are the major limitation in the human stem cell reconstituted NSG mice [97]. Many opportunities for improvement, such as further reduction of the host innate immunity while simultaneously enhancing the development and functionality of the developing human immune system, were already explored and some of them proved to be successful [93]. Beside the genetically modified, by targeted knock-in of human cytokine and growth factor genes and knock-out of mouse genes, the easiest approach to improve this mouse model is to inject the needed factors as recombinant proteins [93, 97, 98]. Many laboratories have already shown that the injection of human IL7, IL15, granulocyte/monocyte-colony stimulating factor (GM-CSF), etc. can facilitate and improve T, NK, myeloid cell, etc. development and functionality in humanized mice [65, 67, 82, 93]. Also, if more robust human immune system reconstitution is needed, the most improved Bone marrow/Liver/Thymus (BLT) humanized model, which is developed by the co-implantation of small pieces of human fetal liver and thymus under the immunodeficient mouse renal capsule and the subsequent transplantation with $CD34^+$ stem cells, all derived from same donor, could be used [45, 47, 67, 93]. Major advantage of the BLT-model is that human T cells develop in the implanted human thymus and are HLA restricted. However the preparation of this model is associated with a large expense and takes more time and effort, and also the developing more robust human system could easily reject the implanted tumor cells if not fully HLA matched. None of the developed humanized mouse models would be optimal to answer all of the questions that might be considered during vaccinia virus-mediated oncolytic therapy [97]. Therefore it is important to choose the right experimental design, mouse model and approach for its improvement for the defined question we have. It might even be considered the use of multiple humanized models to better understand the complex interaction between the virus and the tumor in the context of the human immune system.

6 References

1. American Cancer Society, Atlanta, Georgia, USA, *Global Cancer Facts & Figures 3rd Edition.* 2012.
2. American Cancer Society, Atlanta, Georgia, USA, *Cancer Facts & Figures 2015.* 2015.
3. Hanahan, D. and R.A. Weinberg, *The hallmarks of cancer.* Cell, 2000. **100**(1): p. 57-70.
4. Hanahan, D. and R.A. Weinberg, *Hallmarks of cancer: the next generation.* Cell, 2011. **144**(5): p. 646-74.
5. Bergers, G. and L.E. Benjamin, *Tumorigenesis and the angiogenic switch.* Nat Rev Cancer, 2003. **3**(6): p. 401-10.
6. Woo, Y., P.S. Adusumilli, and Y. Fong, *Advances in oncolytic viral therapy.* Curr Opin Investig Drugs, 2006. **7**(6): p. 549-59.
7. Mullen, J.T. and K.K. Tanabe, *Viral oncolysis for malignant liver tumors.* Ann Surg Oncol, 2003. **10**(6): p. 596-605.
8. Ries, S.J. and C.H. Brandts, *Oncolytic viruses for the treatment of cancer: current strategies and clinical trials.* Drug Discov Today, 2004. **9**(17): p. 759-68.
9. Parato, K.A., et al., *Recent progress in the battle between oncolytic viruses and tumours.* Nat Rev Cancer, 2005. **5**(12): p. 965-76.
10. Thorne, S.H., D.L. Bartlett, and D.H. Kirn, *The use of oncolytic vaccinia viruses in the treatment of cancer: a new role for an old ally?* Curr Gene Ther, 2005. **5**(4): p. 429-43.
11. Harrison, S.C., et al., *Discovery of antivirals against smallpox.* Proc Natl Acad Sci U S A, 2004. **101**(31): p. 11178-92.
12. Henderson, D.A., *The eradication of smallpox.* Sci Am, 1976. **235**(4): p. 25-33.
13. Yu, Q., et al., *Comparative analysis of tropism between canarypox (ALVAC) and vaccinia viruses reveals a more restricted and preferential tropism of ALVAC for human cells of the monocytic lineage.* Vaccine, 2006. **24**(40-41): p. 6376-91.

14. Kirn, D.H. and S.H. Thorne, *Targeted and armed oncolytic poxviruses: a novel multi-mechanistic therapeutic class for cancer.* Nat Rev Cancer, 2009. **9**(1): p. 64-71.
15. Roberts, K.L. and G.L. Smith, *Vaccinia virus morphogenesis and dissemination.* Trends Microbiol, 2008. **16**(10): p. 472-9.
16. Moss, B., *Poxvirus cell entry: how many proteins does it take?* Viruses, 2012. **4**(5): p. 688-707.
17. Schmidt, F.I., C.K. Bleck, and J. Mercer, *Poxvirus host cell entry.* Curr Opin Virol, 2012. **2**(1): p. 20-7.
18. Weibel, S., et al., *Treatment of malignant effusion by oncolytic virotherapy in an experimental subcutaneous xenograft model of lung cancer.* J Transl Med, 2013. **11**: p. 106.
19. Frentzen, A., et al., *Anti-VEGF single-chain antibody GLAF-1 encoded by oncolytic vaccinia virus significantly enhances antitumor therapy.* Proc Natl Acad Sci U S A, 2009. **106**(31): p. 12915-20.
20. Buckel, L., et al., *Combination of fractionated irradiation with anti-VEGF expressing vaccinia virus therapy enhances tumor control by simultaneous radiosensitization of tumor associated endothelium.* Int J Cancer, 2013. **133**(12): p. 2989-99.
21. Doceul, V., et al., *Repulsion of superinfecting virions: a mechanism for rapid virus spread.* Science, 2010. **327**(5967): p. 873-6.
22. Zhang, Q., et al., *Eradication of solid human breast tumors in nude mice with an intravenously injected light-emitting oncolytic vaccinia virus.* Cancer Res, 2007. **67**(20): p. 10038-46.
23. Yu, Y.A., et al., *Visualization of tumors and metastases in live animals with bacteria and vaccinia virus encoding light-emitting proteins.* Nat Biotechnol, 2004. **22**(3): p. 313-20.
24. Hess, M., et al., *Bacterial glucuronidase as general marker for oncolytic virotherapy or other biological therapies.* J Transl Med, 2011. **9**: p. 172.
25. Heo, J., et al., *Randomized dose-finding clinical trial of oncolytic immunotherapeutic vaccinia JX-594 in liver cancer.* Nat Med, 2013. **19**(3): p. 329-36.
26. Chen, N.G. and A.A. Szalay, *Oncolytic vaccinia virus: a theranostic agent for cancer.* Future Virology, 2010. **5**(6): p. 763-784.

27. Chen, N., et al., *A novel recombinant vaccinia virus expressing the human norepinephrine transporter retains oncolytic potential and facilitates deep-tissue imaging.* Mol Med, 2009. **15**(5-6): p. 144-51.
28. Haddad, D., et al., *Insertion of the human sodium iodide symporter to facilitate deep tissue imaging does not alter oncolytic or replication capability of a novel vaccinia virus.* J Transl Med, 2011. **9**: p. 36.
29. Stritzker, J., et al., *Vaccinia virus-mediated melanin production allows MR and optoacoustic deep tissue imaging and laser-induced thermotherapy of cancer.* Proc Natl Acad Sci U S A, 2013. **110**(9): p. 3316-20.
30. Jefferson, R.A., S.M. Burgess, and D. Hirsh, *beta-Glucuronidase from Escherichia coli as a gene-fusion marker.* Proc Natl Acad Sci U S A, 1986. **83**(22): p. 8447-51.
31. Zenser, T.V., V.M. Lakshmi, and B.B. Davis, *Human and Escherichia coli beta-glucuronidase hydrolysis of glucuronide conjugates of benzidine and 4-aminobiphenyl, and their hydroxy metabolites.* Drug Metab Dispos, 1999. **27**(9): p. 1064-7.
32. Ruiz-Hernandez, E., et al., *PEG-pHPMAm-based polymeric micelles loaded with doxorubicin-prodrugs in combination antitumor therapy with oncolytic vaccinia viruses.* Polym Chem, 2014(5): p. 1674-1681.
33. Jefferson, R.A., T.A. Kavanagh, and M.W. Bevan, *GUS fusions: beta-glucuronidase as a sensitive and versatile gene fusion marker in higher plants.* EMBO J, 1987. **6**(13): p. 3901-7.
34. Fang, W., M. Vikerpuur, and M. Sandholm, *A fluorometric beta-glucuronidase assay for analysis of bacterial growth in milk.* Vet Microbiol, 1995. **46**(4): p. 361-7.
35. Workenhe, S.T. and K.L. Mossman, *Oncolytic virotherapy and immunogenic cancer cell death: sharpening the sword for improved cancer treatment strategies.* Mol Ther, 2014. **22**(2): p. 251-6.
36. Lichty, B.D., et al., *Going viral with cancer immunotherapy.* Nat Rev Cancer, 2014. **14**(8): p. 559-67.
37. Fong, L. and E.J. Small, *Anti-cytotoxic T-lymphocyte antigen-4 antibody: the first in an emerging class of immunomodulatory antibodies for cancer treatment.* J Clin Oncol, 2008. **26**(32): p. 5275-83.

38. Pardoll, D.M., *The blockade of immune checkpoints in cancer immunotherapy.* Nat Rev Cancer, 2012. **12**(4): p. 252-64.
39. Buchbinder, E.I. and D.F. McDermott, *Cytotoxic T-Lymphocyte Antigen-4 Blockade in Melanoma.* Clin Ther, 2015. **37**(4): p. 755-763.
40. Schmerling, R.A., *Toxicity of checkpoint inhibitors.* Chin Clin Oncol, 2014. **3**(3): p. 31.
41. McCune, J.M., et al., *The SCID-hu mouse: murine model for the analysis of human hematolymphoid differentiation and function.* Science, 1988. **241**(4873): p. 1632-9.
42. Aldrovandi, G.M., et al., *The SCID-hu mouse as a model for HIV-1 infection.* Nature, 1993. **363**(6431): p. 732-6.
43. Zollner, T.M., et al., *Proteasome inhibition reduces superantigen-mediated T cell activation and the severity of psoriasis in a SCID-hu model.* J Clin Invest, 2002. **109**(5): p. 671-9.
44. Denton, P.W., et al., *Antiretroviral pre-exposure prophylaxis prevents vaginal transmission of HIV-1 in humanized BLT mice.* PLoS Med, 2008. **5**(1): p. e16.
45. Wege, A.K., et al., *Functional and phenotypic characterization of the humanized BLT mouse model.* Curr Top Microbiol Immunol, 2008. **324**: p. 149-65.
46. Namikawa, R., et al., *Long-term human hematopoiesis in the SCID-hu mouse.* J Exp Med, 1990. **172**(4): p. 1055-63.
47. Melkus, M.W., et al., *Humanized mice mount specific adaptive and innate immune responses to EBV and TSST-1.* Nat Med, 2006. **12**(11): p. 1316-22.
48. Bosma, G.C., R.P. Custer, and M.J. Bosma, *A severe combined immunodeficiency mutation in the mouse.* Nature, 1983. **301**(5900): p. 527-30.
49. Greiner, D.L., R.A. Hesselton, and L.D. Shultz, *SCID mouse models of human stem cell engraftment.* Stem Cells, 1998. **16**(3): p. 166-77.
50. Mosier, D.E., et al., *Transfer of a functional human immune system to mice with severe combined immunodeficiency.* Nature, 1988. **335**(6187): p. 256-9.
51. Vormoor, J., et al., *Immature human cord blood progenitors engraft and proliferate to high levels in severe combined immunodeficient mice.* Blood, 1994. **83**(9): p. 2489-97.

52. Christianson, S.W., et al., *Role of natural killer cells on engraftment of human lymphoid cells and on metastasis of human T-lymphoblastoid leukemia cells in C57BL/6J-scid mice and in C57BL/6J-scid bg mice.* Cell Immunol, 1996. **171**(2): p. 186-99.
53. Dorshkind, K., et al., *Natural killer (NK) cells are present in mice with severe combined immunodeficiency (scid).* J Immunol, 1985. **134**(6): p. 3798-801.
54. Czitrom, A.A., et al., *The function of antigen-presenting cells in mice with severe combined immunodeficiency.* J Immunol, 1985. **134**(4): p. 2276-80.
55. Prochazka, M., et al., *The nonobese diabetic scid mouse: model for spontaneous thymomagenesis associated with immunodeficiency.* Proc Natl Acad Sci U S A, 1992. **89**(8): p. 3290-4.
56. Shultz, L.D., et al., *Multiple defects in innate and adaptive immunologic function in NOD/LtSz-scid mice.* J Immunol, 1995. **154**(1): p. 180-91.
57. Greiner, D.L., et al., *Improved engraftment of human spleen cells in NOD/LtSz-scid/scid mice as compared with C.B-17-scid/scid mice.* Am J Pathol, 1995. **146**(4): p. 888-902.
58. Hogan, C.J., et al., *Engraftment and development of human CD34(+)-enriched cells from umbilical cord blood in NOD/LtSz-scid/scid mice.* Blood, 1997. **90**(1): p. 85-96.
59. Gimeno, R., et al., *Monitoring the effect of gene silencing by RNA interference in human CD34+ cells injected into newborn RAG2-/- gammac-/- mice: functional inactivation of p53 in developing T cells.* Blood, 2004. **104**(13): p. 3886-93.
60. Goldman, J.P., et al., *Enhanced human cell engraftment in mice deficient in RAG2 and the common cytokine receptor gamma chain.* Br J Haematol, 1998. **103**(2): p. 335-42.
61. Mazurier, F., et al., *A novel immunodeficient mouse model--RAG2 x common cytokine receptor gamma chain double mutants--requiring exogenous cytokine administration for human hematopoietic stem cell engraftment.* J Interferon Cytokine Res, 1999. **19**(5): p. 533-41.
62. Traggiai, E., et al., *Development of a human adaptive immune system in cord blood cell-transplanted mice.* Science, 2004. **304**(5667): p. 104-7.
63. Ito, M., et al., *NOD/SCID/gamma(c)(null) mouse: an excellent recipient mouse model for engraftment of human cells.* Blood, 2002. **100**(9): p. 3175-82.

64. Macchiarini, F., et al., *Humanized mice: are we there yet?* J Exp Med, 2005. **202**(10): p. 1307-11.
65. Shultz, L.D., et al., *Human lymphoid and myeloid cell development in NOD/LtSz-scid IL2R gamma null mice engrafted with mobilized human hemopoietic stem cells.* J Immunol, 2005. **174**(10): p. 6477-89.
66. Ishikawa, F., et al., *Development of functional human blood and immune systems in NOD/SCID/IL2 receptor {gamma} chain(null) mice.* Blood, 2005. **106**(5): p. 1565-73.
67. Wege, A.K., et al., *Humanized tumor mice--a new model to study and manipulate the immune response in advanced cancer therapy.* Int J Cancer, 2011. **129**(9): p. 2194-206.
68. Dias, J.D., et al., *Targeted cancer immunotherapy with oncolytic adenovirus coding for a fully human monoclonal antibody specific for CTLA-4.* Gene Ther, 2012. **19**(10): p. 988-98.
69. Riss, T.L., et al., *Cell Viability Assays*, in *Assay Guidance Manual*, G.S. Sittampalam, et al., Editors. 2004, Eli Lilly & Company and the National Center for Advancing Translational Sciences: Bethesda (MD).
70. Tsien, R.Y., *The green fluorescent protein.* Annu Rev Biochem, 1998. **67**: p. 509-44.
71. Shcherbo, D., et al., *Bright far-red fluorescent protein for whole-body imaging.* Nat Methods, 2007. **4**(9): p. 741-6.
72. Mestas, J. and C.C. Hughes, *Of mice and not men: differences between mouse and human immunology.* J Immunol, 2004. **172**(5): p. 2731-8.
73. Tsoneva, D., *Oncolytic viral therapy- Immunological characterization of vaccinia virus-mediated cancer therapy in T-cell-deficient and humanized mice implanted with human cancer cells or stem cells and evaluation of novel biomarker tests*, in *Department of Bichemistry*. 2012, University of Würzburg.
74. Angarita, F.A., et al., *Mounting a strategic offense: fighting tumor vasculature with oncolytic viruses.* Trends Mol Med, 2013. **19**(6): p. 378-92.
75. Strowig, T., et al., *Priming of protective T cell responses against virus-induced tumors in mice with human immune system components.* J Exp Med, 2009. **206**(6): p. 1423-34.
76. Murphy, K., *Janeway's Immuno Biology*. 2012, London and New York: Garland Science, Taylor & Francis Group, LCC.

77. Rea, I.M., S.E. McNerlan, and H.D. Alexander, *CD69, CD25, and HLA-DR activation antigen expression on CD3+ lymphocytes and relationship to serum TNF-alpha, IFN-gamma, and sIL-2R levels in aging.* Exp Gerontol, 1999. **34**(1): p. 79-93.
78. Caruso, A., et al., *Flow cytometric analysis of activation markers on stimulated T cells and their correlation with cell proliferation.* Cytometry, 1997. **27**(1): p. 71-6.
79. Buckner, J.H., *Mechanisms of impaired regulation by CD4(+)CD25(+)FOXP3(+) regulatory T cells in human autoimmune diseases.* Nat Rev Immunol, 2010. **10**(12): p. 849-59.
80. Piccirillo, C.A., *Regulatory T cells in health and disease.* Cytokine, 2008. **43**(3): p. 395-401.
81. Arnon, T.I., G. Markel, and O. Mandelboim, *Tumor and viral recognition by natural killer cells receptors.* Semin Cancer Biol, 2006. **16**(5): p. 348-58.
82. Strowig, T., et al., *Human NK cells of mice with reconstituted human immune system components require preactivation to acquire functional competence.* Blood, 2010. **116**(20): p. 4158-67.
83. Munz, C., et al., *Mature myeloid dendritic cell subsets have distinct roles for activation and viability of circulating human natural killer cells.* Blood, 2005. **105**(1): p. 266-73.
84. Poli, A., et al., *CD56bright natural killer (NK) cells: an important NK cell subset.* Immunology, 2009. **126**(4): p. 458-65.
85. Yokota, M., et al., *Role of NKp46 expression in cytokine production by CD56-positive NK cells in the peripheral blood and the uterine endometrium.* Am J Reprod Immunol, 2013. **69**(3): p. 202-11.
86. Crome, S.Q., et al., *Natural killer cells regulate diverse T cell responses.* Trends Immunol, 2013. **34**(7): p. 342-9.
87. Mandelboim, O. and A. Porgador, *NKp46.* Int J Biochem Cell Biol, 2001. **33**(12): p. 1147-50.
88. Smyth, M.J., et al., *New aspects of natural-killer-cell surveillance and therapy of cancer.* Nat Rev Cancer, 2002. **2**(11): p. 850-61.
89. Lee, S.H., T. Miyagi, and C.A. Biron, *Keeping NK cells in highly regulated antiviral warfare.* Trends Immunol, 2007. **28**(6): p. 252-9.

90. McNerney, M.E., et al., *Role of natural killer cell subsets in cardiac allograft rejection.* Am J Transplant, 2006. **6**(3): p. 505-13.
91. Bose, A., et al., *Cutting edge: perforin down-regulates CD4 and CD8 T cell-mediated immune responses to a transplanted organ.* J Immunol, 2003. **170**(4): p. 1611-4.
92. Beilke, J.N., et al., *NK cells promote islet allograft tolerance via a perforin-dependent mechanism.* Nat Med, 2005. **11**(10): p. 1059-65.
93. Brehm, M.A., et al., *Generation of improved humanized mouse models for human infectious diseases.* J Immunol Methods, 2014. **410**: p. 3-17.
94. Tanaka, S., et al., *Development of mature and functional human myeloid subsets in hematopoietic stem cell-engrafted NOD/SCID/IL2rgammaKO mice.* J Immunol, 2012. **188**(12): p. 6145-55.
95. Gille, C., et al., *Monocytes derived from humanized neonatal NOD/SCID/IL2Rgamma(null) mice are phenotypically immature and exhibit functional impairments.* Hum Immunol, 2012. **73**(4): p. 346-54.
96. Watanabe, Y., et al., *The analysis of the functions of human B and T cells in humanized NOD/shi-scid/gammac(null) (NOG) mice (hu-HSC NOG mice).* Int Immunol, 2009. **21**(7): p. 843-58.
97. Shultz, L.D., et al., *Humanized mice for immune system investigation: progress, promise and challenges.* Nat Rev Immunol, 2012. **12**(11): p. 786-98.
98. Willinger, T., et al., *Improving human hemato-lymphoid-system mice by cytokine knock-in gene replacement.* Trends Immunol, 2011. **32**(7): p. 321-7.

7 Appendix

7.1 Abbreviations

°C	Degree Celsius
%	Percent
β	Beta
ɣ	Gamma
ɣc	Gamma chain
µg	Microgram
µl	Microliter
4-MU	4-Methylumbelliferone
4-MUG	4-Methylumbelliferyl-β-D-glucuronide
Ab	Antibody
APCs	Antigen-presenting cells
ATP	Adenosine triphosphate
BLT	Bone Marrow/Liver/Thymus
BSA	Bovine serum albumin
CEV	Cell-associated enveloped virus
CH_3COOH	Acetic acid
CH_3OH	Methanol
C_2H_2OH	Ethanol
CMC	Carboxymethylcellulose
CMUG	6-Chloro-4-methylumbelliferyl β-D-glucuronide
CO_2	Carbon dioxide
CTLA4	Cytotoxic T-lymphocyte Antigen 4
DAMPs	Danger-associated molecular pattern
DCs	Dendritic cells
ddH_2O	Double distilled water
DMEM	Dulbecco’s Modification of Eagle’s Media
DMSO	Dimethyl sulfoxide
DNA	Deoxyribonucleic acid

DPBS	Dulbecco’s Phosphate-Buffered Saline
dph	Days post humanization
dpi	Days post infection
EBV	Epstein-Barr virus
E.coli	*Escherichia coli*
EDTA	Ethylenediaminetetraacetic acid
EEV	Extracellular enveloped virion
EGFR	Epidermal growth factor receptor
ER	Endoplasmic reticulum
FACS	Fluorescent Activated Cell Sorting
FBS	Fetal bovine serum
FDGlcU	Fluorescein Di-β-D-glucuronide
g	Gramm
GFP	Green fluorescent protein
Gluc	*Gaussia* luciferase
GVHD	Graft versus host disease
GusA	*E. coli* β-glucuronidase
h	Hour
hpi	Hours post infection
HBSS	Hank's Balanced Salt Solution
HMGB1	High-mobility group box 1
HSCs	Hematopoietic stem cells
IEV	Intracellular enveloped virion
IMV	Intracellular mature virion
i.v.	Intravenous
M	Molar
mAb	Monoclonal antibody
min	Minute
mg	Milligram
ml	Milliliter
MHC	Major histocompatibility complex
MOI	Multiplicity of infection
NK cells	*Natural killer cells*

NOD/SCID	Nonobese diabetic/ severe combined immunodeficient
NSG	NOD/SCID/IL2rγ^{null}
OD	Optical density
PAMPs	Pathogen-associated molecular pattern
PBMCs	Peripheral blood mononuclear cells
pfu	Plaque forming units
ph	Post humanization
PMA	Phorbol 12-myristate 13-acetate
p.t.	Posttransplantation
R^2	Correlation coefficient
RAG2	Recombinase activating gene-2
RFU	Relative fluorescence units
Rluc	*Renilla* luciferase
r.o.	Retroorbitally
rpm	Revolutions per minute
RT	Room temperature
rVACV	Recombinant vaccinia virus
s.c.	Subcutaneously
scAb	Single-chain antibody
SCID	Severe combined immunodeficient
SFEM	Serum-Free Expansion Medium
TAA	Tumor-associated antigens
TCR	T cell receptor
Th	Helper T cell
Treg	Regulatory T cell
VAA	Virus-associated antigens
VACV	Vaccinia virus
VGF	Vaccinia growth factor
WHO	World Health Organization

7.2 Acknowledgement

First of all, I would like to express my great thankfulness to Prof. Dr. Aladar Szalay for giving me the opportunity to accomplish my doctoral thesis in his group. In addition I want to thank him for challenging me with this very interesting and exciting topic and for his constant interest about my progress.

I would like to express my gratitude to Dr. Boris Minev for his continuing support and guidance through planning and performing all experiments.

I also want to thank PD. Dr. Jochen Stritzker for his scientific guidance through our cooperative work on the “Drug-encoded Biomarkers for Monitoring Biological Therapies” project and for his contribution to the resulting manuscript.

I also want to thank Prof. Dr. Friedrich Grummt for final proofreading of the entire doctoral thesis.

I would also like to thank Prof. Dr. Thomas Dandekar for agreeing to be the second reviewer for my thesis.

I would like to thank Dr. Qian Zhang and Dr. Alexa Frentzen for the scientific knowledge they shared with me and the support they gave me whenever I needed it.

I also want to thank the virus production team of Genelux Corporation, Dr. Nanhai Chen, Dr. Qian Zhang, Dr. Alexa Frentzen and Jason Aguilar, for providing me with all viruses used.

My special thanks to Terry Trevino, Uma Patel and Jason Aguilar for their excellent technical assistance.

I also want to thank Duong, Prisca, Sandeep, Ivan, Ricky, Lisa, Klaas, Marion and all the others for their help, support and friendship. I would like especially to thank Christina for helping me to print my thesis in Würzburg and also for all the support throughout our study at the University of Würzburg.

I also would like to thank the whole Genelux team and AG Szalay at the University of Würzburg for teaching me so many new methods, giving me countless practical advises and for creating such a lovely and pleasant work environment.

I would like to express my gratitude to Dr. Anja Wege for welcoming me in her Laboratory at the University of Regensburg and training me on the Humanized mouse model.

I would like to thank Dina Sirypangno and Neal Sekiya from the Flow Cytometry CORE Research Facility at VA Hospital, San Diego, CA, for introducing me to the basics of the flow cytometry analyses and for their continuous assistance.

Furthermore I would like to thank my Family for their love and emotional support during my study. I could not have done it without you.

I would like to express my gratitude to my mother, Pavlina, who was always on my side, made my dream to study Biomedicine in Germany possible, and therefore paved the way to where I stand today.

I also would like to thank my brother, Atanas, for the moral support and for being the best brother ever.

I would especially like to thank my husband and best friend, Boyan, who was always there for me with his love and continued support. Thank you for encouraging me and for giving up precious family time through this journey.

I am very happy that I had the chance to study at the University of Würzburg. I am thankful to all my professors and colleagues for giving me all the knowledge and these wonderful years in Würzburg and in San Diego and preparing me for my future professional carrier.

Thank You very much!

7.3 Affidavit

Erklärungen nach §4 Abs. 3 Satz 3, 5, 8 der Promotionsordnung der Fakultät für Biologie

Affidavit

I hereby declare that my thesis entitled: „ Humanized mouse model: a system to study the interactions of human immune system with vaccinia virus-infected human tumors in mice" is the result of my own work.

I did not receive any help or support from commercial consultants. All sources and / or materials applied are listed and specified in the thesis.

Furthermore I verify that the thesis has not been submitted as part of another examination process neither in identical nor in similar form.

Eidesstattliche Erklärung

Hiermit erkläre ich an Eides statt, die Dissertation: „Humanized mouse model: a system to study the interactions of human immune system with vaccinia virus-infected human tumors in mice", eigenständig, d. h. insbesondere selbständig und ohne Hilfe eines kommerziellen Promotionsberaters, angefertigt und keine anderen, als die von mir angegebenen Quellen und Hilfsmittel verwendet zu haben.

Ich erkläre außerdem, dass die Dissertation weder in gleicher noch in ähnlicher Form bereits in einem anderen Prüfungsverfahren vorgelegen hat.

_____ _____

Place and date Signature